Thresholds of Axial Vibration Induced Fretting Corrosion in Electrical Connectors

by

Haoyue Yang

A thesis submitted to the Graduate Faculty of
Auburn University
in partial fulfillment of the
requirements for the Degree of
Master of Science

Auburn, Alabama
May 5, 2013

Keywords: electrical contacts, fretting corrosion, modeling

Approved by

George T. Flowers, Chair, Professor of Mechanical Engineering
Subhash C. Sinha, Professor of Mechanical Engineering
Robert L. Jackson, Associate Professor of Mechanical Engineering

Abstract

Vibration induced fretting corrosion has been considered an important cause of failure in electrical contacts. In previous research, the basic mechanism that controls the inchoation and development of such fretting degradation has been well understood. However the vibration exciting the motion of connector systems is limited in the direction that is perpendicular to the connector and wire lead with it. In the present research, random noise and single frequency vibration tests in the axial direction of the connector system are used to induce the fretting corrosion in the connector contacts. Vibration characteristics and vibration threshold amplitudes of the connector systems with various wire lead lengths are studies by the vibration tests.

The experimental results exhibit the transverse vibration of the connector pairs and wire leads with them induced by the axial vibration excitation. Several vibration modes were found in the vibration tests. The axial vibration with micrometer-scale amplitude is able to trigger the fretting degradation of this kind of connector systems. The threshold behavior at various frequencies for the onset of fretting corrosion is displayed by the experimental results. Typically the threshold amplitudes at natural frequencies are apparently lower than the ones at other frequencies. With the increase of lengths of wire leads of the connector systems, natural frequency of the major mode decreases, and the threshold amplitudes of the

mode vary as a function with a non-monotonic curve. This threshold behavior is explained experimentally and by latter modeling results.

A simple mathematical model is developed to relate the threshold amplitude to the dynamic properties of connectors and wiring configuration. This spring-mass-damper vibration model is built according to the vibration characteristics and fretting mechanism of the connector systems that are validated by vibration tests. The results of this model are well correlated with the experimental results.

Acknowledgements

Sincerely, I hope to express my deep appreciation to my Advisor George T. Flowers for his guidance in the completion of my research work in Auburn University. His wise instruction and patient support provides me with constant help to deal with every academic problem.

I also would like to thank my committee members, Dr. Subhash C. Sinha and Dr. Robert L. Jackson for their academic instruction and assistance.

Special thanks would be given to all my friends, especially Mr. Pregassen Subramany, Mr. Yang Xu, Mr. Rujian Fu, which without their constant support, this "journey" would have been very difficult to accomplish.

Finally, I would like to express my greatest gratitude and gratefulness to my parents, Donghai Yang and Jie Wen, whose love, care and perpetual support have been invaluable for the completion of this degree (Master of Science).

Table of Contents

List of Tables

List of Figures

Nomenclature

A input vibration amplitude (μm) (page 69), a point in modeling

a_o acceleration of shaker head (m/s^2)

$a_{G'}$ acceleration of center of mass of receptacle (m/s^2)

AO simplified connector

AG' simplified blade

c_1 horizontal damping $(\mathrm{N \cdot s/m})$

c_2 vertical damping $(\mathrm{N \cdot s/m})$

F_1 horizontal force of spring and damper (N)

F_2 vertical force of spring and damper (N)

Ff friction force (N)

F_n normal force at contacting interface (N)

F_{ox} x axis component of support force of shaker head

F_{oy} y axis component of support force of shaker head

G center of mass of connector

G' center of mass of receptacle

g gravity (m/s^2)

I moment of inertia of connector about its root

k stiffness (N/m)

k_0 ngular stiffness (N/rad)

k_1 horizontal stiffness (N/m)

k_2 vertical stiffness (N/m)

l length of AO (m)

L_G length of OG (m)

$L_{G'}$ length of OG' (m)

M magnitude of Transfer Function (non-dimensional)

M_{k0} moment of angular spring ($N \cdot m$)

M_O moment about point O ($N \cdot m$)

m mass (kg) (Page 63), mass of connector (kg)

m' mass of receptacle (kg)

OG simplified receptacle

X_A initial position of point A in x axis (m)

x_A position of point A in x axis (m)

x_G position of point G in x axis (m)

$x_{G'}$ position of point G' in x direction (m)

Y_A initial position of point A in x axis (m)

y_A position of point A in y axis (m)

y_G position of point G in y axis (m)

$y_{G'}$ position of point G' in y direction (m)

y_O position of point O in y direction (m)

Z_F relative motion (mm)

Greek Letters:

α angular acceleration of AO about point O (rad/s^2)

β initial angle between AO and y axis (*rad*)

γ initial angle between OG and y axis (*rad*)

δ intial angle between OG' and y axis (*rad*)

θ angle of vibration (*rad*)

Ø phase angle (*rad*)

ω_n angluar velocity of natural frequency (rad/s)

ω angular velocity (rad/s)

Superscript:

$\hat{\imath}$ index in the x direction

$\hat{\jmath}$ index in the y direction

$\hat{\imath}'$ index in the x' direction

$\hat{\jmath}'$ index in the y' direction

CHAPTER 1 INTRODUCTION AND LITERATURE REVIEW

Fretting corrosion is widely considered a serious cause of failures of electrical contact. In recent decades, many researchers have worked and contributed to understanding causes, mechanisms and precaution of the fretting degradation. As the fundamental factor of such corrosion, the chemical reaction between contact surface material and the corrosive environments around it, like oxygen and chlorine, has been deeply researched and well understood. From the mechanical engineering prospective, vibration, thermal and tribology research has been focused on the small amplitude relative motion of contact surfaces, the other vital cause of fretting corrosion.

1.1 Fretting Corrosion

Fretting Corrosion is a phenomenon that happens due to mechanical stresses and chemical reactions; primarily because of chemical reactions (Waterhouse [1]). Fretting corrosion occurs at the interface of contacting metal surfaces that are subject to relative slip. The slipping is usually oscillatory motion, with small amplitudes, which can be resulted from mechanical vibration, changing temperatures, differential thermal expansion of contacting metals, load relaxation and junction heating as the power is switched on and off. When slipping happens at the interface, oxidation usually takes place as well.

The after effect of the fretting corrosion is characterized by discoloration of the metal surfaces by the formation of pits and grooves along with various corrosion products surrounding them (Fontana [2]). “Reddish brown debris” is found if the materials of one or both of the contacting surfaces contain iron (Williams [3]). With the rapid chemical conversion from metal to oxide, fretting corrosion is detrimental to dimensional accuracy and satisfactory tolerance. The corrosion products could also cause seizing or clogging for moving parts.

In multiple fields, the fretting corrosion has been causing serious problems. It usually leads to failures of suspension springs, bolt and rivet heads, king pins in auto steering mechanisms, jewel bearings, variable- pitch propellers, shrink fits, contacts of electrical relays, connecting rods, and other parts of vibrating machinery. Multiple bridges have collapsed caused by fretting at essential parts of the bridge design. As one reason of the substitute of artificial hips every nine years, fretting corrosion loosens femoral stems. One of the earliest documented examples of this corrosion was about automobiles shipped by railroad from Detroit to the West Coast. Because ball-bearing races of wheels were severely pitted by fretting, the automobiles were not operable on arrival. Based on its significance and influences, fretting corrosion is one of the topics under research at the Corrosion Technology Laboratory at the NASA Kennedy Space Center.

Multiple environmental factors have been researched by laboratory experiments. Moist air causes less corrosion damages compared to dry air. Nitrogen decreases the rate of progression of fretting corrosion. Parameters, including

amplitudes of slippage, the number of cycle slippage and normal load that keeps contacting surfaces compressed, are directly proportional to the rate of occurrence of fretting corrosion (Waterhouse [1]).

1.2 Mechanism of Fretting Corrosion

From the prospective of tribology, any flat surface is full of micro-scale asperities. Contact of two surfaces compressed together only occurs at the asperities. During relative motion of the surfaces, asperities rub clean tracks on the opposite surface. The track may oxidize superficially. By the repeated slip, the oxides are wiped off by the asperities. This slip activates a repeated conversion from metal to oxides, which is wiped off in turn, forming another fresh metal track. As shown in Figure 1-1, the oxide particles moving relatively to the metal surface fret the contacting surface after a run-in period [4]. Thus electrical resistance between the surfaces increases from a low value and remains high.

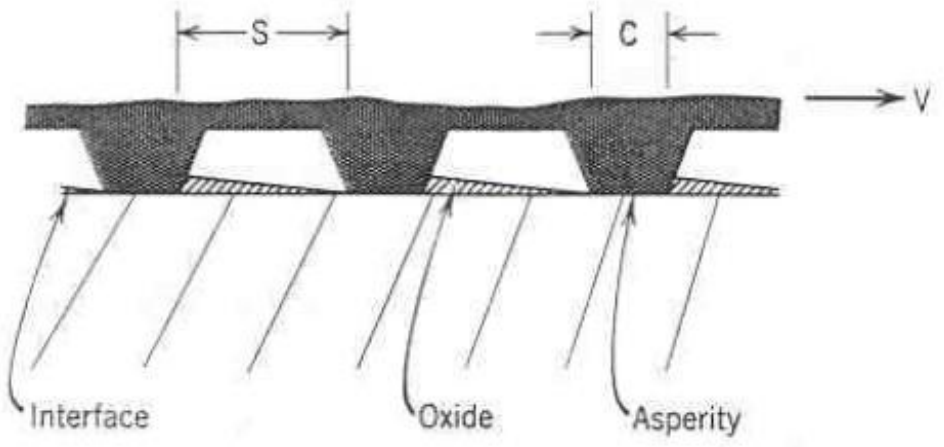

Figure 1-1: Idealized Model of Fretting Action (Feng et al. [4])

Oxidation usually takes place at interfaces of metallic surfaces that relatively

slip. Two mechanisms called wear- oxidation and oxidation- wear theories are used to explain how oxidation occurs. As shown in Figure 1-2 which illustrates the wear-oxidation theory, the oxidation of particles is caused by the asperities that are broken by frictional forces. The oxidation- wear theory, shown in Figure 1-3, is the opposite of wear-oxidation theory. It is believed that the wear- oxidation theory takes place first with the alternate occurrence of these theories after that (Fontana [2]).

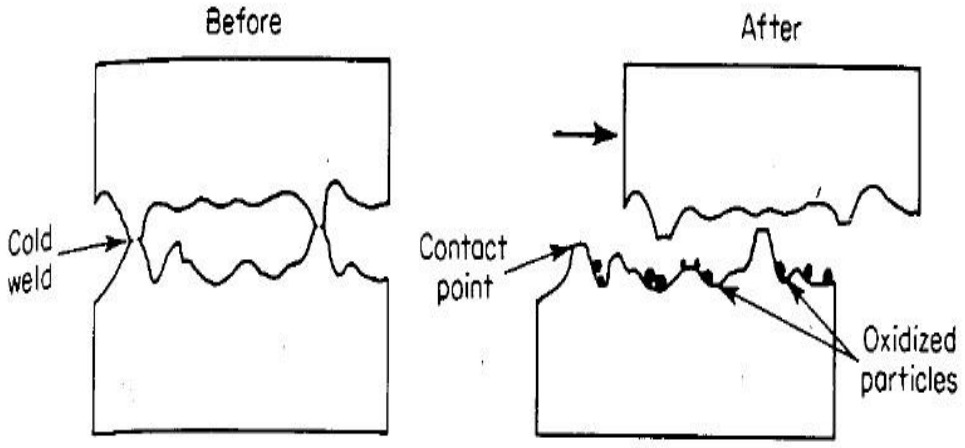

Figure 1-2: Mechanics of Wear- Oxidation Theory (Fontana [2])

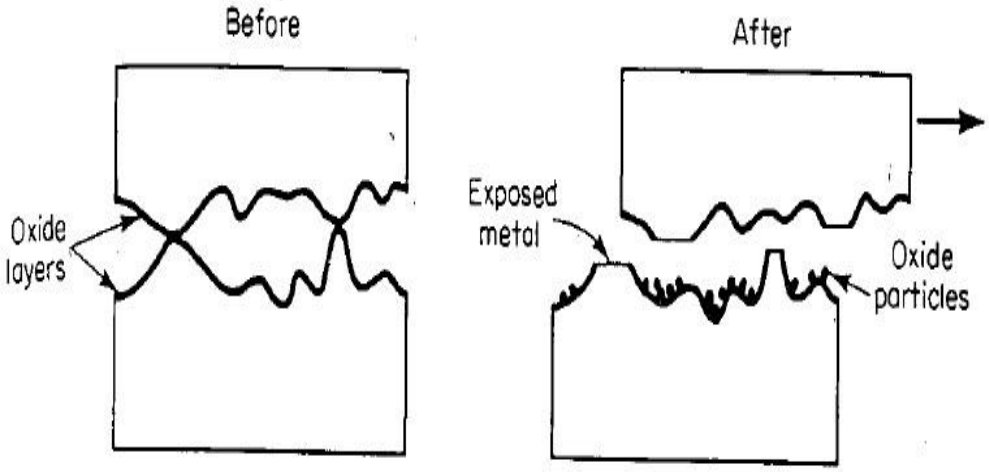

Figure 1-3: Mechanics of Oxidation- Wear Theory (Fontana [2])

As shown in Figure 1-4, Bryant introduced a mechanism of fretting corrosion on electrical connectors [5]. During the process of fretting, the initial rubbing of

asperities is ignored. Fretting motions expose the asperity contacts to corrosive attack and films are formed. The reversal fretting motions shears off corrosive layers and/or drag layers into contact. Further motion exposes contact to repeated corrosive attack. After a while, fretting motions induce plastic deformation of asperities, breaking the corrosive layers between the contacting asperities and mix this corroded material with the asperity metal. The asperities become contaminated with corrosion product and electrical resistance increases. Finally, after this series of events, the connector fails.

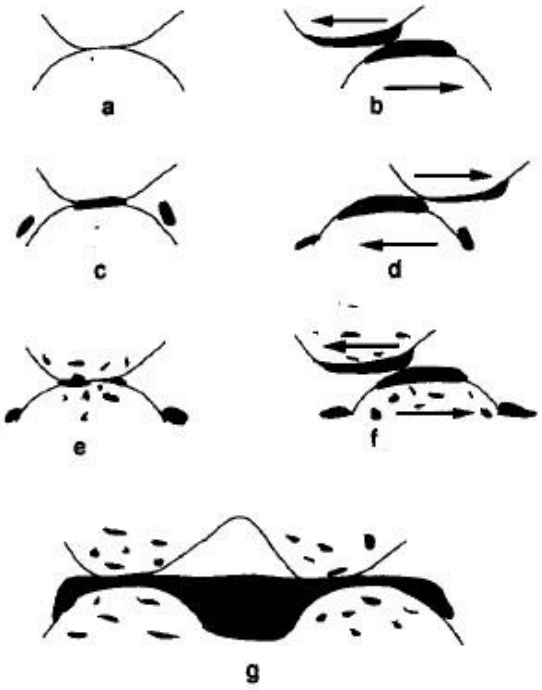

Figure 1-4: Mechanism of Connector Degradation due to Fretting (Bryant [5])

1.3 Literature Review of Fretting Corrosion in Electrical Contacts

Fretting corrosion is a significant problem affecting performance of various electrical and electronic equipments that contains expensive components. The detrimental influence of fretting to the electrical connections was not widely recognized until some failures of electrical connectors and Bock and Whitley's

subsequent work [6] in 1974. In their work, commonly used non- noble contact materials experienced large increases of electrical resistance during fretting actions, which occurs on electrical contacts as a result of vibration, mechanical motion or differential thermal expansion. Lubricants were proved to be able to exclude oxygen and other oxidizing gases from the contacts, thus preventing oxidation of the wear. After these findings, a lot of research was focused on the influences of different material properties and coatings of the contact surfaces. Some research was focused on the thermal, vibrational, tribologcical factors affecting the fretting corrosion [7-9]. Furthermore, mathematical models and FEA models have been widely built to predict the onset and progression of the fretting corrosion [10-14].

In 1984, a comprehensive review of fretting corrosion is offered [15]. In the study, the mechanism of phenomenon of this corrosion was discussed, such as transfer, wear, oxidation, and frictional forces that influence the fretting; the influence of the cycle rate and force on electrical resistance change of contact surfaces; an analysis of fretting behaviors of different materials; and a survey of lubricants that control fretting based on contact materials. The determination factors of connector designs, the expected connector lifetime and the reliability requirement were investigated. Shock and vibration tests of hardware were recommended to be conducted for new material incorporation and contact design of electrical connectors. By fretting corrosion, the contact resistance ordinarily becomes more unstable with longer time, and resistance transients are considerably higher than static contact resistance. Lubricants that can reduce the oxidation rate by retarding the wear rate of thin noble

metals on film- forming substrates are able to stabilize the contact resistance. By the category of fretting process based on regimes [16], stick regime happens for motions of approximate 1 μm according to the contacting material, geometry and other factors. In this regime, relative motion between contact surfaces is accommodated by elastic deformation of the parts near contacting regions. Not until the parts are separated, the asperities are joined and there is no surface damage. Mixed stick- slip regime occurs with central stick areas surrounded by ring slip regions at which crack formation, fretting fatigue and wear debris may take place. In gross slip regime with 10 to 100 μm movement of contact surfaces, all asperity contacts are broken and asperities rub others of the opposing surface during each cycle. Fretting corrosion occurs in reciprocating sliding regime with large displacements of surface movement more than 100 to 200 μm. In research of Hannel et al. [17], the relative motion is divided into partial slip and gross slip conditions. The stabilized partial slip sliding condition allows direct metal/metal interactions operating where inner stick domain maintains low and stable contact resistance. Under the stabilized gross slip condition, wear leads to debris that oxidizes, and generates an insulating oxide layer. Stable metal/metal interactions are no longer possible and the electrical contact resistance becomes high and unstable, controlled by random oxide debris movement through the interface. During gross slip process, the coating is necessary to display noble properties to prevent the formation of oxide debris and a high wear resistance.

As one of the most critical fields affected by fretting corrosion, vehicle electronics are in the environment combing mechanical vibration, harmful

temperature and humidity. In 1987, Lee and Mamrick [18] reported a study about the fretting corrosion of tin- plated copper alloy used for stepping motor/precision stage assembly. The objective of this study is to explain the physical phenomenon of electrical conduction by tin- plated contacts subjected to fretting corrosion and the effect of electric load on the process of fretting corrosion. The rise of contact resistance of tin- plated copper alloy was studied under minute cyclical motion. By the tests over the range of circuit voltage and current, electrical load did not affect the electrical conduction of slightly corroded contacts. With the heat from further corrosion, the temperature rose more and resulted in the melting, sublimation and decomposition of oxides and finally vaporizing tin. The complexity of fretting corrosion in vehicle environment was reported by Swingler et al. in 2000 [19]. In their study, the temperature of automotive connectors was being monitored during real operation to evaluate stress levels. According to real environmental data gained from tests, an empirical model of temperature behaviors of various electrical connectors was presented. For improving this study, some micro-sensors were embedded in a connector housing, which provided real information about phenomena taking place at the connector interface for the first time.

In recent years, a lot of research has been focused on the performance of different materials as coatings of electrical connectors to retard the fretting corrosion. Song et al. indicated that there is a strong correlation between the rate of wear and lifetime of electrical contacts [20]. In the research of Bouzera et al. [21], the amplitude of transition where fretting begins was measured by a method of

incrementing amplitude at the micro- displacement scale test. Different types of materials are considered in this research. It was found that hard materials like nickel needs higher motion amplitude than softer material like tin to enable fretting corrosion whereas coating material in connector needs higher amplitude than pure metal without coating. The lifetime of electrical contact of noble materials is unlimited. For non-noble material, the lifetime is limited, and the contact resistance sharply increased at amplitude as low as a few micrometers. Fouvery et al. explained the reason and mechanism that noble coatings like gold and silver last longer than non- noble material like tin [22]. It's concluded that electrical contact endurance under established gross slip conditions is controlled by the kinetics of oxide debris layer formation and by the evolution of its composition of the debris. For non-noble coatings, like tin, the electrical conductivity decays as soon as the debris layer fully separates the interface, resulted from the high current resistivity of tin oxides. And for noble materials, electrical failure is controlled by the progressive elimination of the noble element from the oxide debris layer. When the content of noble atoms in the lay has been low, the conductivity of the interface decreases and the electrical contact fails. BNi- Au contact pair was proved to be able to replace Au-Au contact pair only under limited conditions of short fretting lifetime with several thousand cycles [23]. And it's better for BNi to be used as probe than as coupon, where contact pair displays rather low and stable fretting resistance within during thousands of cycles, longer than BNi(coupon)- Au(probe). Park et al. [24-27] proved that higher current load was useful to break oxide film and establish a good electrical

contact. Tin plated copper was suggested not to be used in over 85℃ as the tin would soften and cause an increase in the thickness of oxidation film. Neol et al. did the first study that aimed at relating the electro-deposition process with the microstructure of the layers [28], characterizing the properties of different layers for a given application. Bright nickel was compared to matte nickel in a fretting test that simulated the micro displacements resulted from vibrations. A drastic increase of the electrical resistance was observed with bright nickel. This behavior is linked to the microstructure of the coating that depends on the mechanisms of texture development in nickel electro-deposits.

For predicting contact resistance behavior of electrical connectors under fretting corrosion, mathematical models are necessary but difficult to be developed. In the early 1990s, two previously developed models, which dealt with contact resistance and oxide built- up under fretting corrosion, were combined into an analytical model by Malucci [29-30]. This model is able to predict the average influences of contact forces and fretting amplitudes on contact degradation. By modeling results, the results of fretting tests on tin plated contacts were explained. By this study, the fretting degradation is proved to be increased by increasing fretting amplitude or decreasing contact force. This phenomenon is attributed to either more asperity deformation by larger contact force or an increased number of asperity deformations per cycle under longer fretting amplitudes, which are able to increase the buildup of oxides. In addition, the relationship between the temperature swing and acceleration factor was studied by the analysis of the data of thermal shock experiments. By these results and

analysis, a basis of modeling of fretting corrosion based on fretting cycles and temperature swing is provided. To sum up, according to the necessary experimental parameters, the field degradation is able to be estimated by this model which simulates the acceleration factor of fretting corrosion.

A mathematical model, combing the tribology properties of contact surfaces and the chemical reaction of such corrosion, was also put forward by Bryant [5] in 1994. This comprehensive model is able to predict the contact resistance during specific fretting cycles and the lifetime of the ultimate failure of contacts. In this model, contact wipe, fretting vibration amplitude and frequency, contaminant chemistry, material properties, plating thickness, asperity deformations, normal load, electrical load, surface topography were taken into consideration. The fretting mechanism proposed by him is the basis of the model. Both the filling of surface valleys with debris produced by fretting and contamination of surface asperities by the corrosion products are considered to be the causes of fretting corrosion. Based on the mechanism, the model calculated the amount of corrosive products generated on the exposed surfaces during cycles of fretting. Assumptions which correlate mixing to plastic flow and modern composite theory are used to estimate the conductivity in the contaminated asperity. The asperity resistance that produced by the integration over the asperity volume and the total resistance were predicted by Greenwood's theory.

Bryant's theory and model is able to explain the general trend of the progression of electrical resistance, as shown in Figure 1-5 [31]. This figure reveals

transients of the resistance of electrical connectors under the vibration test with single frequency and single amplitude. During cycles of relative motion of contacting surfaces, the electrical resistance increased slowly first, and then rose tremendously after a critical fretting cycle. Based on Bryant's model and mechanism of fretting corrosion, the phenomenon can be generally divided into three stages. At the first stage, the contact micro structures- asperities and valleys - only have the elastic deformation. Secondly, the fretting motion begins and wear debris is generated. The escape of debris from the metal to metal contacts was facilitated by fretting actions. So the low contact resistance is maintained. At the third stage, insulating layers containing oxides and wear debris accumulate. Metallic contacts are lost and contact resistance fluctuates. Eventually, contact resistance becomes high and the connector fails.

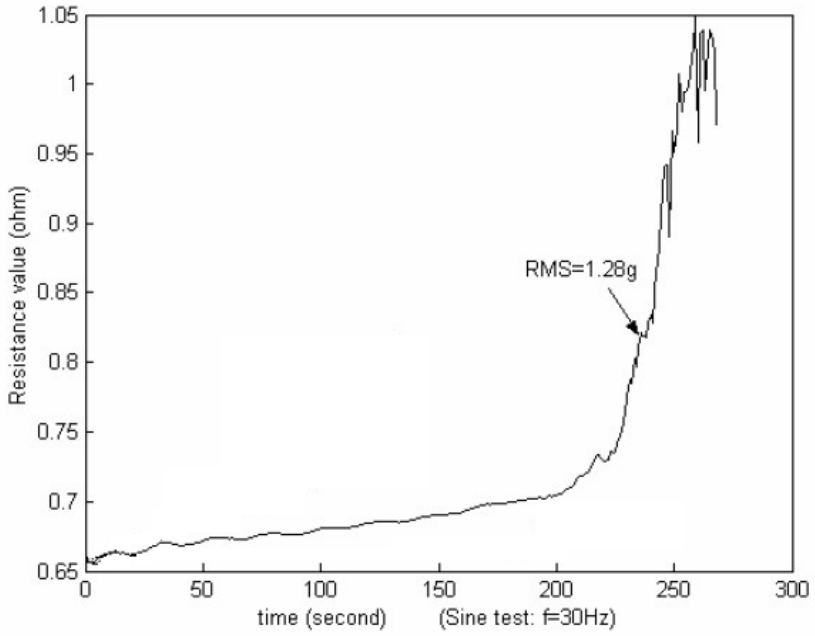

Figure1-5: Typical Fretting Curve in Sine Vibration Test (Xie [31])

In recent years, many new applications of the studies of fretting corrosion in

electrical contacts are extended by computer simulations. This technology has been being used to assist and guide the experiments and analyses of many companies and researchers. In 1996, Villeneuve et al. [32] at Ford Motor Company used finite element method to model the terminal crimping process of vehicle connectors. In his model, the terminal grip cross section, the punch tooling and wire strands were involved. For simulating the real application, the grip was forced into the punch as it sits on an anvil. In terms of results, the friction between the grip surface and the punch surface was found to be crucial to a "good" crimp. In 2005, Monnier et al. [33] applied FEM for simulating the performance of a sphere-plane electrical contact as a high current flowed through it. In this simulation, the mechanical, electrical and thermal coupling was involved. The validity of the model was confirmed by the high consistency of the simulation and experimental results. The contact terminal voltage, the contact resistance of the system and the solid temperature, which are not able to be measured in experiments, were provided by the simulation.

Compared to the research on multiple fields, relatively few researchers are focused on the vibration threshold in electrical connectors. From 2002， Flowers et al. [34], [35], [36] researched on the relationship between vibration excitation levels and fretting rates under single frequency vibration tests. In their works, the flexible cables connected with metal connectors was taken into account in vibration tests, as shown in Figure 1-6, and figure 1-7.

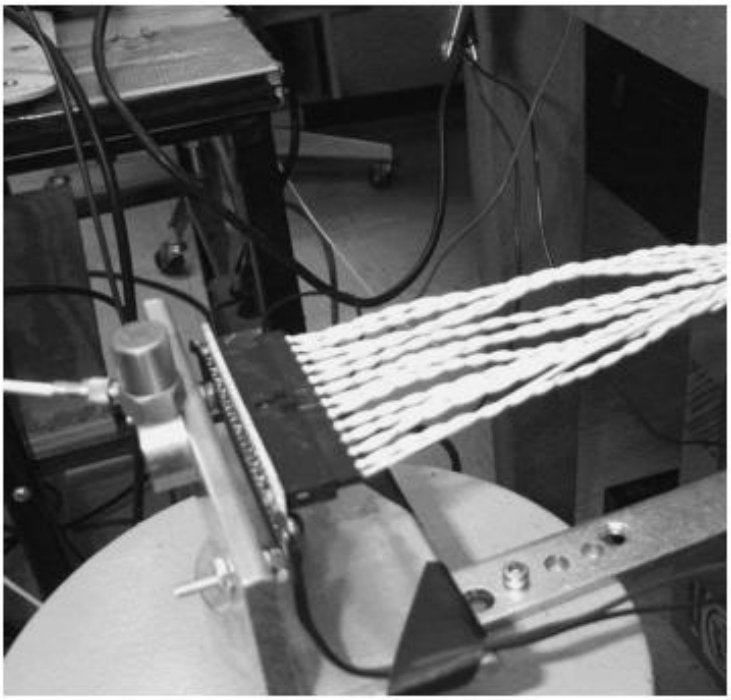

Figure 1-6: Experimental Setup Used by Flowers et al. [36]

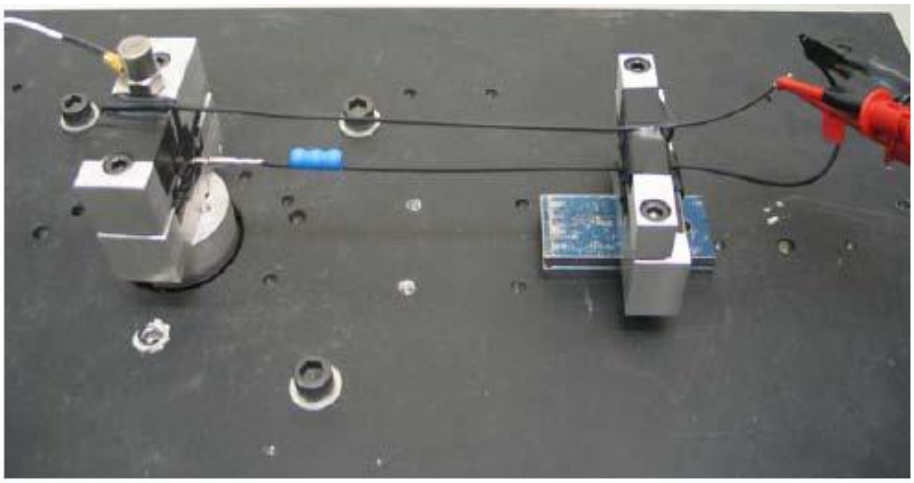

Figure 1-7: Experimental Setup Used by Xie et al. [37]

By the effect of the cables, relative motions between contact surfaces of connector pair are avoided under the vibration with small amplitudes. The threshold levels of excitation for fretting corrosion, above which the fretting corrosion occurs, were revealed by the results of the study. With the increase of excitation levels above the threshold, fretting rates rise monotonically. This phenomenon is illustrated by Figure 1-8. With the vibration excitation, smaller than 5 Grms, the electrical

resistance did not rise. With excitation levels that are larger than 6 Grms, the rate of the increase of the resistance rises monotonically. The threshold g-level should be between 5 to 6 Grms, and the accuracy of the measurement depends on the period of the test run- in. The researchers also found that the threshold g-level varies as a function of the dynamic behavior of the connector, the tie-off configurations and the mass and stiffness properties.

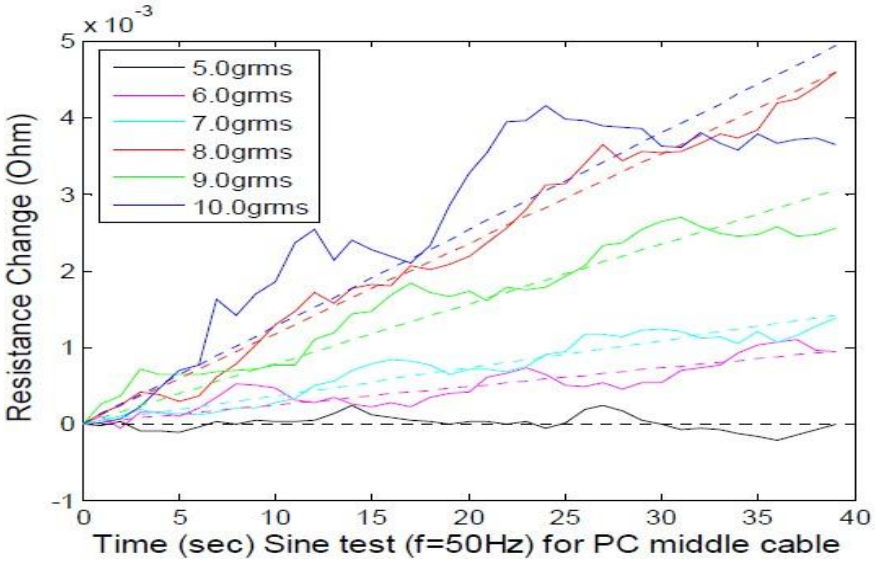

Figure 1-8: Electrical Resistance Transients under Excitation Levels (Xie [31])

In this study, the direction of exciting vibration, which is perpendicular to cable and connector pair, results in the rocking motion between contact pair. The primary mode of connector interface motion (rocking- type motion), the relative motion at the contacting location, served as an indicator of the fretting rate. The rocking motion leads one side of connector pin to be exposed to air, and to isolate another side from the air. As shown in Figure 1-9, the fretting corrosion mostly happened on the side of the pin that contacts air. It also indicated that the moment applied as the result of the given excitation level and frequency was reasonably

estimated by a transfer matrix model. An empirical fit of the data was in a good correlation with the model as the damping was considered. The analysis demonstrated that the bending moment caused by the excitation levels and tie- off configurations at the contact interface was significant to analyze and predict the threshold level. The researchers concluded that the dynamic behavior of the mechanical system under different excitation levels and tie- off configuration influences the performance of the connector system under vibration stresses.

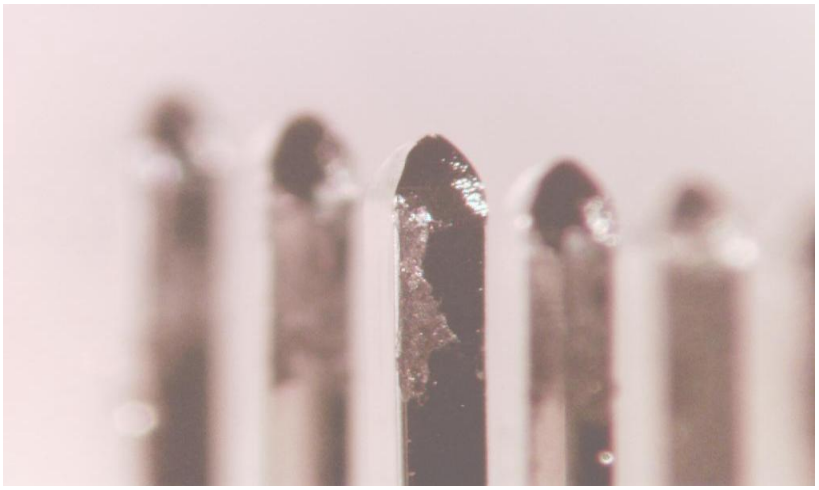

(a)

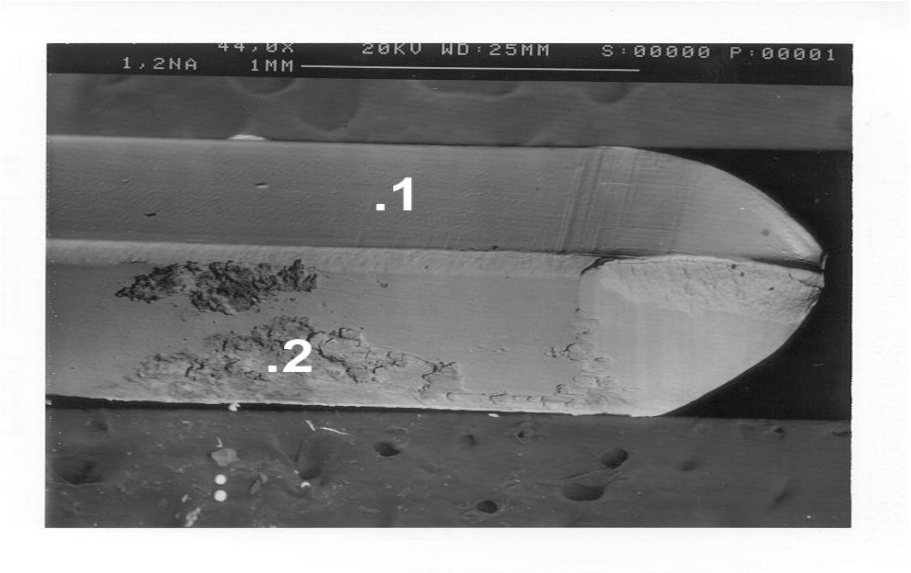

(b)

Figure 1-9: Corrosion Spots on Connector Pins Caused by Fretting (Flowers et al. [34])

Chen et al. [38-39] continued these research topics in FEA field. They have made two-dimensional and three dimensional FEA models to predict the vibration characteristics and thresholds of rocking- motion style vibration of connector systems. With the threshold levels measured experimentally, approximate amplitudes of relative motion at contact interface were obtained by the FEM model. In addition, the calculation cost of the two- dimensional model, with the comparative calculation accuracy, has been proven to be much better than the three- dimensional model. Ibrahim et al. [11] studied the influence of thermal factors on the fretting in electrical connectors. The results exhibited the non effect of temperature on the threshold and early stage performance. Gao et al. [40] researched on fretting corrosion on electrical connectors with contaminants between contact interfaces. It was proved that the failure of fretting degradation occurs much more easily than with the clean surfaces.

Another approach to measure the relative motion inducing fretting corrosion was reported by Lam et al. in 2005 [41]. In the study, a novel thick film sensor measuring the displacement at the connector interface was used to test for environmental effects on fretting corrosion in electrical contacts. This sensor was assembled into a connector sample to replace the male component. While the relative motion at the interface happened, the relative displacement of the contact point resulted in a corresponding electrical resistance change, which was measured by the connection of male and female parts. After the validation by a series of experiments, the sensors were subsequently used in a field test to research on the relationships between the fretting influences and temperature, humidity and differential pressure.

The researchers found that the differential pressure dominates the relative movement behavior at the interface of connector samples in condition that the influences of temperature and humidity on measured relative motion are negligible.

Fu et al. investigated the fretting mechanisms of silver-plated high power connectors induced by vibrations [42]. His results indicated that the variation of electrical contact resistance (ECR) of connectors subjected to vibration is primarily due to periodic changes of contact area caused by relative motion between the contact pairs, rather than other fretting corrosions. This finding was reinforced by observing a good correlation between relative motion and the variance of ECR under vibration. When a vibration stopped, the ECR decreased to a value that was slightly higher than the original value. A surface analysis showed no apparent degradation until the coating was worn away. An FEA model to predict the instant electrical resistance change during vibration was developed in his research.

In 2008, Angadi et al. [7] proposed a multi-physics coupled simulation with the mechanical, thermal and electrical interactions predicting contact forces, electrical contact resistance (ECR) and thermal contact resistance (TCR) in the rough surface contact regions. This model was developed in terms of multi- scale sinusoidal rough surface (MSRS) contact model using a MATLAB code that communicates with ANSYS. In the bulk connector material, it provided predictions of the stresses, strains, Joule heat effects, current flow, electric potential and the temperature distributions between the spring and pin parts of the connector. Finally the results illustrated the significant proportional rise in voltage drop and

temperature across the bulk regions of connector parts.

1.4 Overview of Current Work

This thesis discusses an experimental study and a mathematical model which are focused on axial vibration thresholds of fretting corrosion of electrical connectors.

The thesis has been divided into four chapters. Chapter one is the literature review and introduction. It demonstrated the concept and mechanism of fretting corrosion. The research on fretting corrosion in electrical connectors in recent years has been also introduced in this chapter.

In chapter two, two experiments that utilized the same apparatus are described. In the first experiment, the transfer function test and the threshold test were conducted on one type of electrical connectors. The experimental results are analyzed to study the relationship between the single frequency thresholds for fretting corrosion and the excitation frequency. In the second experiment, transfer function and threshold tests were conducted on sample connectors with various wire lead lengths. Vibration characteristics of the connector systems and influence of the tie-off configuration to thresholds of fretting corrosion are analyzed based on the testing results.

Chapter three describes a discrete mass-spring-damper vibration model. This model was programmed and run in MATLAB. In this model, the beginning of the relative motion at the interface of connector pair was assumed as the indicator of

fretting corrosion. A couple of experiments were conducted to measure several input dynamic properties of connectors, including stiffness and static friction force at the contact interface.

Chapter four provides a summary and conclusion of this work. Suggested future work is also discussed.

CHAPTER 2 EXPERIMENTAL STUDY OF THRESHOLD OF FRETTING CORROSION IN ELECTRICAL CONNECTORS UNDER AXIAL VIBRATION

2.1 Experimental Configuration

In this chapter, two experiments are performed to study the vibration and threshold behaviors and how tie-off configurations affect threshold of fretting corrosion in electrical connectors under axial vibration. For studying vibration characteristics and threshold behavior of the connector samples, a vibration system and electrical resistance measuring equipment are used for both experiments.

2.1.1 Experimental Equipment

The experimental equipment used in this study consist of a Keithley Model 2010 multimeter that is applied for the tests of the values of connector resistance; Polytec laser vibrometers systems measuring the displacements of the selected locations on connector samples; an HP 35665A dynamic signal analyzer, which generates different types of excitation signals (such as sine wave, random noise, etc) for the shaker and analyzes the frequency response; a vibration system that consists of a Dactron vibration control system, a PA500L Amplifier and a V408 Shaker. The details of these major components are mentioned below.

2.1.1.1 Keithley Model 2010 Multimeter

The Model 2010 is a $7\,^1/_2$-digit high-performance digital multimeter. It has 0.0018% 90-day basic DC voltage accuracy and 0.0032% 90-day basic resistance accuracy [43]. During tests, the multimeter was working in a four-wire mode with a resistance measurement range of 1uΩ to 120MΩ. Furthermore, the dry circuit method is indicated in Figure 2-1. It is an efficient type of low resistance measurement method which is made on contact devices such as switches and relay contacts. The purpose of this method is to determine whether fretting corrosion increases the resistance of the contacts. If the voltage across the contacts during the test is too high, the oxidation film might be punctured and render the test meaningless. Therefore dry circuit testing limits the voltage across the DUT to 20mV or less.

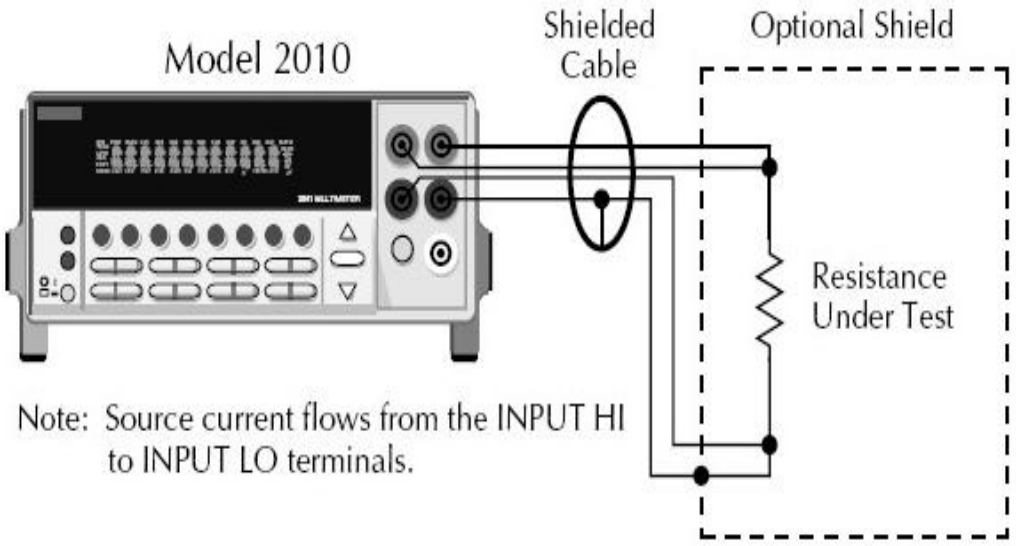

Figure 2-1: Resistance Measurement (Keithley Instruments Inc. [43])

2.1.1.2 Polytec Laser Vibrometer System

As shown in Figure 2-2, the Polytec laser vibrometer system is used in the

experiment for the non-contact displacement measurements [44]. The system consists of two Polytec OFV 353 sensor heads (lasers), and two Manfrotto tripods to hold the lasers and two Polytec OFV 2610 controllers. The system provides the methods for a displacement measurement based on the fringe counter principle. An analog voltage signal is available at its output that is proportional to the vibration amplitude of the measurement object. This signal can be visualized with an oscilloscope or can be entered into a data acquisition and processing system, such as the HP 35665A dynamic signal analyzer. Table 2-1 shows its displacement decoder specifications.

Figure 2-2: Photograph of the Polytec Laser Vibrometer System

Table 2-1: Displacement Decoder Specification of the Laser Vibrometer System

Measurement Range	**Full Scale Output(Peak to Peak)**	**Resolution**	**Max Vibration Frequency**	**Max. Velocity**	**Max. Acceleration**
µm/V	Mm	Mm	kHz	m/s	G
20	0.32	0.08	20	1.6	20,000
80	1.3	0.32	20	1.6	20,000
320	5.2	1.3	20	1.6	20,000
1280	20.5	5	20	1.6	20,000
5120	82	20	20	1.6	20,000

2.1.1.3 HP 35665A Dynamic Signal Analyzer

As shown in Figure 2-3, HP 35665A dynamic signal analyzer is a two-channel fast Fourier transform (FFT) spectrum/network analyzer with a frequency range that extends from 0.19531 Hz to 102.4 kHz in the single channel mode and from 0.097656 to 51.2 kHz in the two channel mode [45]. The analyzer has a built-in signal source providing random noise, burst random noise, periodic chirp, pink noise, and fixed sine. Measurements can be saved to an internal 3.5-inch flexible disk drive, or an external HP SS-80 disk drive, or can be directly printed out. The main characters of this analyzer applied in this study are listed as below:

- Input Noise Level: < -140 db
- Full Span FFT Noise Floor: < -76 db (-85 db typical)
- FFT Cross-Channel Gain Accuracy: ± 0.04 db (0.46%)
- FFT Cross-Channel Phase Accuracy: ± 0.5 degree
- Minimum Frequency Resolution: 122 μHz (Two Channel Mode)

Figure 2-3: Photograph of HP 35665A Dynamic Signal Analyzer

2.1.1.4 Vibration System

The vibration system utilized in this research comprises a PA500L Amplifier and a V408 Shaker, as shown in Figure 2-4 and Figure 2-5 respectively. The shaker provides the vertical vibration and a set of fixtures are designed and attached on the shaker for the experimental setup.

The configuration of the vibration control system is shown in Figure 2-6. The vibration system generates time-domain signals containing the required frequency domain characters or profile and sends them to the amplifier. Then the powerful amplified signal drives the shaker to vibrate with a larger current and voltage. The accelerometer installed on the payload senses the vibration on the shaker and converts it into an electrical signal that is then sent back to the vibration control system. The time-domain signal is processed by the vibration control system and is transferred into the frequency domain by FFT. And then the frequency-domain characteristics of this signal are compared with the original setting by this control system. If differences exist, the output signal will be revised by the vibration control system accordingly. This process repeats until the frequency-domain characteristics of the signal on the shaker match the required characteristics specified by the original setting.

Figure 2-4: PA 500L Amplifier

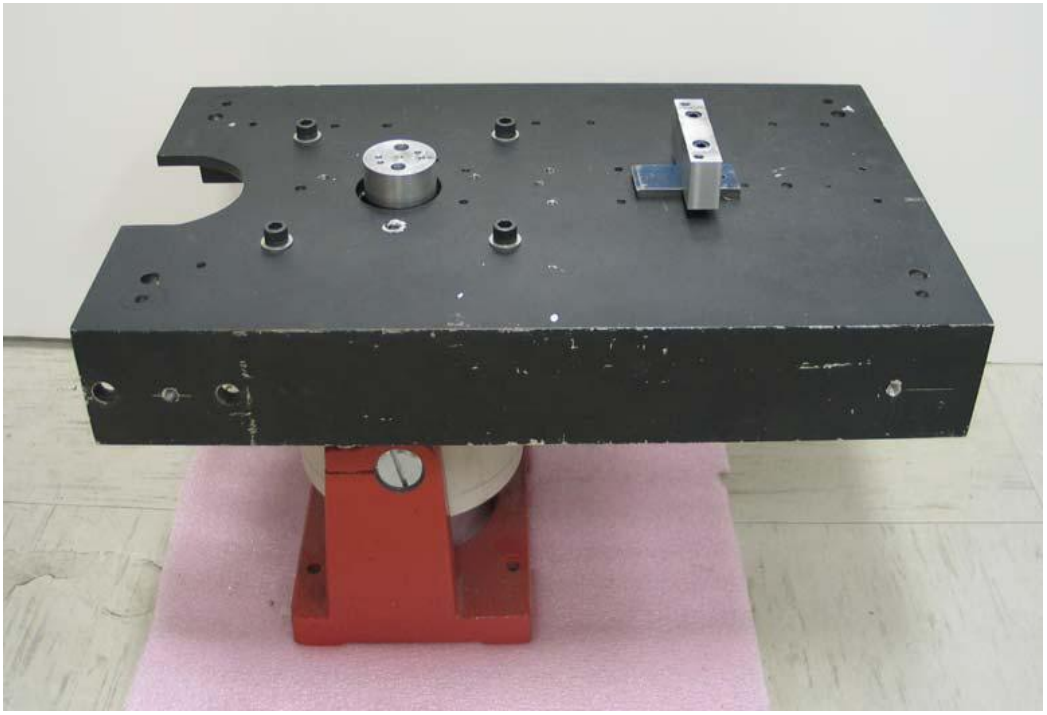

Figure 2-5: V408 Shaker and Fixture Table

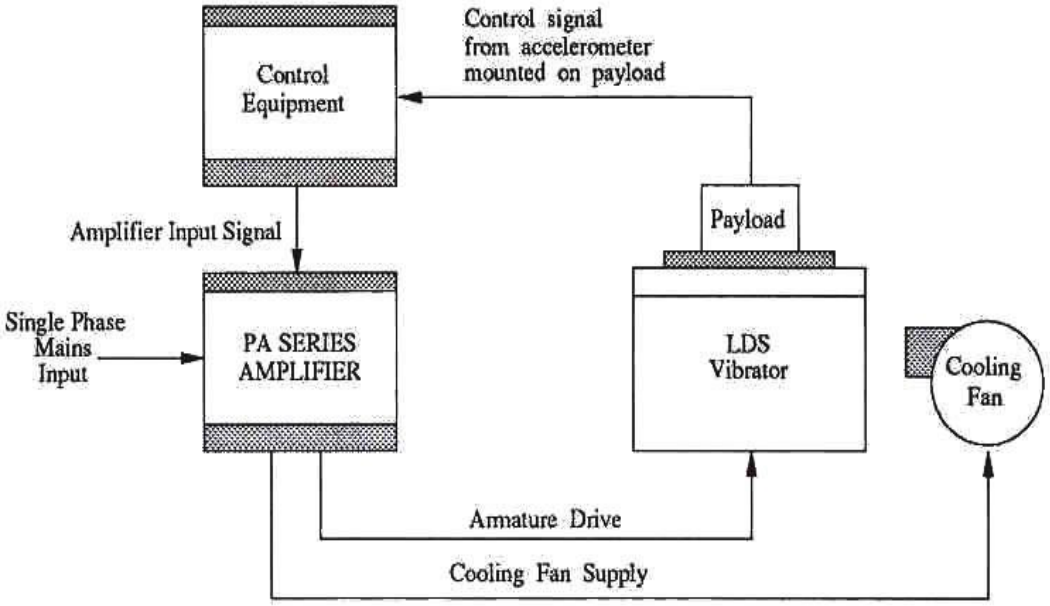

Figure 2-6: Typical Vibration System

2.1.2 Experimental Samples

As shown in Figure 2-7, a type of single blade/receptacle connector pair is applied in this research. The sample fundamentally comprises two components: the blade part on the left and the receptacle part on the right. Inside the receptacle, there is a spring part connected to the top of the inner layer of the receptacle. A gap exists between the end of this spring and the inner side of the bottom of part. Some degree of normal force should be produced between the blade and receptacle to keep the stable contact between the two parts, thus the gap is designed shorter than thickness of blade. As shown in Figure 2-8, when the blade is inserted into the receptacle, the spring bends and the contact force leads to friction force forming the contact pair.

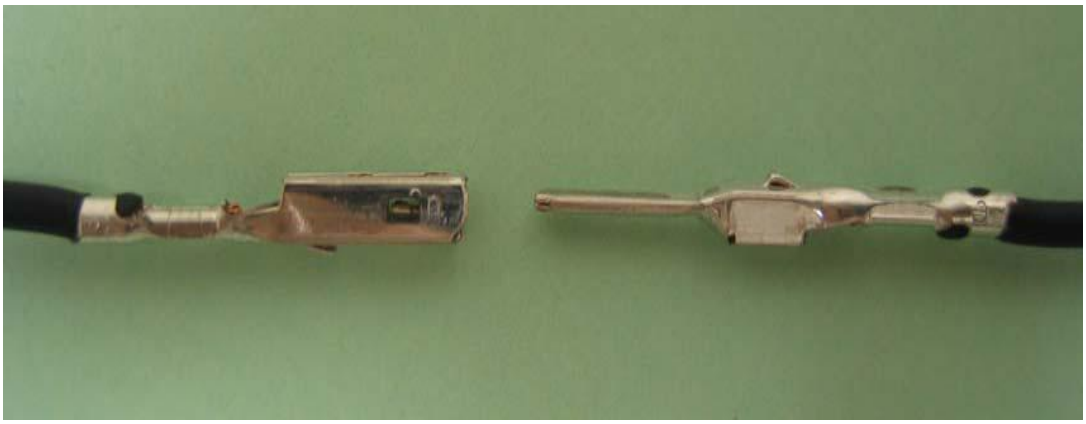

Figure 2-7: Photograph of the Blade and Receptacle Pair

Figure 2-8: Photograph of the Mated Blade/Receptacle Pair

Figure 2-9: Photograph of the Receptacle with a Single Wire Lead

As shown in Figure 2-9, a single wire lead is connected with the receptacle. Inside the rubber cover, a copper wiring bundle is connected with the metal part of

receptacle to transmit electronic power. For a high quality of the measurement, the samples are processed at several positions. The processes on connector samples and detailed experimental setup for two experiments are demonstrated below.

2.2 A Study on Vibration Threshold Amplitudes at Various Frequencies

In the author's work, single frequency vibration tests are used to measure the thresholds of fretting corrosion of electrical connectors. During each test, the connector system is forced to vibrate at the frequency of that of the vibration excitation. At various frequencies, different threshold amplitudes are possibly necessary to trigger fretting corrosion of the electrical connectors. Vibration transfer functions are measured as the significant vibration characteristics of the connector system. Comparison between the thresholds and transfer functions is conducted to study the relation between the threshold behavior and frequency response.

2.2.1 Experimental Setup

2.2.1.1 Experimental Samples

In the initial trials of vibration tests, increase of electrical resistance induced by fretting corrosion hardly happened. Based on the observation and analysis of processes and results of the experiment, it is attributed to the plastic deformation of wire leads connected with receptacles, which is resulted from the axial vibration and causes the blade to get stuck in receptacle. Thus it is necessary to increase the stiffness of the single wire lead to avoid the plastic deformation. As shown in Figure

2-10, two more wire leads are bundled with the original one and they are tied up by thermal shrink tubing. In this experiment, the connector samples with 4 cm cable are used for transfer function and threshold tests. The lengths of additional wire leads and the thermal shrink tubing are 4 cm.

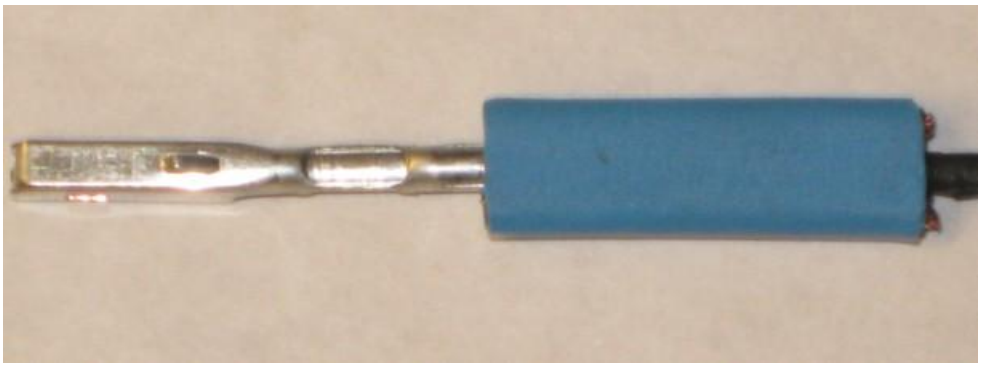

(a)

(b)

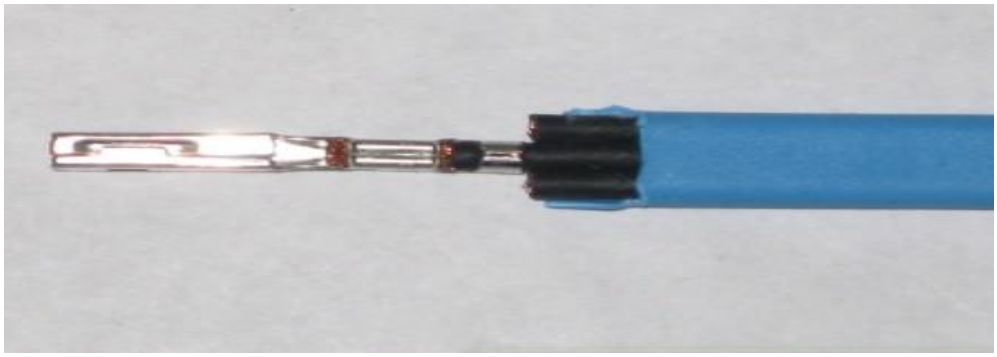

(c)

Figure 2-10: Receptacle with the Strengthened Wire Lead Bundled by Thermal Shrink Tubing

For high- quality laser signal used to measure the vibration behaviors of the connector system, reflectors made by laser sensitive material are necessary to be attached on the measurement positions. In this study, reflectors are fixed on the blade and receptacle to obtain the relative motion between blade and receptacle. To measure the axial vibration amplitudes of the blade, an annulus and a washer with light weights, which provide with the space for attachment of reflectors, are fixed on it by super glue, as shown in Figure 2-11.

Figure 2-11: Photograph of Blade Attached with an Annulus and Washer

2.2.1.2 Experimental Setup of Transfer Function Measurement

It's commonly agreed that relative motion between contacting interfaces is one of the fundamental causes of fretting corrosion. For the case of electrical

connectors, the fretting degradation resulted from micro- scale relative motions between the blade and receptacle leads to the rise of the electrical resistance. In previous study, Flowers et al. [12-16] have described the measurement methods and testing procedures for determining the transfer functions and fretting threshold. The transfer function for each sample is determined by comparing the output vibration response at the connector interface to the input excitation at the vibratory shaker head or the connector part fixed on the fixture on the shaker head. The ratio of the steady-state output amplitude to the input amplitude at a certain excitation frequency is the magnitude of the transfer function at that frequency. The phase difference between the steady-state output and input responses for a given frequency is the phase of the transfer function at that frequency.

From a dynamic modeling perspective, a transfer function is a functional relationship, in the frequency domain, between the magnitude (M) and phase (ø) of an input motion and the corresponding output motion. For example, a transfer function magnitude of 1 and zero phase shift indicates that there is no relative motion between the respective input and output measurement points. Similarly, a transfer function with a magnitude of 2 and a 45°phase indicates that the output motion is twice as large as that of the input and that it lags the input response by 45°. For most dynamic systems, there is a peak magnitude for input excitations at one or more of the resonant frequencies.

Typically, the phase shift is small for low frequency excitations and increases dramatically as the driving frequency approaches and exceeds the primary resonance

value. Another way of thinking of the transfer function is in terms of a complex number where the real part is M cos (ø) and the imaginary part is M sin (ø). Therefore, the transfer function can be expressed by the following equation:

$$Transfer\ Function\ =\ Mcos(ø)\ +\ i \cdot Msin(ø)\ or\ M\ \angle ø$$

Based on the above transfer function, the relative motion between the two-half interfaces is defined by:

$$Z_F = \sqrt{(1 - \mathrm{Mcos}\ (ø))^2 + (\mathrm{Msin}\ (ø))^2}$$

where Z_F is the relative motion, and M cos (ø) and M sin (ø) are the real part and imaginary part of the transfer functions, respectively.

As shown in Figure 2-12, the vibration behavior of the connector system is measured by the basic setup of the transfer function measurement for the blade/receptacle connector pair. By emitting and receiving laser rays, laser heads and the controllers process and send the data of dynamic displacements to the analyzer. The analyzer processes the data to show them on a screen. When testing by a single laser head, vibration displacement of one measurement position is tested. By the cooperation of two laser heads, the dynamic displacements of two positions are tested, and the transfer function of them are calculated by the analyzer. Though the laser heads are fixed by tripods horizontally, the laser rays can be reflected into different directions with the mirrors attached in front of them.

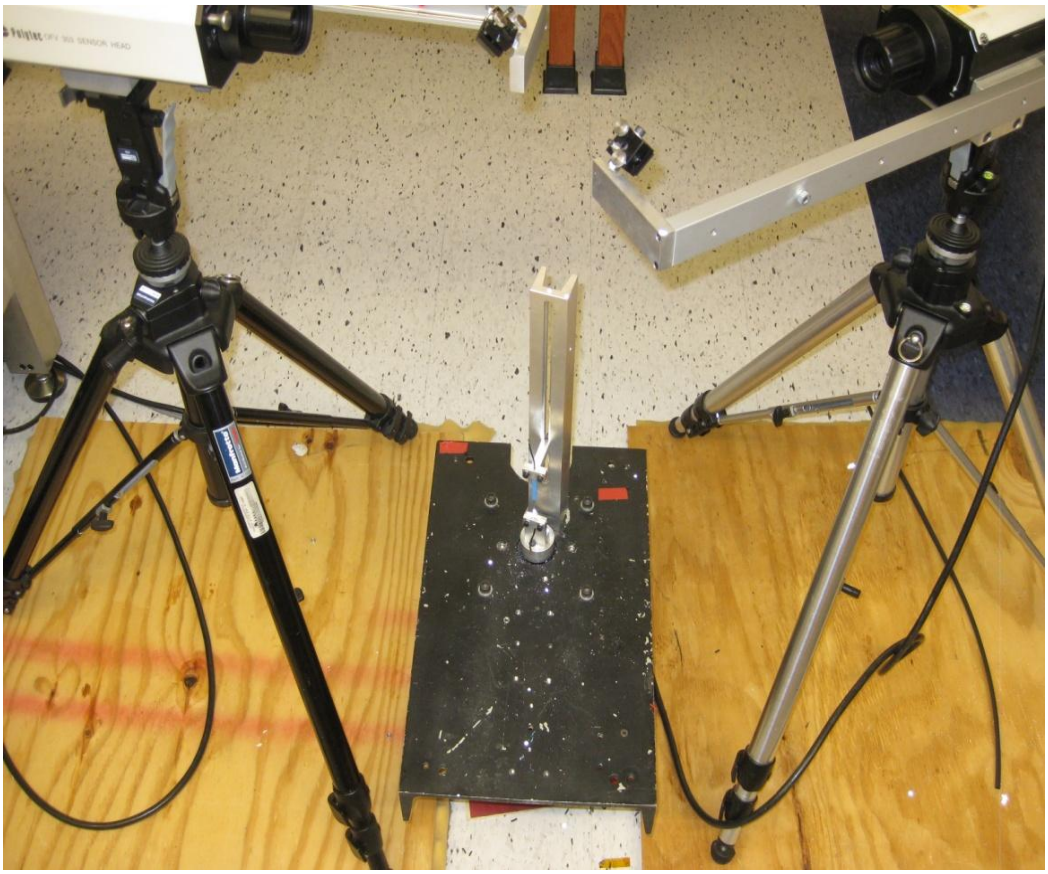

Figure 2-12: Experimental Setup of the Transfer Function Measurement

As shown in Figure 2-13, a set of fixture is fabricated to fix the electrical connectors for the axial vibration tests. The connector pair is assembled vertically. As source of the vibration excitation, a shaker head is set to vibrate vertically. A blade that is mated with the receptacle is fixed on a fixture on the shaker head. Without the connection of wire leads with the fixture, the metal part of the blade is clamped on the fixture. The end of the wire lead connected with the receptacle is fixed to a movable fixture. The movable fixture can be fixed at different heights in a groove of a stand which is stationary on a testing table. As the height of the movable fixture changes, different wire lengths can influence the vibration characteristics of the connector system.

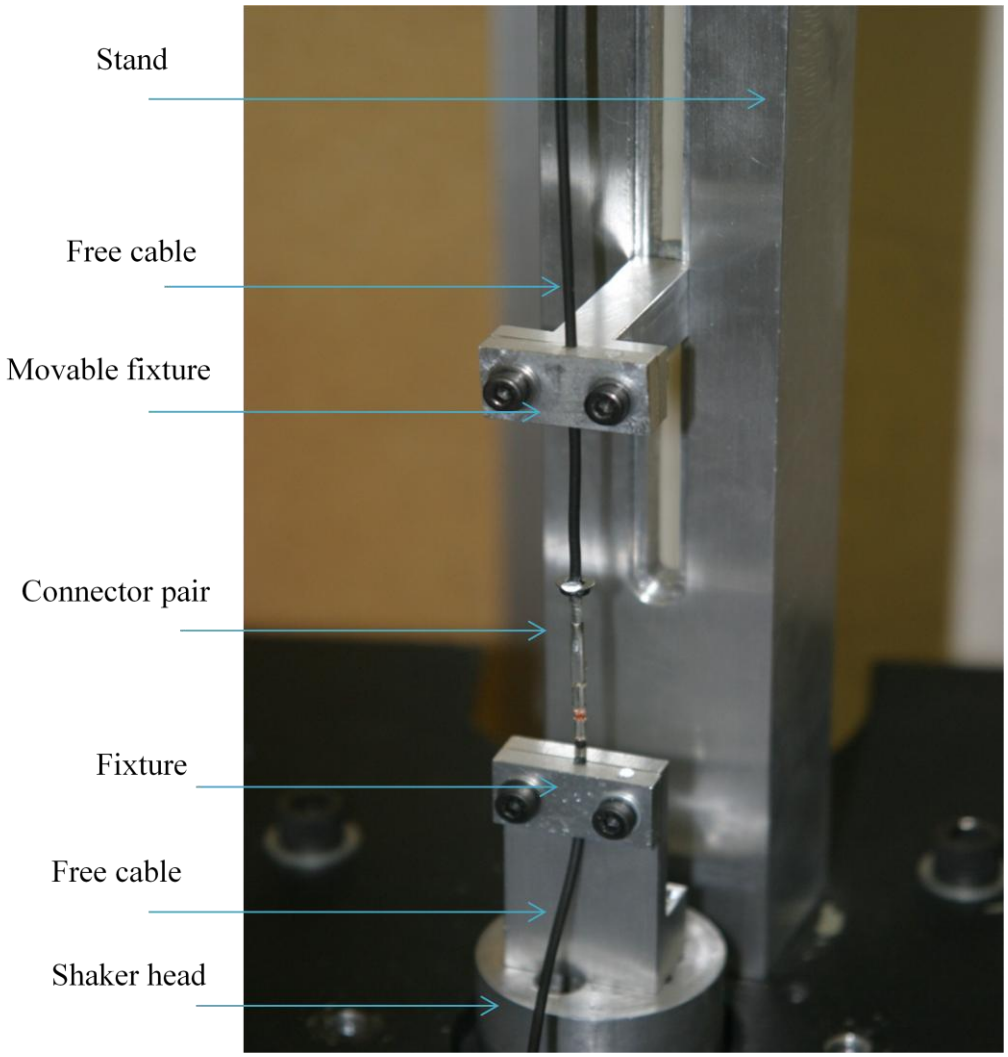

Figure 2-13: Photograph of Fixture for Experiments

The fretting corrosion of electrical connectors is considered to be triggered by micro-scale relative motions between the contact pair, the contact interfaces of blade and receptacle. Thus, the output and input of vibration positions for the transfer function tests are focused on the blade and receptacle. The axial amplitude of the blade is measured by the attached reflector as the vibration input. As the results of the initial trials of vibration tests, the transverse vibration of connector systems is observed. The reflectors are taped on the blade and receptacle to measure the transverse vibration as another input and outputs. The positions of reflectors are

shown in Figure 2-14.

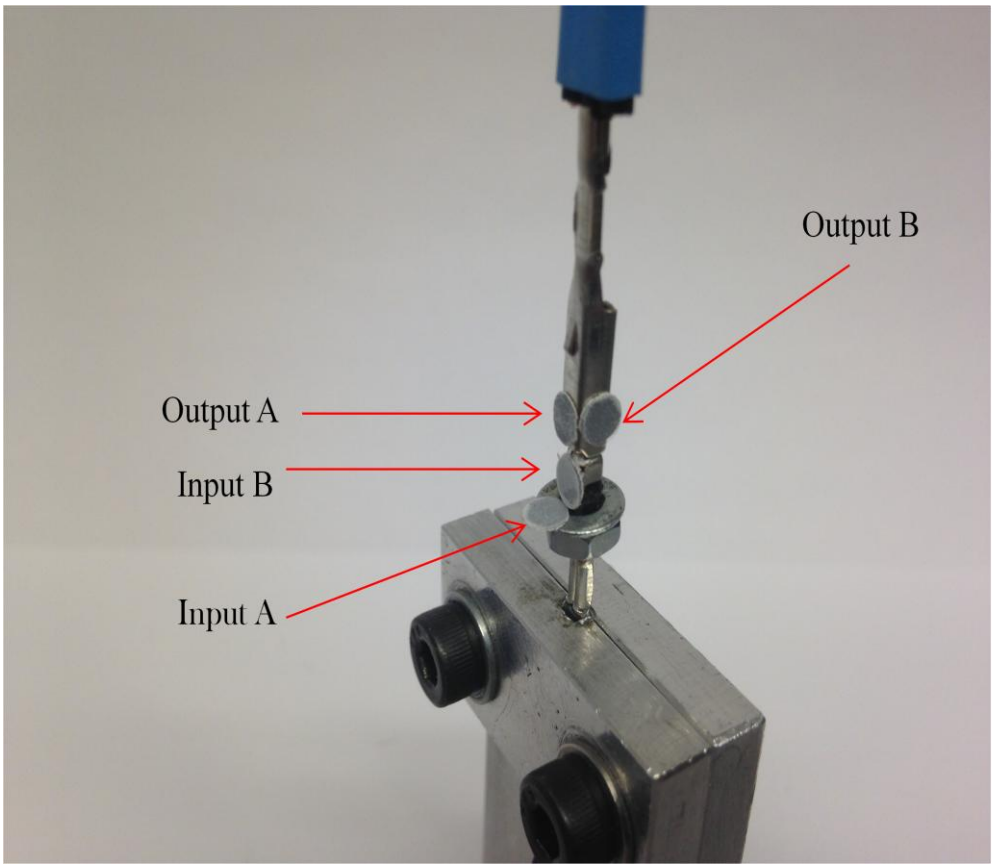

Figure 2-14: Reflector Positions for Transfer Function Test

After the process of wires by the thermal shrink tubing, the shape of cross section of flexible wire turns to be similar to rectangular, which may bring about various vibration modes in different vibration directions. Therefore the output reflectors are attached on two sides of receptacle to test the vibration behaviors of the connector system. As shown in Figure 2-14, the reflectors taped on the blade and receptacle respectively are set to measure the vibration in different directions as Input A and B and Output A and B. The directions of the laser beams emitted from the laser heads are shown in Figure 2-15 (a) and (b).

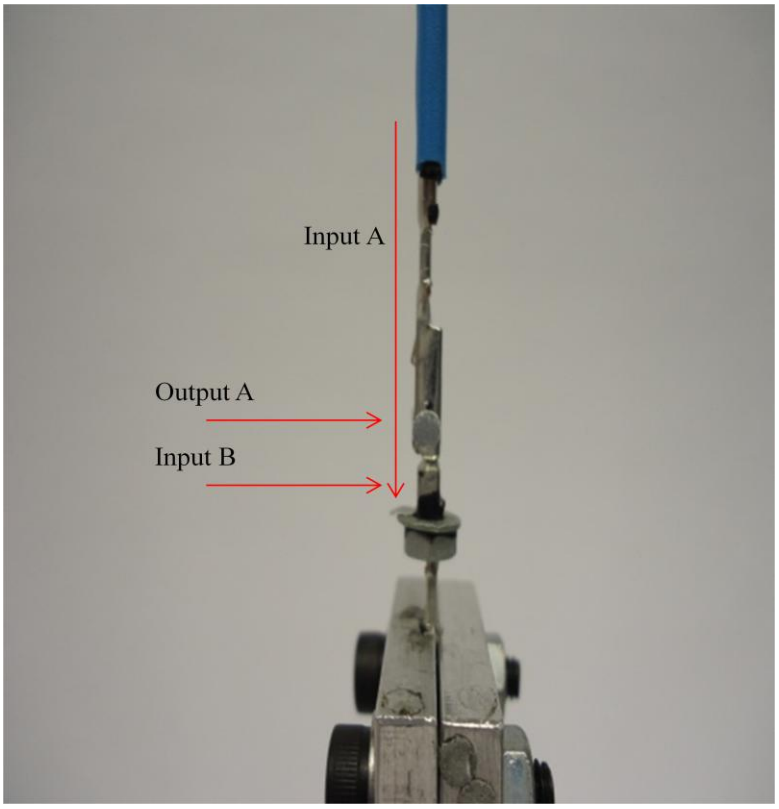

(a)

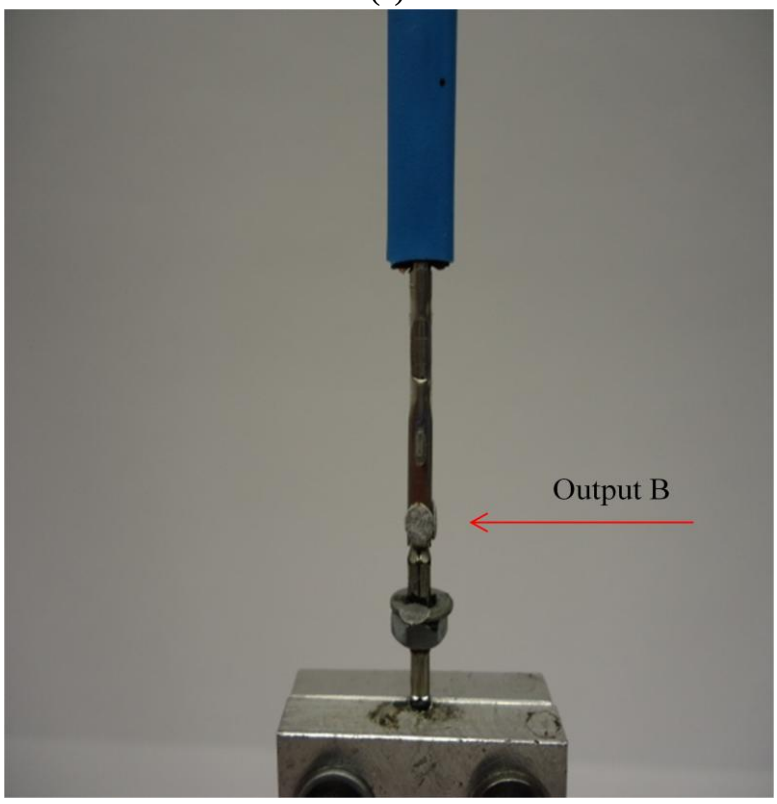

(b)

Figure 2-15: Displacement Measurement System Laser Beam Directions and Positions

2.2.1.3 Experimental Setup of Fretting Threshold Measurement

The setup of the fretting threshold level measurement is shown in Figure 2-16. For measuring the electrical resistance, the most significant indicator of fretting corrosion in electrical connectors, Keithly Model 2010 Multimeter connects the wires of connector systems. Free wire leads, which are not under vibration that are shown in Figure 2-13, are used to connect with the measurement equipment.

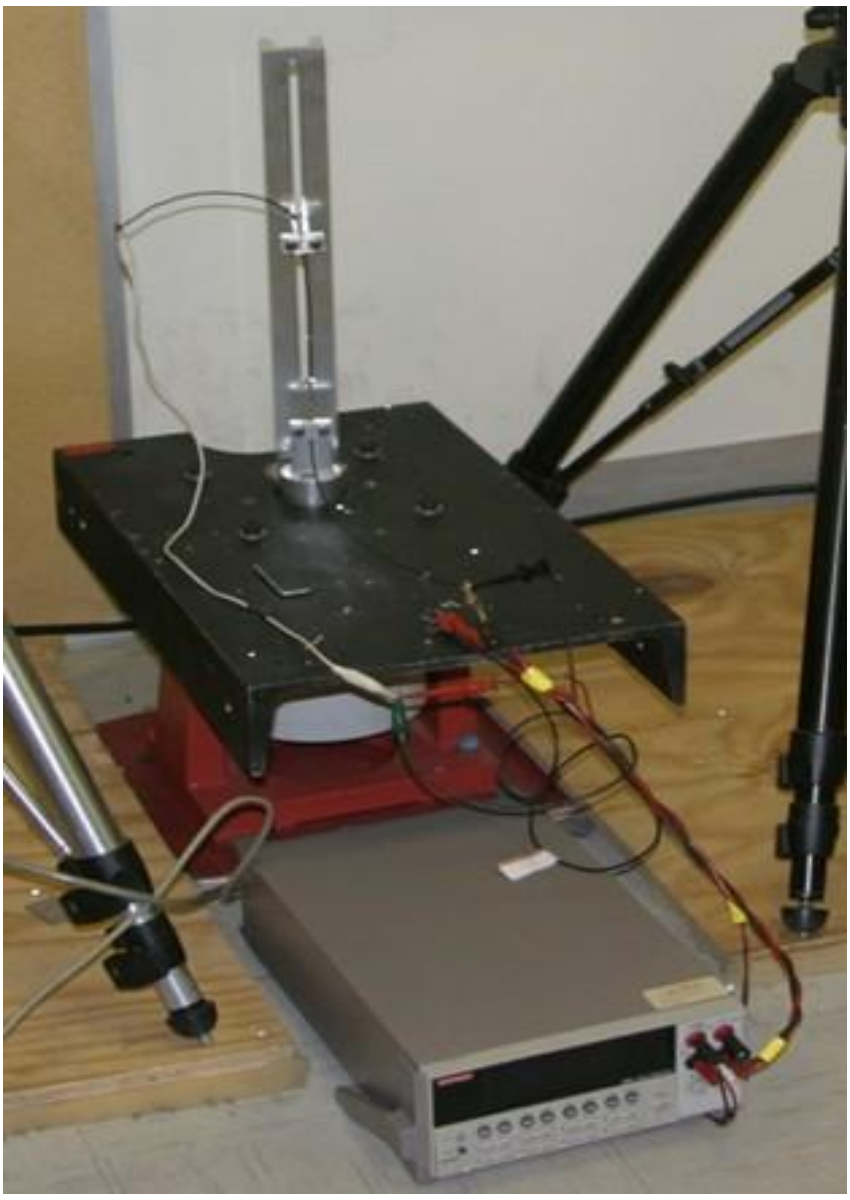

Figure 2-16: Photograph of the Fretting Threshold Amplitudes Experimental Setup

The electrical resistance is measured during vibration by the same experimental setup of vibration test. Sinusoidal signals are generated from the vibration control system, and the real- time resistance change is then observed and recorded by a computer system with a Labview program. The complete experimental setup of the threshold test is shown in Figure 2-17.

Figure 2-17: Complete Experimental Setup for Threshold Measurement

In this threshold test, single frequency vibration is used to excite electrical connectors with wire leads 4cm in length at various frequencies. The transients of electrical resistances are inspected under incremental excitation amplitudes. The lowest vibration amplitude that induces the fretting corrosion is recorded as the threshold. At each frequency, repeated measurements are conducted to obtain an average result. The range of frequency is limited between 100 HZ to 550 HZ

according to the power limitation of the vibration system. Generally there is just one frequency measured about per 50 HZ. But if the thresholds at two adjacent frequencies are close, one more frequency between them is chosen to be measured again. In each test, vibration amplitude increments from zero by amplified power of signal of the analyzer. With the each vibration amplitude, the test is run for at least five minutes for observing the transients of electrical resistance. If no obvious increase of the resistance is found, the vibration amplitude is increased in a small scale. By the initial trials, the fretting corrosion can be triggered by micro-meter scale amplitudes. Thus, the increase scale should be lower than 0.1μm, which is limited by the accuracy of the vibration system.

By initial trials, it is found that apparent corrosion spots appear on the contact surfaces of the connector pair if the fretting corrosion happens no matter how long the vibration takes. A fresh connector sample is used for each threshold test. If failed samples are used for the test again, the vibration amplitude that is much lower than the threshold can lead to the obvious fluctuation and increase of electrical resistance.

2.2.2 Experimental Results

2.2.2.1 Experimental Results of Transfer Function Measurement

Figure 2-18 shows two transfer functions measured by Input A-Output A, and Input A-Output B shown in Figure 2-14. Two natural frequencies of the connector system are found around 310 HZ and 450 HZ. In Figure 2-18 (a), two

peaks of magnitude exist and there are two 180-degree phase shift appear at the corresponding frequencies in Figure 2-18 (b). Figure 2-19 shows another transfer function measured by Input B-Output A, which indicates the natural frequency of relative rocking motion between receptacle and blade.

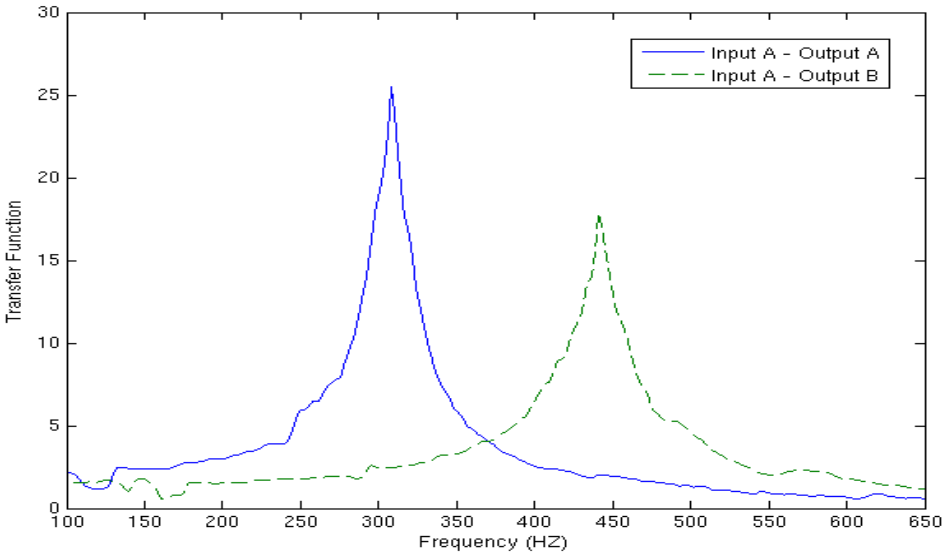

(a) Magnitude Plot

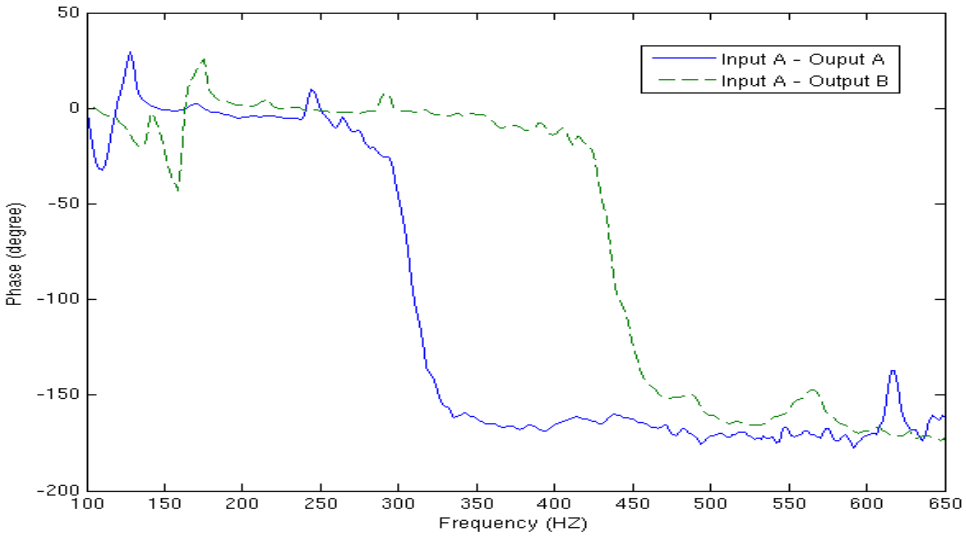

(b)Phase Plot

Figure 2-18: Transfer Function Plot with Input A (Sample with Wire Lead 4 cm in Length)

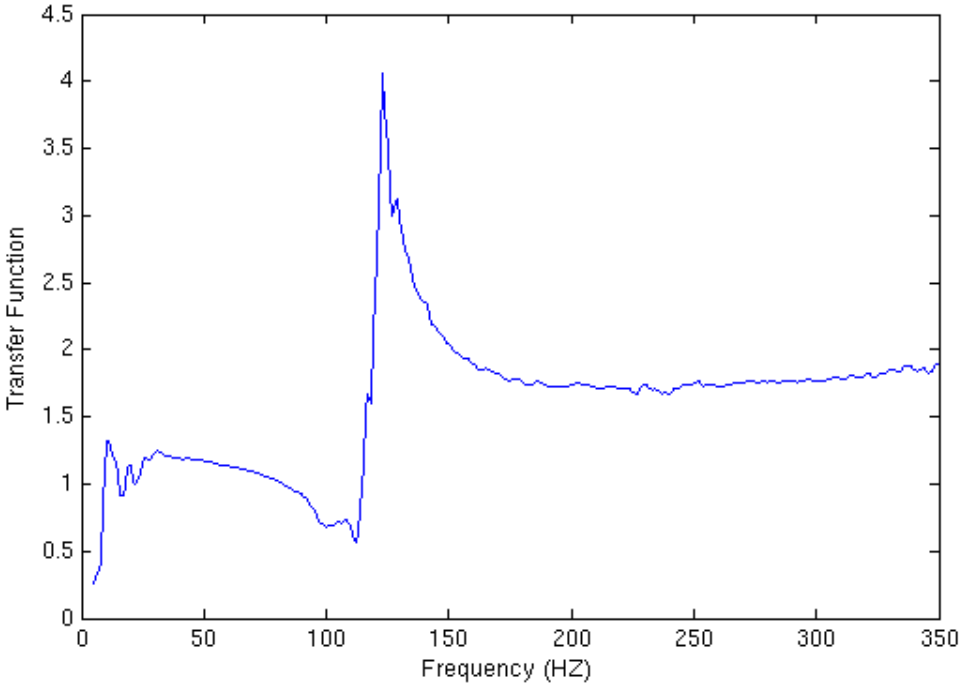

Figure 2-19: Transfer Function Plot with Input B- Output A (Sample with Wire lead 4cm in Length)

2.2.2.2 Experimental Results of Fretting Threshold Measurement

As shown in Figure 2-20, threshold amplitudes of axial vibration on electrical connectors are different at various frequencies. The threshold decreases tremendously from 100 HZ to 300HZ, where the amplitude is lowest. From 300 HZ to about 350 HZ, the threshold increases, and the second valley appears at about 450 HZ. Then threshold amplitude increases largely at frequencies higher than about 470 HZ. The two lowest threshold amplitudes appear around two natural frequencies as shown in Figure 2-18. As the frequency 'gets away' from the natural frequencies, the threshold amplitude increases largely. The threshold amplitude at the natural frequency of the mode measured by Input A- Output A (Mode A-A) is the lowest.

For this type of connector sample, the mode of relative rocking motion between blade and receptacle does not influence the threshold behavior obviously.

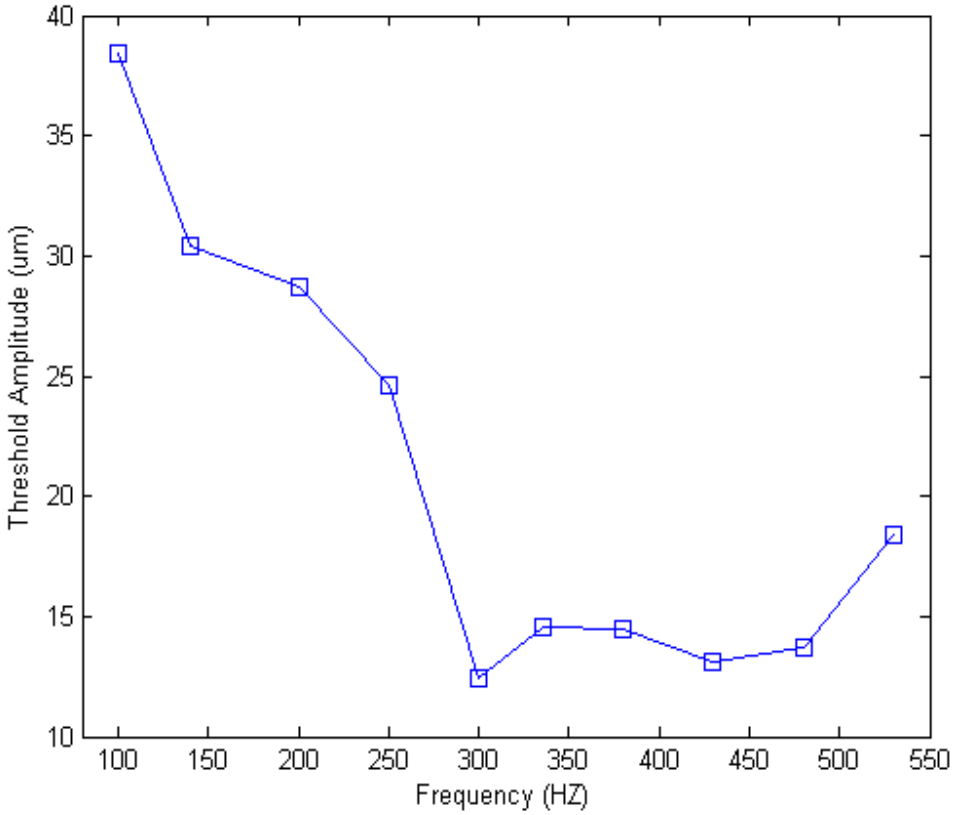

Figure 2-20: Averaged Thresholds at Various Frequencies (Sample with Wire Lead 4cm in Length)

2.2.3 Discussion

Based on the results of the transfer function test, three natural frequencies are found. The reason that the two modes (as shown in Figure 2-18) exist should be linked to the cross section shape of the strengthened cable. After the strengthening process by thermal shrink tubing and supplementary cables, the cross-section of the cable turns to be close to rectangular from circle. The structural change induces the

variation of the moments of inertia of the cable, stiffness and damping characteristics of the transverse vibration in two directions. By the influence of these factors, the natural frequency of the second mode is higher than that of the first mode.

As shown in Figure 2-20, the threshold amplitudes gets lower as the vibration frequency is closer to the natural frequencies as shown in Figure 2-18. At the natural frequency of Mode A-A, the threshold amplitude is lowest. In other words, the relative motion of the contact pair is easiest to occur at this frequency. In contrast, the relative rocking motion between blade and receptacle did not contribute major effect to the threshold behavior.

A large number of electrical connector samples are involved to obtain the average results in the transfer function and threshold tests. The natural frequencies and threshold amplitudes of the repeated trials fluctuate in a small range. The experimental results shown above are all averaged values.

2.3 A Study on Vibration Thresholds of Electrical Connectors with Various Wire Lengths

In last experiment, random noise and single frequency vibration tests were used to measure transfer functions and thresholds of fretting corrosion of electrical connectors with wire leads 4cm in lengths. By testing the vibration in two directions, the natural frequencies of three vibration modes of the connector systems were found. Compared to the thresholds at other frequencies, the threshold amplitude at Mode A-A is lowest.

With the increase of the lengths of wire leads of electrical connectors, the natural frequencies of the Mode A-A possibly change and threshold amplitudes at this natural frequencies are also possibly different. Thus, in this part, transfer functions and thresholds of electrical connectors with multiple lengths of wire leads are tested. The influence of wire lengths on vibration behaviors and threshold amplitudes of this type of electrical connector is studied.

2.3.1 Experimental Setup

In this experiment, transfer function measurement and threshold test are conducted by random noise and single frequency vibration. The vibration system and threshold measurement equipment used in last test are also applied for the tests in this experiment. The operation of these equipment is almost as the same as that of the last research.

2.3.1.1 Experimental Samples

Since the axial vibration induces plastic deformation on the wire leads, which causes the blade to get stuck in receptacle, it is necessary to strengthen wire leads connected with electrical connectors. By the same method mentioned in last experiment, the originally single wire lead connected with the receptacle is bundled with two more wire leads by thermal shrink tubing. The electrical connector samples involved in the test are with multiple lengths of wire leads. The lengths of supplementary wires and shrink tubing are equal to the lengths of the original cables. The processed samples with various lengths of wire leads are shown in Figure 2-21.

In the tests, lengths of wire leads connected with the receptacles are chosen from 2 cm to 18 cm.

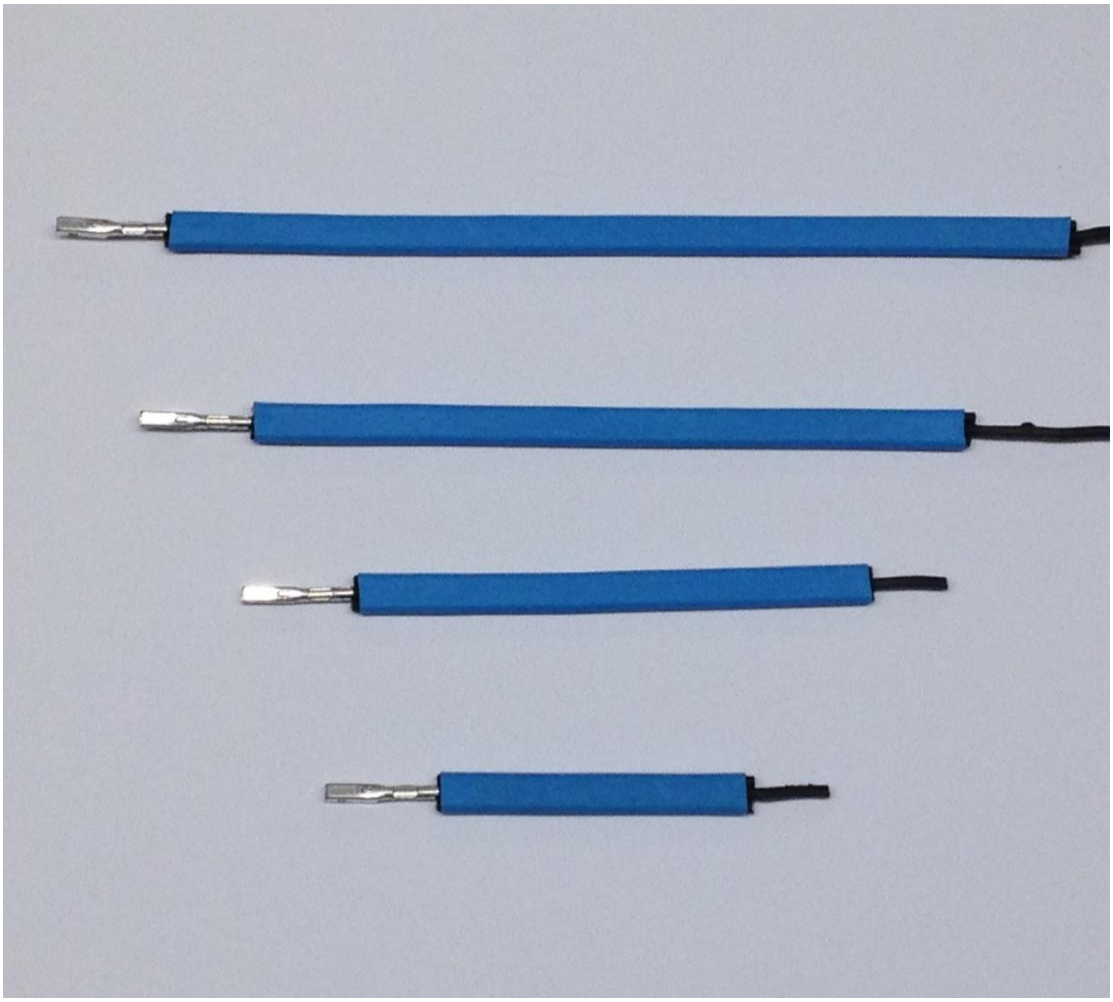

Figure 2-21: Connector Samples with Strengthened Wire Leads

Through the same process described in last experiment, an annulus and a washer are attached on the blade. The reflector, used for reflecting the laser ray back to laser head, is taped on the annulus. The weights and shapes of them are small enough to have nearly no influence on the vibration behavior of the blade.

2.3.1.2 Experimental Setup for Vibration and Threshold Tests

Aiming to obtain the better testing accuracy by the non-contact displacement

measurements, the reflectors, made by laser- sensitive material, are attached on the measured objects to reflect the laser rays. Based on the experimental results of last experiment, the threshold amplitudes of single frequency vibration at different frequencies are different. For this type of electrical connector systems with wire leads 4cm in length, threshold at the natural frequency of Mode A-A is lower than the threshold amplitudes at other frequencies. Thus natural frequencies of Mode A-A of connector systems with multiple lengths of wires are tested in this part.

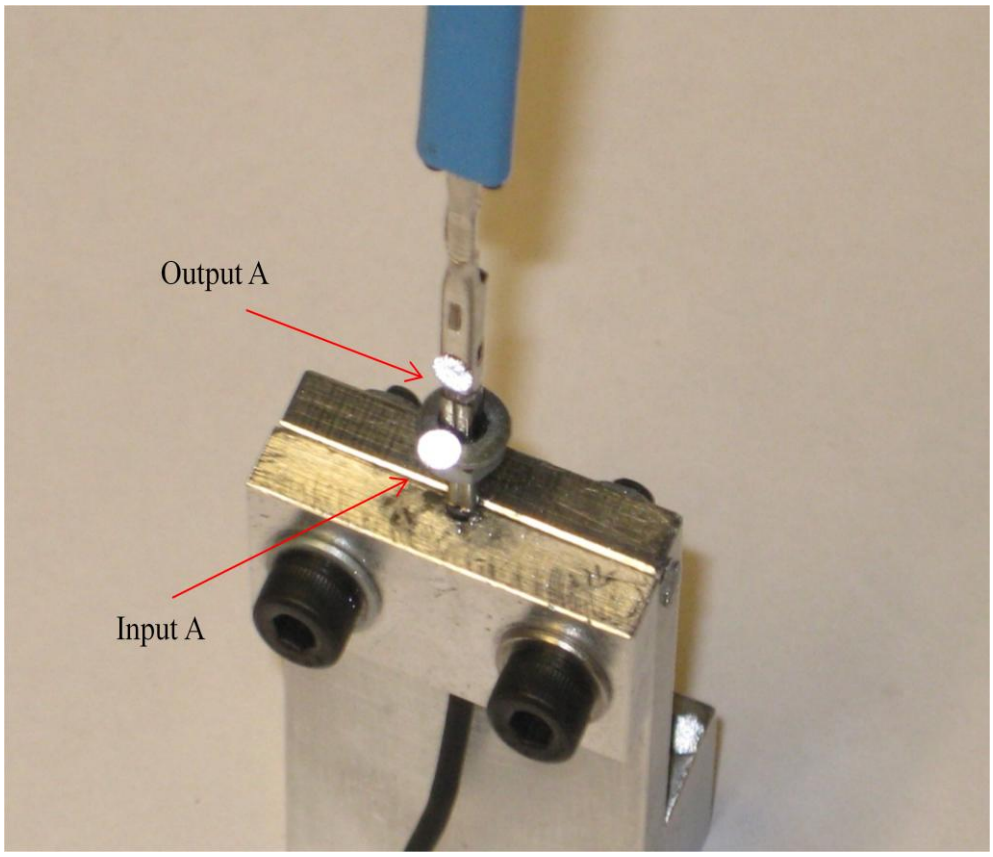

Figure 2-22: Reflector Positions on the Blade and Receptacle

As shown in Figure 2-22, the reflector measuring vibration input is taped on annulus that is attached on the blade. Because of the axial excitation of the shaker head, the input reflector measures the axial vibration of the blade (Input A). The output reflector A is taped on one side of receptacle to measure the transverse

response of the connector system. Based on experimental results of last experiment, the Mode A-A is tested in this transfer function test. For a comprehensive understanding of the vibration behavior, output reflector B (as shown in Figure 2-14) is attached to inspect the relative rocking motion of the connector pair. For the connector samples with different lengths of wire leads, the structures of connector pairs are the same. Blades are fixed on the fixture at the same position. The output reflectors are taped at the same positions of receptacles.

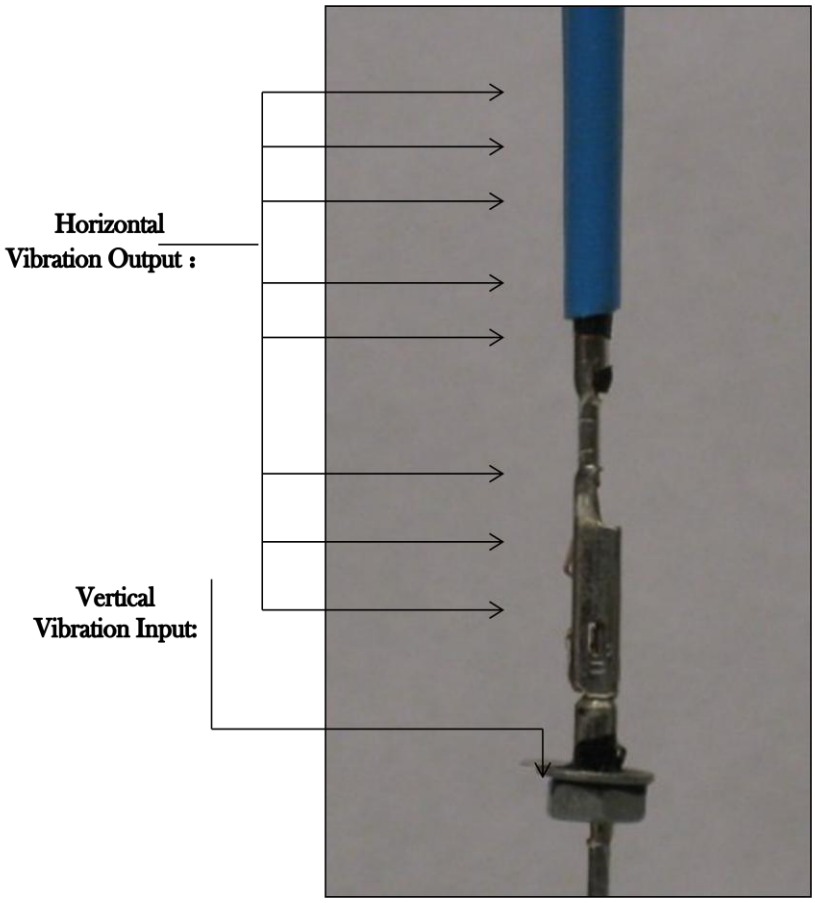

Figure 2-23: Measuring Positions of Laser Beams on the Wire Lead

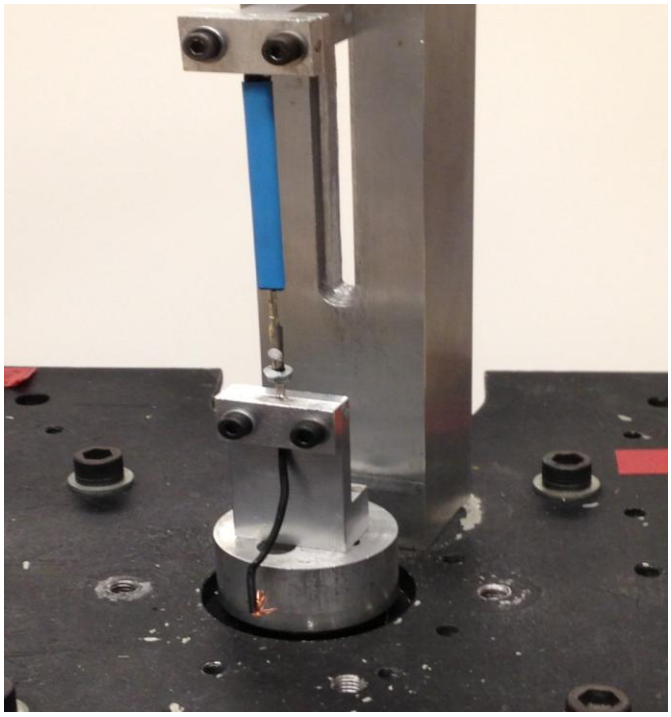

(a) Wire Length = 6cm

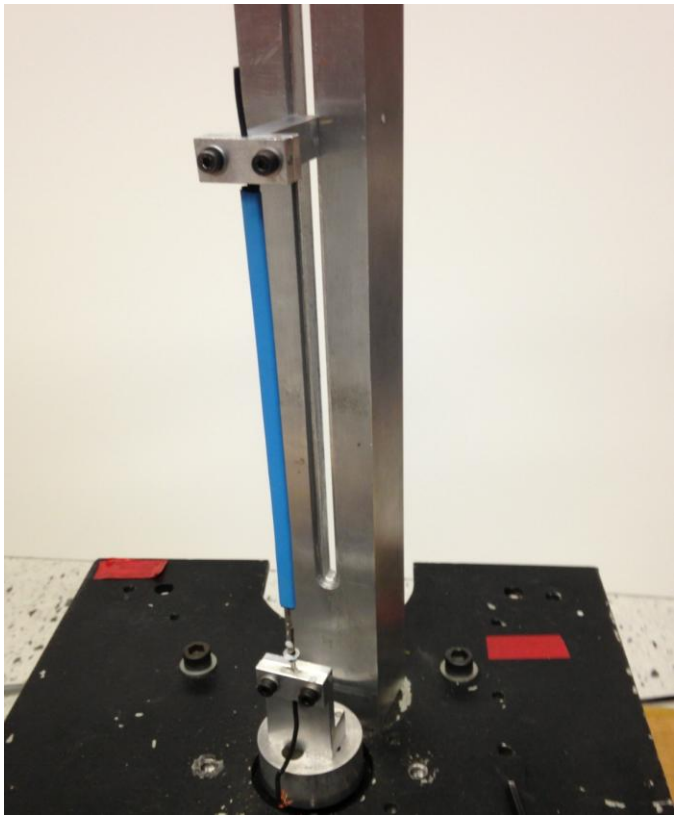

(b) Wire Length = 18cm

Figure 2-24: Fixture Setup for Connectors with Various Wire Lengths

In addition of the transfer function measurement, the detailed vibration

behavior of the connector system is studied by measurement of the transverse vibration of the whole sample body. As shown in Figure 2-23, reflectors are attached on receptacles and wire leads to measure the vibration posture of the Mode A-A.

The electrical connectors with wire lengths of 2cm, 3cm, 4 cm, 5 cm, 6 cm, 8 cm, 10 cm, 12 cm, 14 cm, 16 cm and 18 cm are tested. The fixture shown in Figure 2-13 is able to fix the connector samples with different wire lengths by the height changes of the movable fixture. The fixture setup for different samples is shown in Figure 2-24.

In the threshold test, the threshold amplitude at the natural frequency of the Mode A-A of the connector system is measured. The transfer function of each connector sample is not the same. Thus, the threshold test of the connector sample is conducted after the transfer function measurement of it. In the threshold test, the vibration amplitude increases until the electrical resistance rises continuously. The resistance increase under one certain vibration amplitude is observed for at least five minutes. Natural frequencies and threshold amplitudes are averaged after all testing trials.

2.3.2 Experimental Results

The transfer function measurement of connectors with various lengths of wire leads is conducted. Figure 25- 29 show transfer functions of the connector samples with wires 2cm, 3cm, 5cm, 6cm, 8cm in lengths. The transfer function of one electrical connector sample with 2 cm wire, which is close to the averaged result,

is shown in Figure 2-25. In Figure 2-25 (a), an obvious peak appears around 565 HZ. In Figure 2-24 (b), a typical 180 degrees phase shift is around 565 HZ, too.

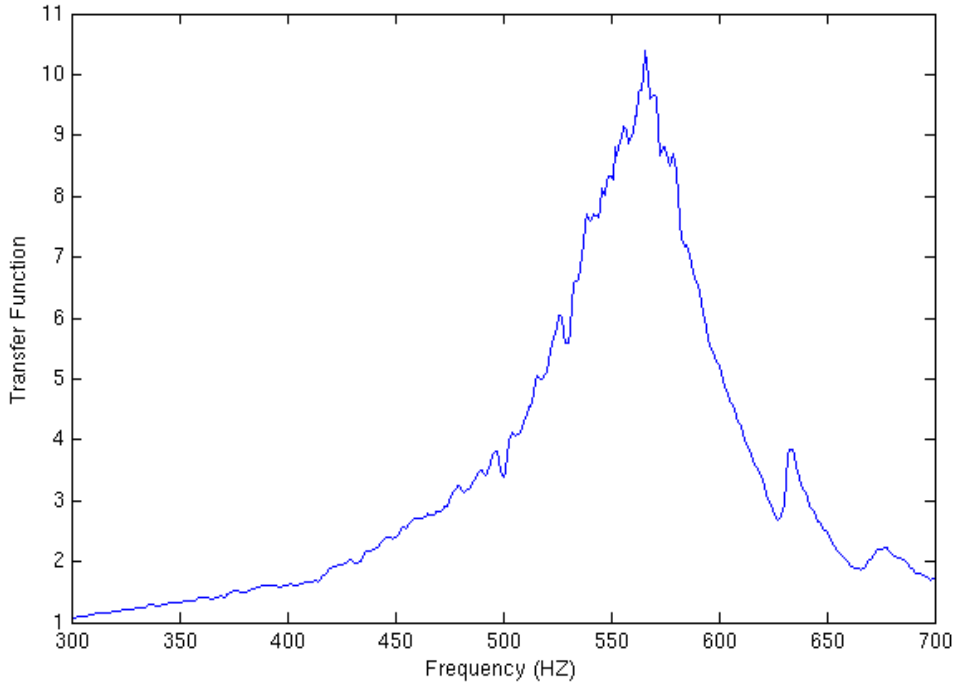

(a) Magnitude Plot

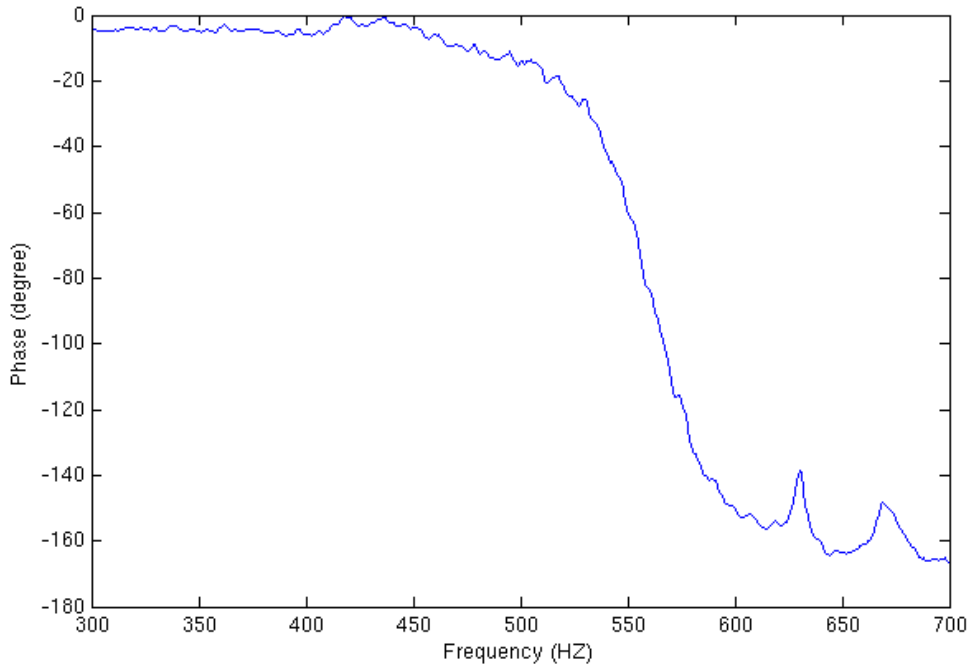

(b) Phase Plot

Figure 2-25: Transfer Function of Connector with Wire Lead 2cm in Length

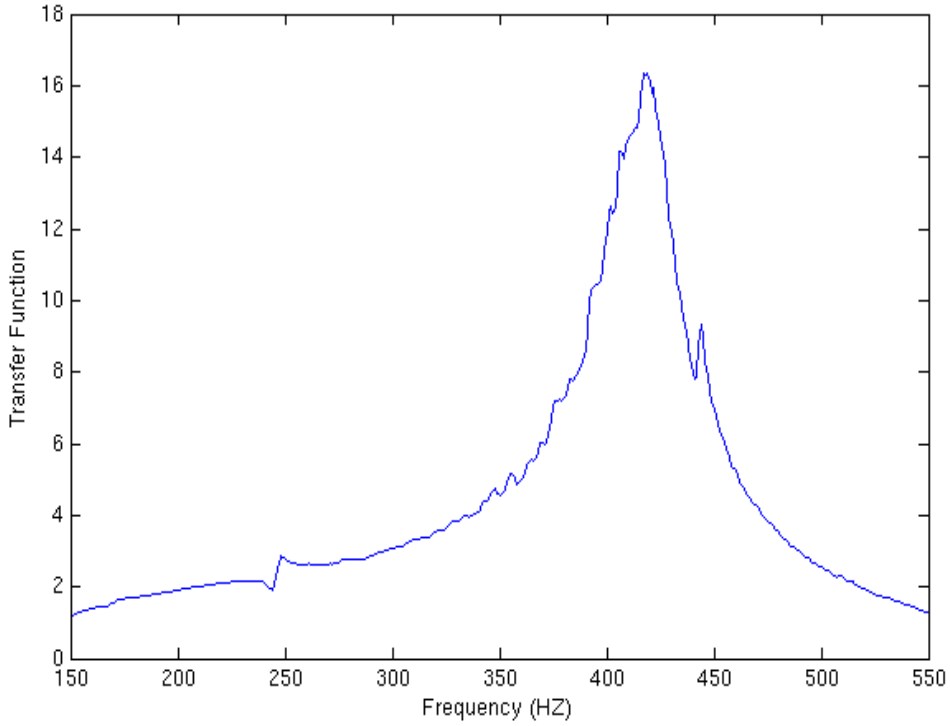

(a) Magnitude Plot

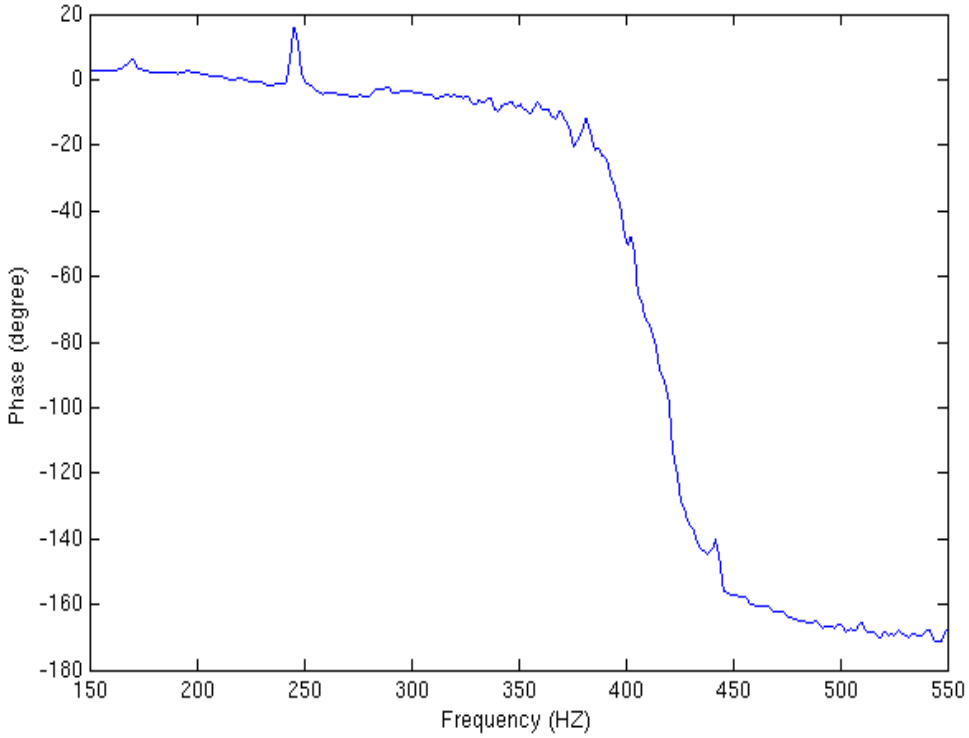

(b) Phase Plot

Figure 2-26: Transfer Function of Connector with Wire Lead 3cm in Length

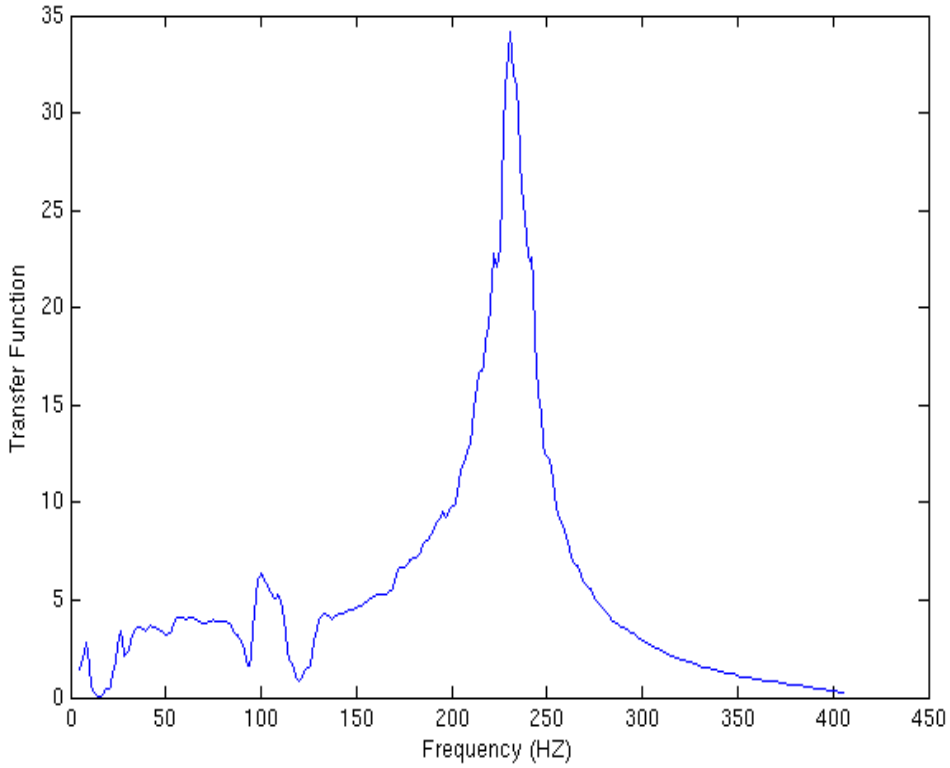

(a) Magnitude Plot

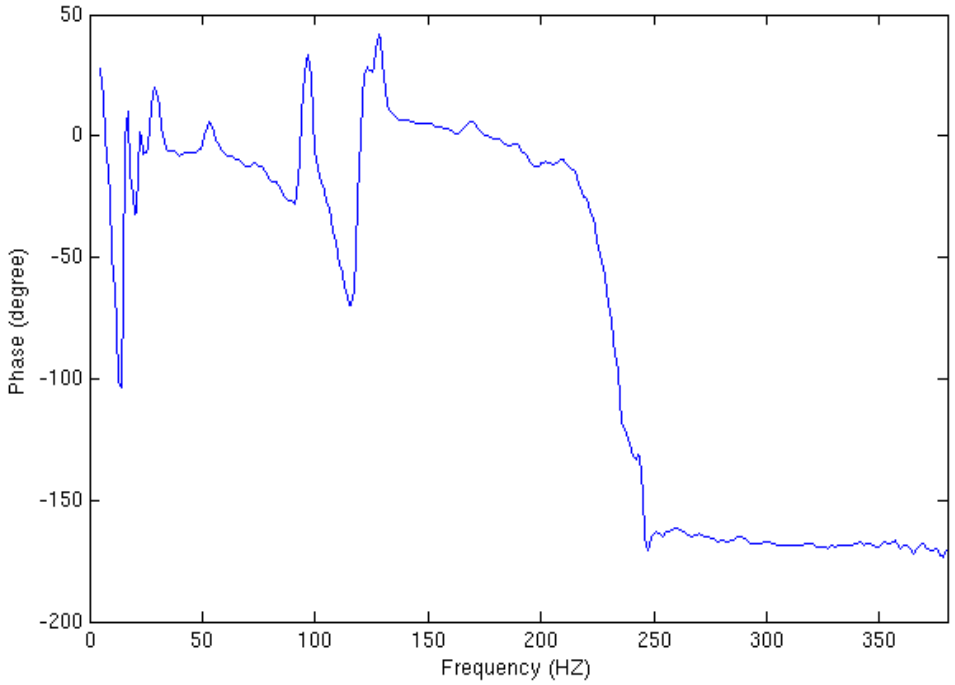

(b) Phase Plot

Figure 2-27: Transfer Function of Connector with Wire Lead 5cm in Length

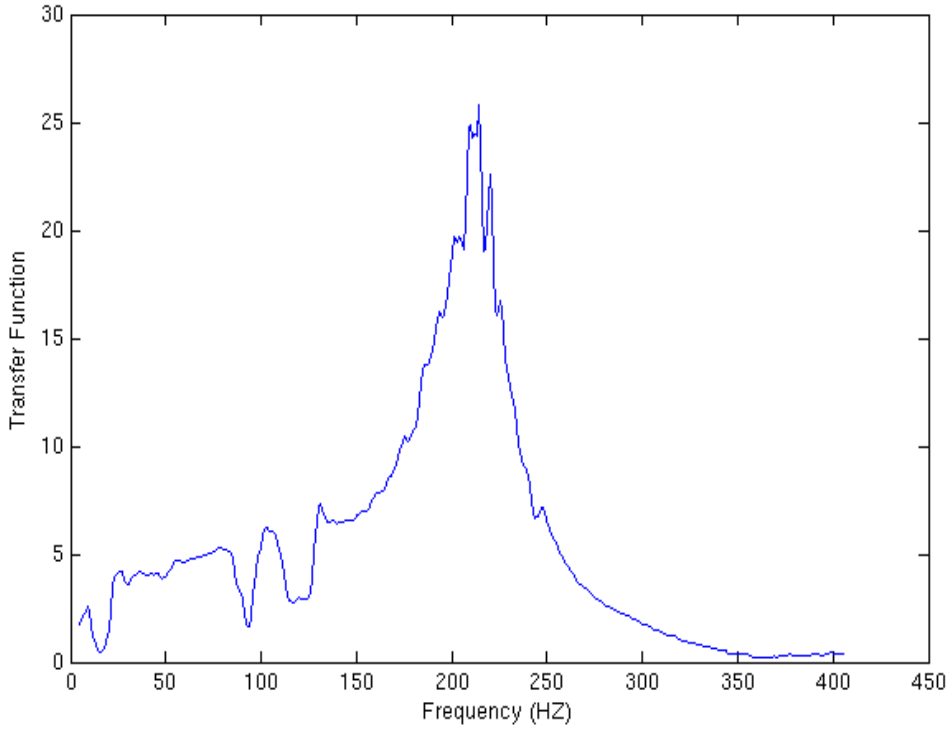

(a) Magnitude Plot

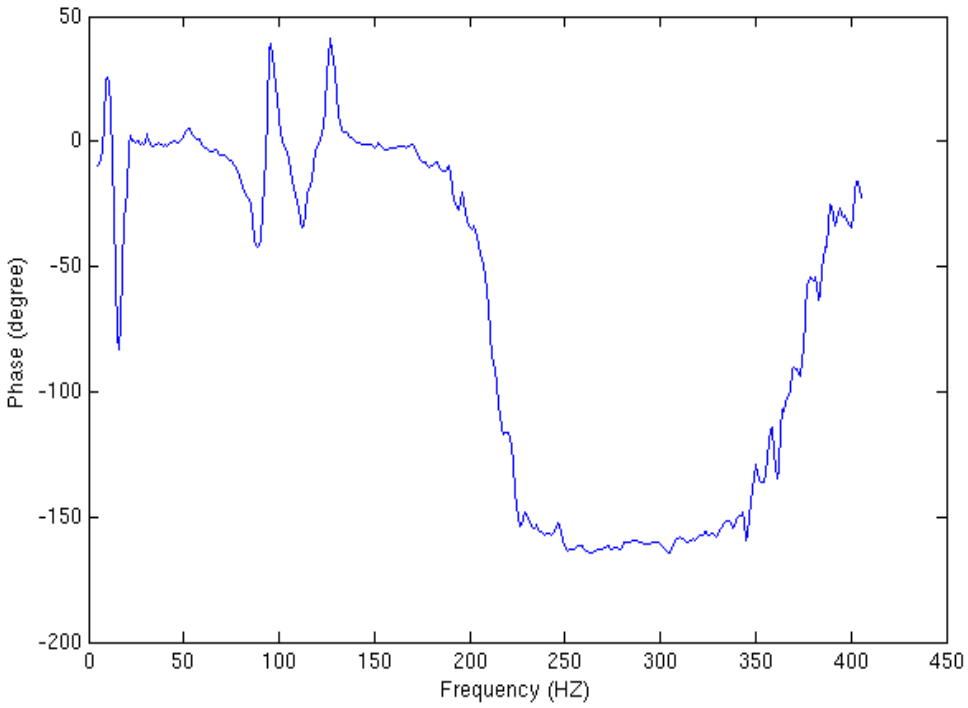

(b) Phase Plot

Figure 2-28: Transfer Function of Connector with Wire Lead 6cm in Length

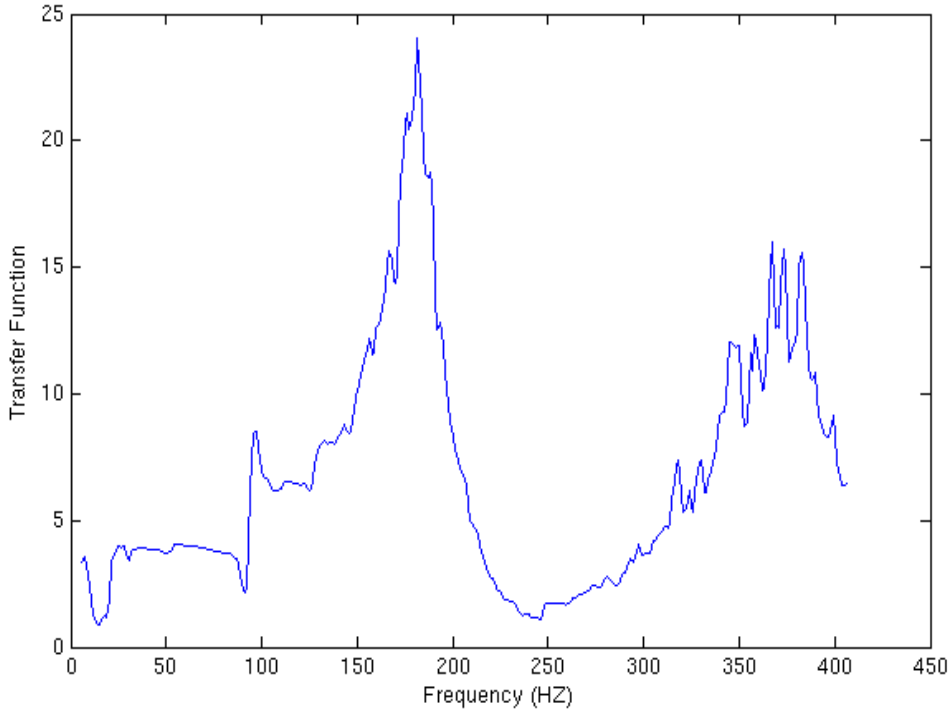

(a) Magnitude Plot

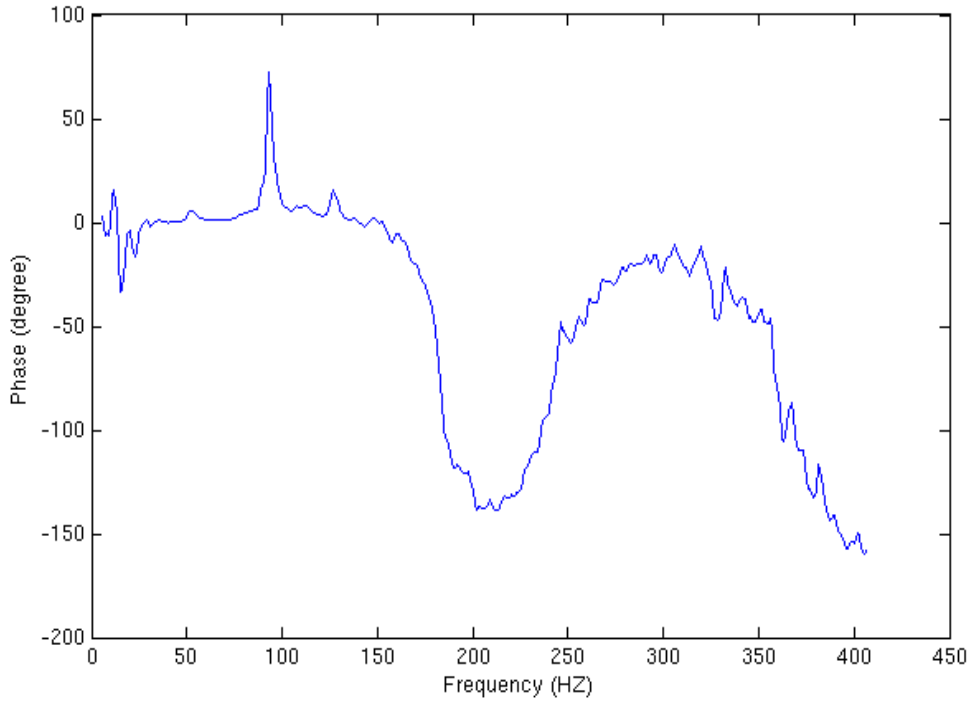

(b) Phase Plot

Figure 2-29: Transfer Function of Connector with Wire Lead 8cm in Length

The averaged natural frequencies tested of electrical connectors with multiple wire lengths are shown in Figure 2-30. With the longer wires, the natural frequencies of the connector systems decrease. For the connector sample with wire lead 18cm in length, the natural frequency is around 100 HZ. By Input B- Output A, natural frequencies of relative rocking motion between blade and receptacle of connectors with various wire lengths are measured. It is found that the natural frequency of this mode is not affected by the tie- off lengths, which is constantly around 120HZ, as shown in Figure 2-19.

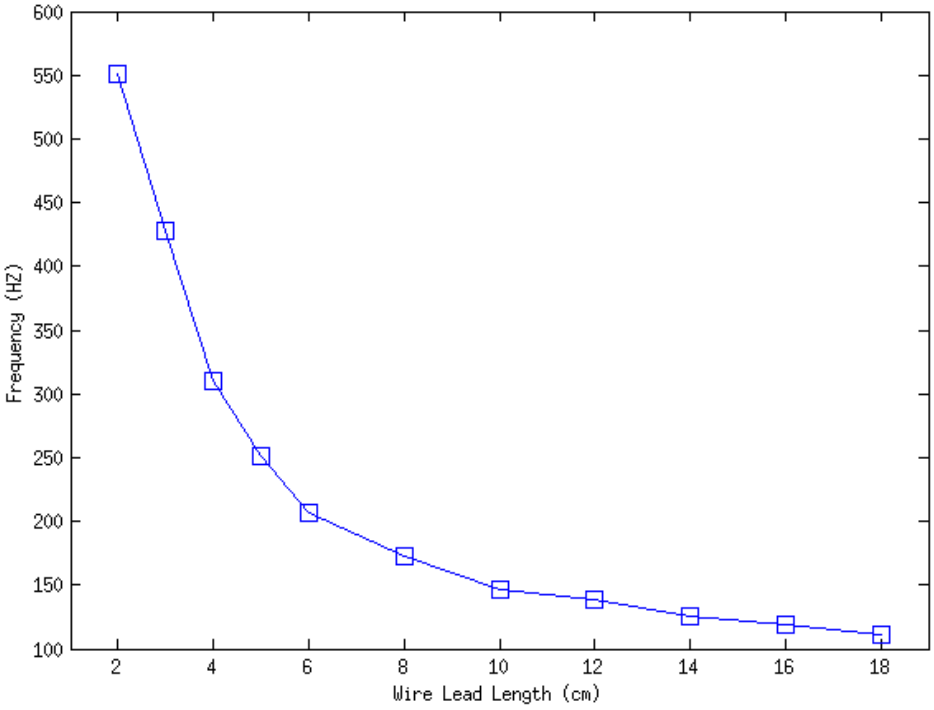

Figure 2-30: Natural Frequencies of Connectors with Various Wire Lengths (Mode A- A)

The transfer functions with outputs at various positions on the blades and receptacles are illustrated in Figure 2-31 (wire length = 2cm). The output positions

are at the height of 1mm, 3mm, 11mm and 14 mm above the root of blade, the part clamped by the fixture on shaker head. For a single sample, the natural frequencies at different output positions are almost the same, except for the ones at the root of the blade, which is close to the fixture on shaker head. In addition, it's indicated that the change of magnitude is close to a linear increase with the heightened position of output on connector. However this phenomenon only exist for the connector with wire length shorter than 10 cm, because the relative rocking motion is activated while the natural frequency of Mode A-A moves closer to 120HZ.

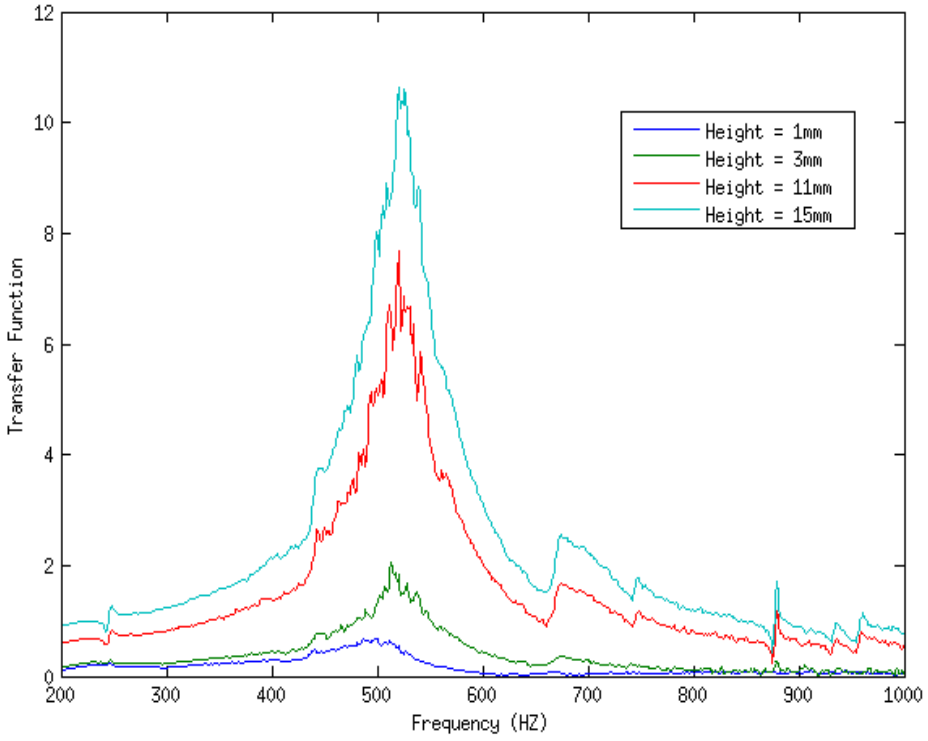

Figure 2-31: Transfer Functions with Outputs on Blade and Receptacle at Different Heights (Wire Length = 2cm)

Based on the vibration information above, the estimation of the vibration posture of blade and receptacle at Mode A- A is showed in Figure 3-32. Only the

root of the blade bends during vibrating. For connectors with short wires, relative rocking motion between receptacle and blade can be ignored according to the linearly increasing vibration magnitude which is illustrated in Figure 2-31. Only the tangentially translational relative motion between connector pair is considered. For connectors with long wires, translational and rocking motions at the contacting interface are both possibly activated by the single frequency vibration at Mode A- A. The vibration information above and this estimation provide significant foundation of the mathematical model simulating the vibration and fretting behavior of the connector system.

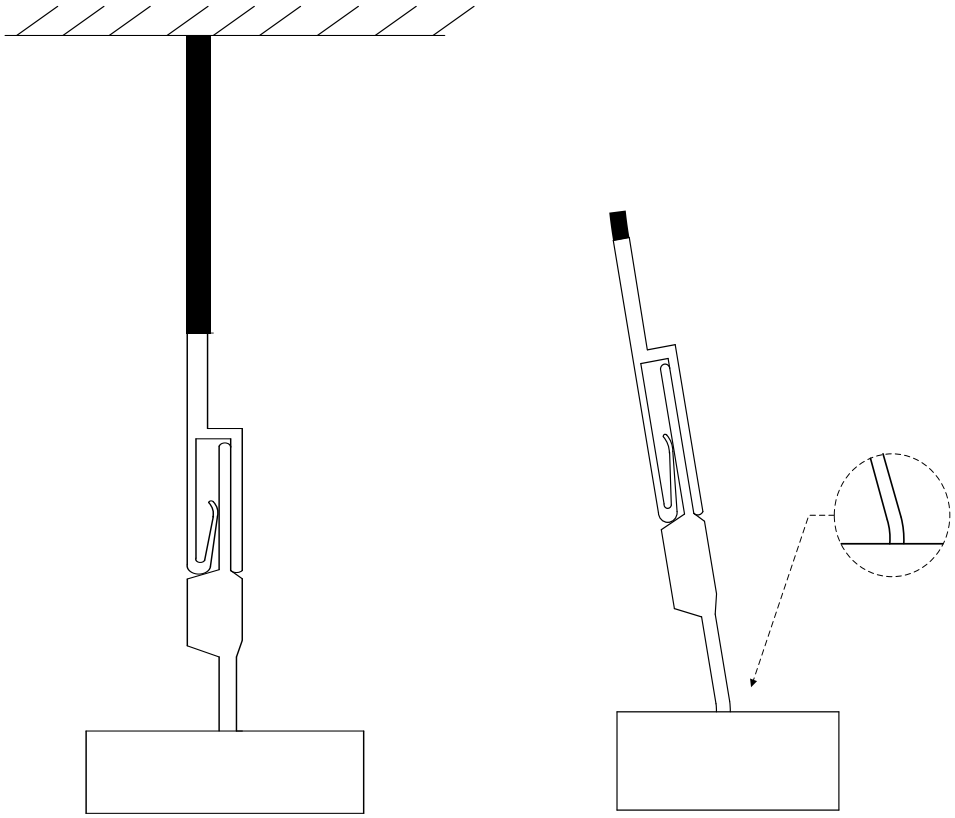

(a) Initial Posture without Deformation (b) Deformation of Blade

Figure 2-32: Estimation of Vibration of Connector Pair for Connectors with Short Wires

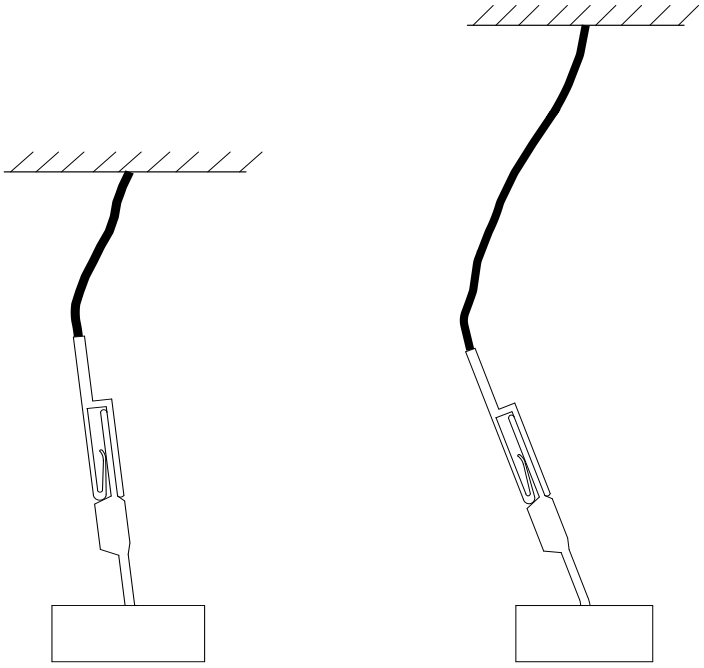

(a) Wire Length = 2cm (b) Wire Length = 4cm

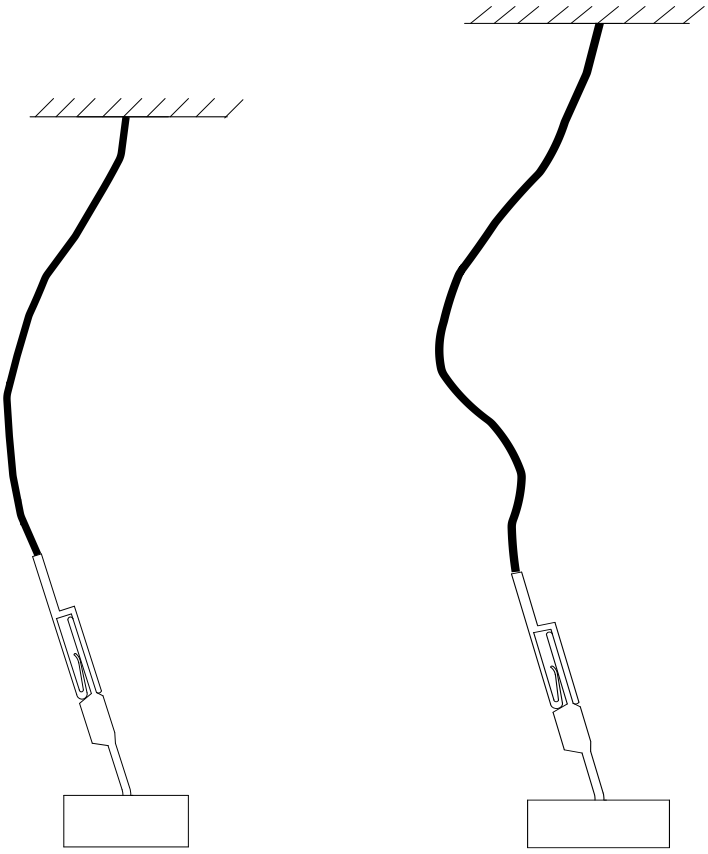

(c) Wire Length = 6cm (d) Wire Length = 8cm

Figure 2-33: Vibration Postures of Connectors with Various Wire Lengths

Figure 2-33 demonstrates the transverse vibration postures of the connector systems including connector pairs and wire leads, at the natural frequencies of Mode A- A. The top and end of the connector systems are fixed at fixtures, which do not allow any transverse vibration amplitudes. The vibration patterns of the wire leads convert continuously as the wire length increases, which becomes obvious while the length is 8cm.

The experimental results: thresholds with the error bands of electrical connector samples with different lengths of wires are shown in Figure 2-34. As shown in the figure, the threshold amplitude of sample with 4 cm wire is lowest. As the lengths of wire leads increase from 4 to 18cm, threshold increases monotonously. The results are also illustrated in Table 2-2.

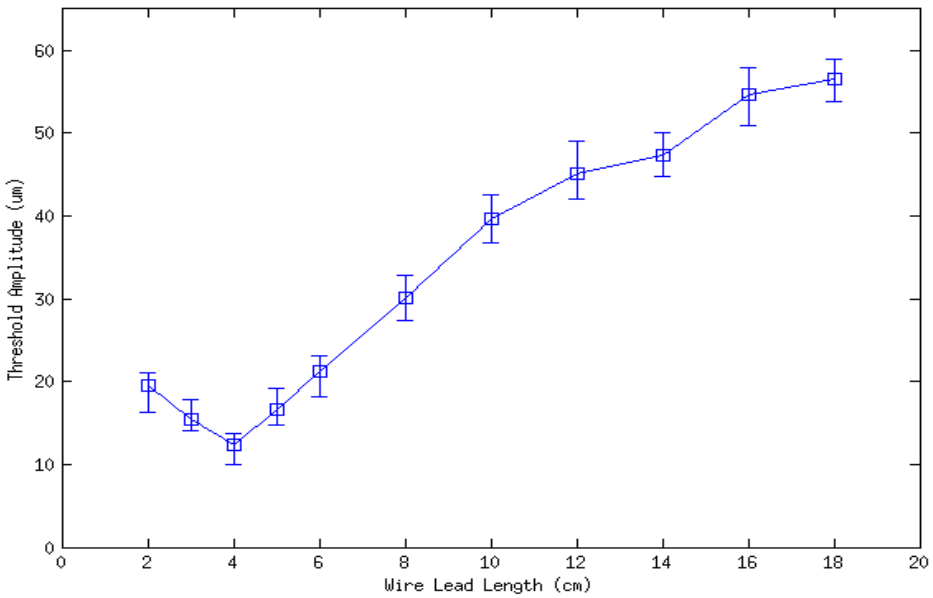

Figure 2-34: Vibration Threshold Amplitudes of Electrical Connectors with Various Wire Lengths

Table 2-2: Experimental Threshold Amplitudes of Electrical Connectors with Various Wire Lengths

Wire length(cm)	**2**	**3**	**4**	**5**	**6**	**8**	**10**	**12**	**14**	**16**	**18**
Averaged Threshold (μm)	19.5	15.5	12.4	16.7	21.3	30.1	39.7	45.2	47.3	54.6	56.5
Largest Threshold (μm)	21.1	17.9	13.8	19.2	23.2	32.9	44.0	48.4	51.1	59.2	58.0
Smallest Threshold (μm)	16.3	14.4	9.0	13.4	18.2	27.4	35.4	42.0	44.5	50.2	54.8

2.3.3 Discussion

In this experiment, the transfer function and threshold tests are conducted by the vibration system and electrical resistance measurement equipment used for last tests. Natural frequencies of Mode A- A and relative rocking motion of connector pairs for sample with various wire lengths are conducted. The threshold tests are conducted at natural frequencies of Mode A- A. The vibration amplitude of the fixture holding the blade that triggers the fretting corrosion is the threshold. For the convenience of threshold tests, wires with connectors are strengthened by supplementary wires and thermal shrink tubing. For samples with different lengths of wire leads, the blade and receptacle parts have no differences. The laser reflectors are located at the same positions on connectors with different cable lengths.

As shown in Figure 2-30, the averaged natural frequency of the Mode A-A of the electrical connector decreases with the increase of the length of cable. This decreasing trend can be attributed to the declined stiffness and larger mass of the connector system with the lengthened wires based on the equation for calculating natural frequency

$$\omega_n = \sqrt{\frac{k}{m}}$$

where ω_n, k and m are respectively natural frequency, stiffness and mass of a vibration system,. In addition, it is found that the natural frequency of relative rocking-style motion of connector pair is not influenced by different tie- off lengths, which is constantly around 120HZ for different samples.

As shown in Figure 2-33, threshold amplitude varies as a function of the wire lengths. This non-monotonic trend of threshold amplitude behavior can be explained by the vibration postures for connectors with various wires, as shown in Figure 2-32. As the vibration mode evolves with the increased wire length, fretting corrosion may occur with lower excitation amplitude. The decreased stiffness of the system with the lengthened wire results in a larger vibration amplitude necessary to induce the relative motion at the interfaces of connectors. While wire lengths are 2- 4cm, the influence of mode conversion is major to lead to a decreasing trend of threshold. For longer wires, the declined stiffness affect the threshold greatly to increase the threshold as the wire length is increased. It is estimated that for connectors with wires shorter than 8cm in lengths, of which fretting corrosion is caused by translational relative motion between blade and receptacle. In the conditions that wire is longer than 8cm, relatively translational and relative rocking motion at the contacting interface both contribute to the degradation.

CHAPTER 3 MATHEMATICAL MODELING AND ANALYSIS OF A BLADE/RECEPTACLE CONNECTOR PAIR OF THE PREDICTION OF AXIAL VIBRATION- INDUCED FRETTING CORROSION

In this chapter, a mathematical model is developed to predict the threshold behavior of certain type of electrical connectors. Based on the experimental study of the vibration behavior, this model simplifies the dimensions and vibration modes of the connector pair to focus on the threshold behavior of the fretting corrosion caused by Mode A- A. Some supplementary experiments are conducted to provide necessary parameters for the modeling.

3.1 Model Development

A spring-mass-damper model is developed to explain and predict the threshold behavior of the connector system. In previous work, the relative rocking motion at contacting interface and fretting behavior caused by it was simulated by FEA modeling method. In current study, modeling objective is fretting degradation caused by translational relative motion at the interface of connector pairs with short wires. The schematic for the model is shown in Figure 3-1.

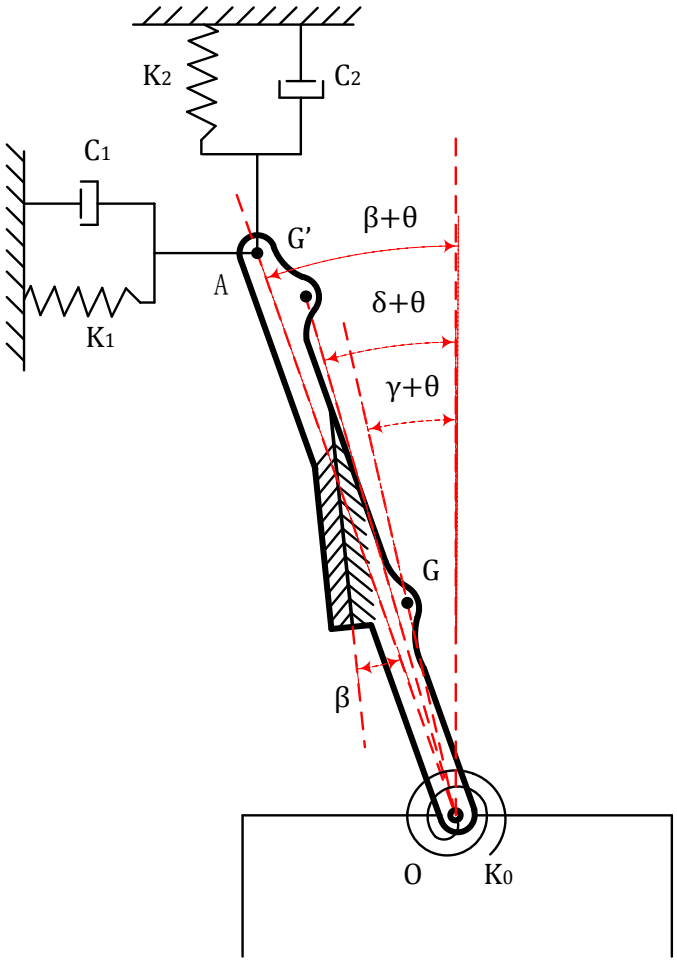

Figure 3-1: Schematic of Model

The connector pair is simplified into two rigid parts including bar OG and bar AG'. Each of them has a friction pad. The two bars are connected by this pair of frictional pads modeling the contacting interface between blade and receptacle where relatively rocking motion is not allowed. As the same as the experimental setup, Bar OG is fixed on the shaker head at point O, and bar AG' is connected with the wire at point A. Point G and G' are respectively the centers of masses of the connector pair and receptacle. According to the experimental results, the blade bends at the root of it during vibrating at natural frequency of Mode A- A. Thus while there is no relative slip at the contacting interface, bars AG' and OG rotate about Joint O without

deformation. For the design of sample connectors, the blade and wire of the sample connector are axially eccentric as shown in Figure 2-31a. While connector is vertically fixed as the initial posture, bars AG' and OG are positioned obliquely with an angle β between AO and vertical axis; the angle between GO and vertical axis is γ; the angle between G'O and vertical axis is δ; the frictional pad interface is vertical. The angle of vibration is θ. The angle between AO and interface of frictional pad is constantly β. Spring k_0 is located at point O to model the moment produced by the deformation of blade root under vibration. The stiffness of k_0 is tested by experiments. The wire is simplified to two springs k_1, k_2 and two dampers c_1, c_2 which represent the effect of vertical and transverse deformation of the wire. The mass of wire is ignored in this model, of which effect is converted into that of springs and dampers.

There are two steps for running this model, including transfer function fitting and threshold calculation. In the first step, springs k_1, k_2 and dampers c_1, c_2, parameters that are difficult to measure experimentally, are determined by fitting transfer functions of the modeling mechanical system with those tested experimentally. In transfer function test with small vibration amplitudes, transients of friction forces at contacting interface are constantly lower than static friction force. Without any relative motion between blade and receptacle, AO is considered to vibrate as a rigid bar. In the second step, the friction force at the contacting interface is considered as the indicator of the occurrence of fretting corrosion. Relative motion occurs at the contacting interface and leads to fretting corrosion only if the friction

force rises over the nominal value of the static friction force with the increase of vibration amplitude. The determined parameters and transient dynamic data obtained from step one are plugged into the equation for calculating transient of the friction force during vibration. The vibration input amplitude that caused the friction force to be equal to the nominal static friction force is recognized as the threshold.

As shown in Figure 3-2, three Cartesian coordinates, including x-y-z, n-t and x'-y' coordinates, are set for the ease of calculation. The n axis is along with vector $\overline{G'O}$; y' axis is parallel to the interface of frictional pad. The x-y-z coordinate is fixed with the origin at the initial position of point O before vibration.

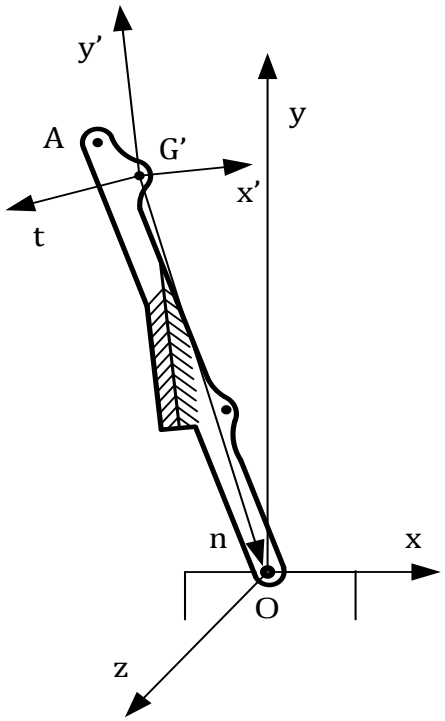

Figure 3-2: Coordinates Used for Calculation

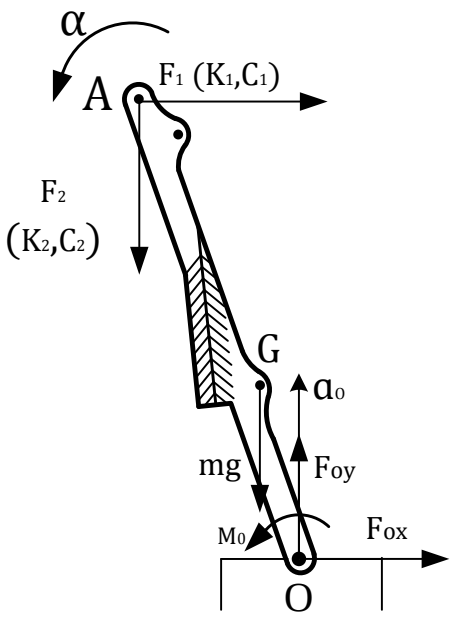

Figure 3-3: Free Body Diagram for Transfer Function Fitting

Free body diagram about 'bar' AO for transfer function fitting is shown in Figure 3-3. F_{ox} , F_{oy} are x and y axes components of the force that the shaker head acts on 'bar' AO at point O; M_0 is the moment produced by k_0; F_1 and F_2 are forces produced respectively by spring k_1, damper c_1, and spring k_2, damper c_2; α is angular acceleration of AO about point O; a_o is acceleration of point O. The resultant moment of 'bar' AO about point O is

$$\sum \bar{M}_O = I_O\bar{\alpha} + \overline{OG} \times m\bar{a}_O = \overline{M_0} + \overline{OA} \times (\overline{F_1} + \overline{F_2}) + \overline{OG} \times m\bar{g}$$

where I_O is moment of inertia of 'bar' AO about point O, m is mass of 'bar' AO. In the initial condition without vibration, a tension in cable in vertical direction keeps the connector system straight. In non-vibration condition, the above equation is simplified:

$$\overline{OA} \times \overline{F_2} + \overline{OG} \times m\bar{g} = 0$$

Matching like components in the preceding conditions leads to

$$\bar{\alpha} = \bar{\ddot{\theta}}, \quad \overline{M_0} = -k_0\bar{\theta},$$

from which we find that

$$\begin{aligned} I_O\ddot{\theta}\hat{k} + m\left[x_G\hat{\imath} + (y_G - y_O)\hat{\jmath}\right] \times a_O\hat{\jmath} \\ = -k_O\theta\hat{k} + \left[x_A\hat{\imath} + (y_A - y_O)\hat{\jmath}\right] \\ \times \left[-(x_A - X_A)k_1\hat{\imath} - \dot{x}_A c_1\hat{\imath} + \frac{mgX_G}{X_A}\hat{\jmath} - (y_A - Y_A)k_2\hat{\jmath}\right. \\ \left. - \dot{y}_A c_2\hat{\jmath}\right] + \left[x_G\hat{\imath} + (y_G - y_O)\hat{\jmath}\right] \times (-mg)\hat{\jmath} \end{aligned}$$

where x_G, y_G are the position of point G; x_A, y_A are the position of point A; y_O is the position of point O on y axis; X_A, Y_A are initial position of point A before vibration. The equation of motion for transfer function fitting is

$$\ddot{\theta} = \frac{1}{I_O}[-k_0\theta + (x_A - X_A)(y_A - y_O)k_1 + \dot{x}_A c_1(y_A - y_O) + \frac{mgX_G x_A}{X_A} - (y_A - Y_A)x_A k_2 - \dot{y}_A x_A c_2 - mgx_G - mx_G a_O]$$

The position, velocity, and acceleration items in above equations are

$$a_O = -A\omega^2 sin\omega t$$

$$x_G = -L_G sin\,(\gamma + \beta)\ ; \quad \dot{x}_G = -L_G\dot{\theta}\,cos(\gamma + \beta)$$

$$x_A = -Lsin(\beta + \theta)\ ; \quad \dot{x}_A = -L\dot{\theta}cos(\beta + \theta)$$

$$\ddot{x}_A = L\dot{\theta}^2 sin(\beta + \theta) - L\ddot{\theta}cos\,(\beta + \theta)$$

$$y_A = y_O + Lcos(\beta + \theta) = \mathrm{A}\,sin\,\omega t + Lcos(\beta + \theta)$$

$$\dot{y}_A = \dot{y}_O - L\dot{\theta}\,sin(\beta + \theta) = A\omega\,cos\,\omega t - L\dot{\theta}sin\,(\beta + \theta)$$

$$\ddot{y}_A = \ddot{y}_O - L\dot{\theta}^2\,cos(\beta + \theta) - L\ddot{\theta}sin\,(\beta + \theta)$$

$$\mathrm{X_A} = -Lsin\beta \;\; ; \quad Y_A = Lcos\beta$$

where A is input vibration amplitude; ω is angular velocity of single frequency vibration; L is length of OA; L_G is length of OG. For this model, θ is assumed a small angle. By assuming sinθ and cosθ to be

$$sin\theta = \theta \text{ and } cos\theta = 1$$

in equations expressing the position, velocity, and acceleration items, these equations are linearized:

$$x_G = -L_G(sin\gamma + \theta cos\gamma)$$

$$\dot{x}_G = -L_G\dot{\theta}(cos\,\gamma - \theta sin\gamma)$$

$$x_A = -L(sin\beta + \theta cos\beta)$$

$$\dot{x}_A = -L\dot{\theta}(cos\beta - \theta sin\beta)$$

$$\ddot{x}_A = L\dot{\theta}^2(sin\beta + \theta cos\beta) - L\ddot{\theta}(co\,s\,\beta - \theta sin\beta)$$

$$y_A = \mathrm{A}\,sin\,\omega t + L(cos\beta - \theta sin\beta)$$

$$\dot{y}_A = A\omega\,cos\,\omega t - L\dot{\theta}(sin\beta + \theta cos\beta)$$

$$\ddot{y}_A = \ddot{y}_O - L\dot{\theta}^2(\mathrm{cos}\beta - \theta sin\beta) - L\ddot{\theta}(sin\beta + \theta cos\beta)$$

For each calculation trial, the equations are run by a sine vibration input with single frequency. The frequency response of mechanical system is modeled by inputs over a frequency range of interest.

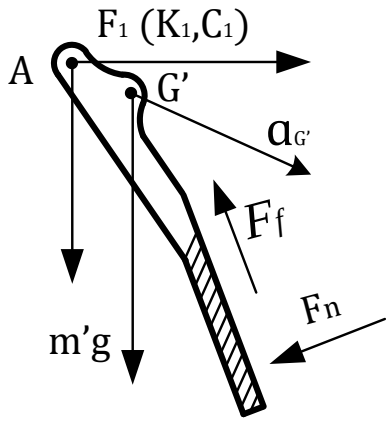

Figure 3-4: Free Body Diagram for Threshold Calculation

Figure 3-4 shows free body diagram of bar AG' for threshold calculation. F_f is the friction force tangent to the contacting interface; F_n is a force normal to the interface acted from bar OG, m' is mass of bar AG'. The resultant force on bar AG' is

$$\sum \bar{F} = m'\bar{a}_{G'} = m'\bar{g} + \bar{F}_f + \bar{F}_1 + \bar{F}_2 + \bar{F}_n$$

Matching like components in the preceding conditions leads to

$$\bar{a}_{G'} = \bar{a}_O + (\bar{a}_{G'/O})_n + (\bar{a}_{G'/O})_t$$

where

$$(\bar{a}_{G'/O})_n = \bar{\dot{\theta}} \times (\bar{\dot{\theta}} \times \overline{OG}) \ , \quad (\bar{a}_{G'/O})_t = \bar{\ddot{\theta}} \times \overline{OG}$$

from which we find that

$$m'\left[a_O - \dot{\theta}(y_{G'} - y_O) + \ddot{\theta}x_{G'}\right]\hat{j} + m'\left[-\dot{\theta}^2 x_{G'} - \ddot{\theta}(y_{G'} - y_O)\right]\hat{i}$$
$$= -m'g\hat{i} + [-(x_A - X_A)k_1 - \dot{x}_A c_1]\hat{i}$$
$$+ \left[\frac{mgX_G}{X_A} - (y_A - Y_A)k_2 - \dot{y}_A c_2\right]\hat{j} + F_f\hat{j}' - F_n\hat{i}'$$

For cancelling out the unknown item F_n, the equation multiplies $\hat{j}'$. Then we find the equation for threshold calculation as shown below.

$$F_f = [-(x_A - X_A)k_1 - \dot{x}_A c_1]sin\theta$$
$$- \left[-m'g - (y_A - Y_A)k_2 - \dot{y}_A c_2 + \frac{mgX_G}{X_A}\right]cos\theta$$
$$+ m'\left\{\left[a_O - \dot{\theta}(y_{G'} - y_O) + \ddot{\theta}x_{G'}\right]cos\theta\right.$$
$$\left. - \left[\left[-\dot{\theta}^2 x_{G'} - \ddot{\theta}(y_{G'} - y_O)\right]sin\theta\right]\right\}$$

For the configuration of the sample connectors, the dimensional parameters are $I_O = 264 \times 10^{-9}\,m^2kg$, $m = 1.10g$, $m' = 0.45g$, $\beta = 0.0283rad$, $\gamma = 0.0205rad$, $\delta = 0.0208rad$, $L = 36.84mm$, $L_G = 15.77mm$, $L_{G'} = 24.11mm$. Based on the free body diagrams and equations of motion, the nominal static friction force at the contacting interface between blade and receptacle is an essential parameter. The experimental measurement of it is described in the latter part.

3.2 Measurement of Nominal Static Friction Force

An MT-200 tension/torsion test system from Wisdom Technology, Inc., shown in Figure 3-5, is applied for sample testing in this research. The system provides an axial displacement resolution of 0.1 microns and a rotation resolution of 0.001°. Tests can be performed in tension, shear, torsion, bending, and combinations of these loadings on small specimens such as thin films, solder joints, gold wire, fibers, etc. Cyclic (fatigue) testing can also be performed at frequencies of up to 5 Hz. In addition, a universal 6-axis load cell was utilized to simultaneously monitor three forces and three moments/torques during sample mounting and testing. In this study, the tensile testing function is applied to measure the nominal static friction force between the contact pair of electrical connector.

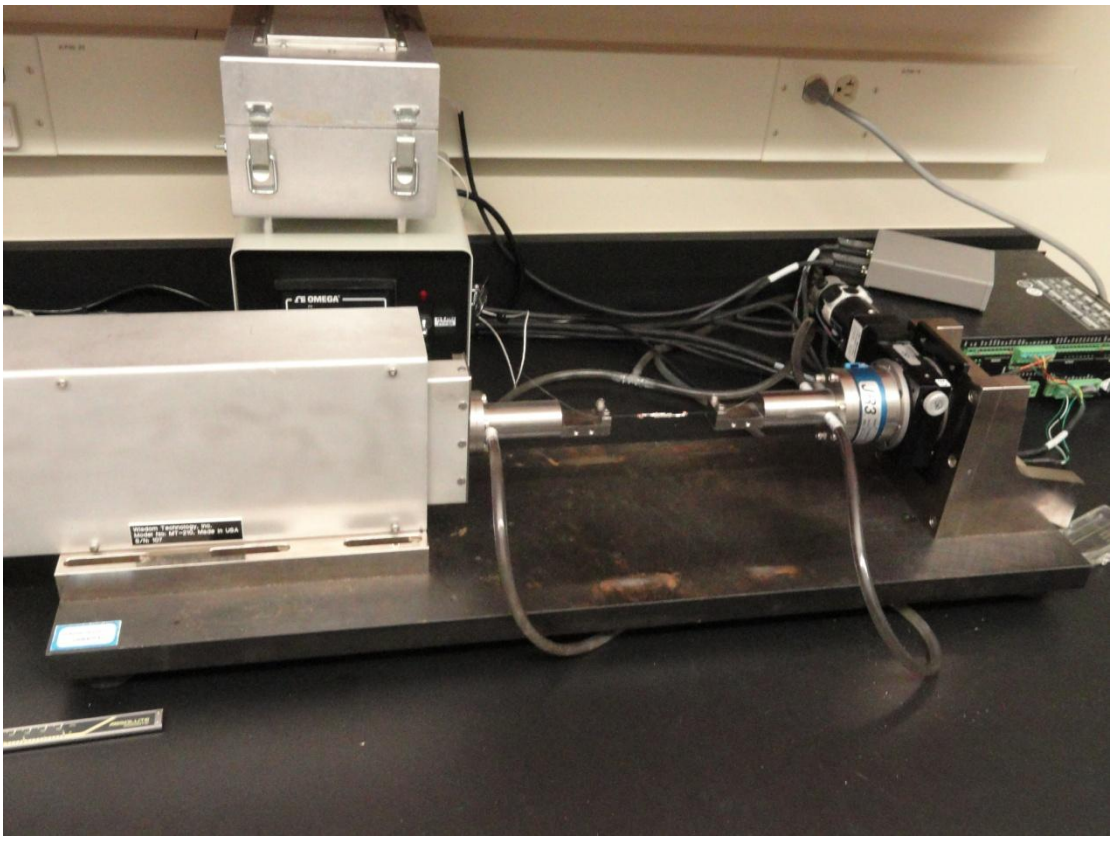

Figure 3-5: Photograph of Small Scale Tensile Machine

The basic setup of the tensile test for measuring the static friction force is shown in Figure 3-6. With two ends of the connector pairs clamped at two aligned fixtures, the tensile machine drove the two ends apart with 0.3 mm/s in speed. During this process, the transient of the force separating the connector pair is recorded. The nominal static friction force is evaluated and averaged by 20 samples and repeated testing trials. In order to decrease the moment at the interface that is potentially resulted from unaligned setup and influence the friction force value, wire leads with connectors were removed and flexible fishing wires were attached to align the axial direction of the connector pair with the driving direction of the tensile machine.

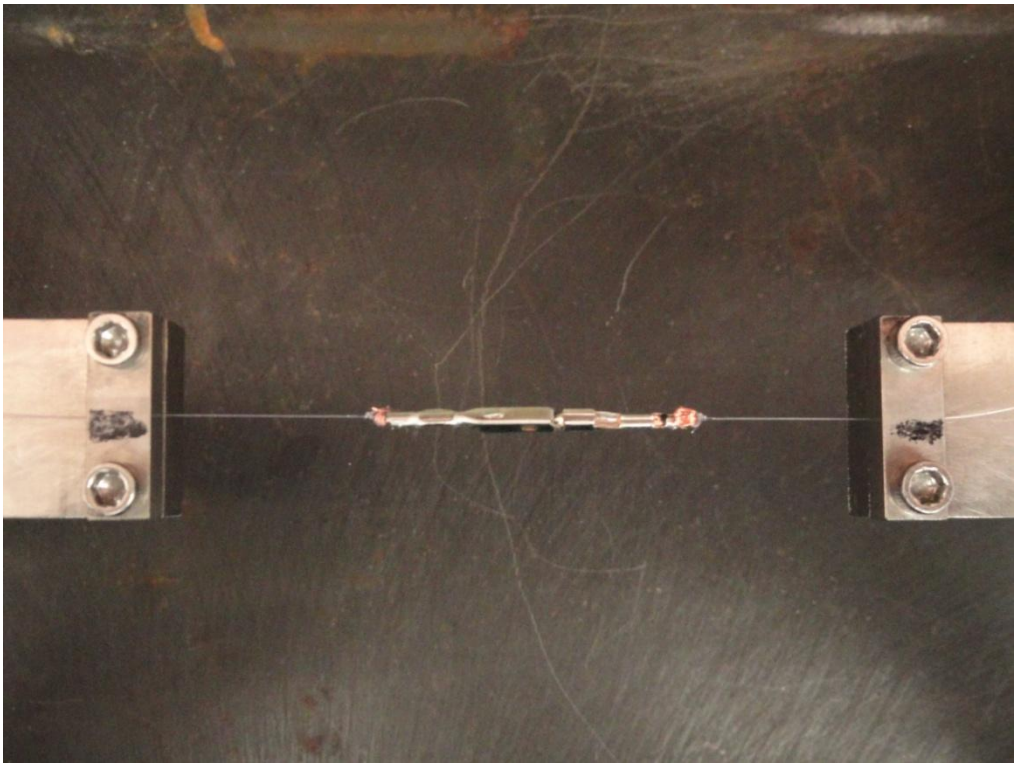

Figure 3-6: Setup of Connector Pair for Tensile Test

Figure 3-7 shows the result of fiction force at the contacting interface of connector pair in the tensile test. As the connector pair is stretched apart, the tensile force needed for keeping the uniformly slow movement is recorded. At the 0.0 mm horizontal displacement point, the machine did not start to move conversely. In the first period of tensile motion, the fish lines with connectors were tightened and the relative slip of contact pair did not occur, thus the tensile force increases monotonically from 0.0 mm to nearly 2.0 mm distance. After that, the fishing lines are already tightened and the blade and receptacle moved apart. The small scale variance of the force is mainly due to stick-slip phenomenon [46], the spontaneous jerking motion that can occur while two objects are sliding over each other. This phenomenon is typically caused by the reality that static friction coefficient is higher

than kinetic friction coefficient at one interface. In this case, as the tensile force became larger than static friction force, relative slip of connector pair occurred and the reduction of the friction to the kinetic friction leaded to a dropped tensile value. In the last period, the tensile force decreases simultaneously and becomes zero as the contact is separated. Based on the mechanism of stick-slip, the tensile force values that indicate the static friction coefficient are focused on the peak magnitudes during jerking motions. Through dozens of samples, the averaged static friction force between blade and receptacle is 2.19N.

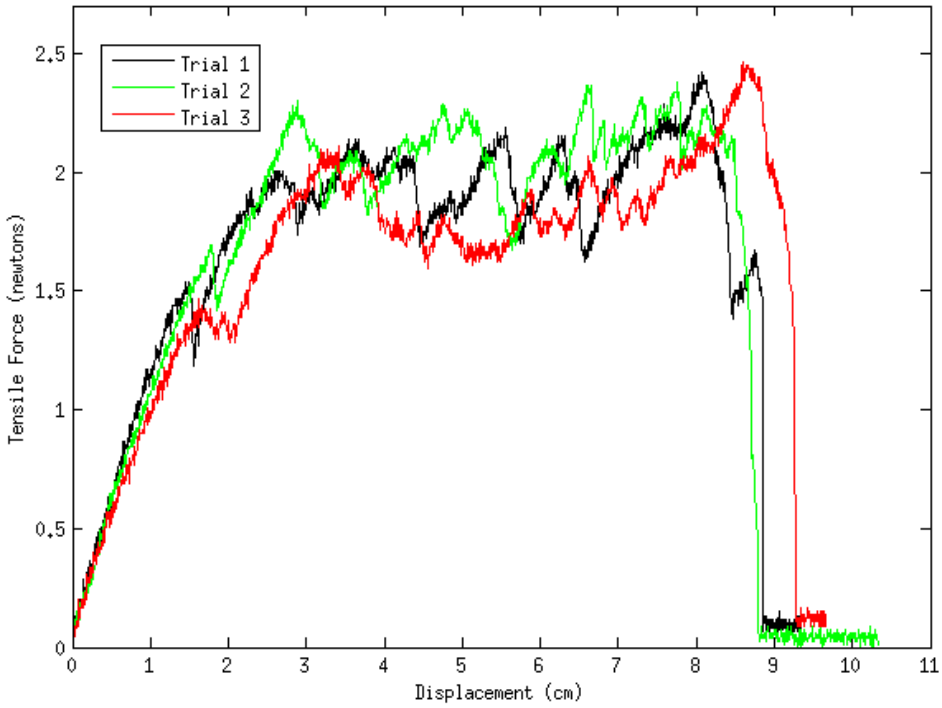

Figure 3-7: Tensile Force Change of Friction Force Measurement

3.3 Modeling Results

As the output of the transfer function fitting, the dynamic responses of mechanical system like $\ddot{\theta}$, $\dot{\theta}$, θ, and determined stiffness and damping parameters

are plugged into the equation for threshold prediction. As shown in Figures 3-8 to Figure 3-10, with a sine vibration input, $\ddot{\theta}$, $\dot{\theta}$, θ are all at periodic functions, with stable magnitudes after a short time fluctuation. The results for transfer function fitting are shown in latter figures.

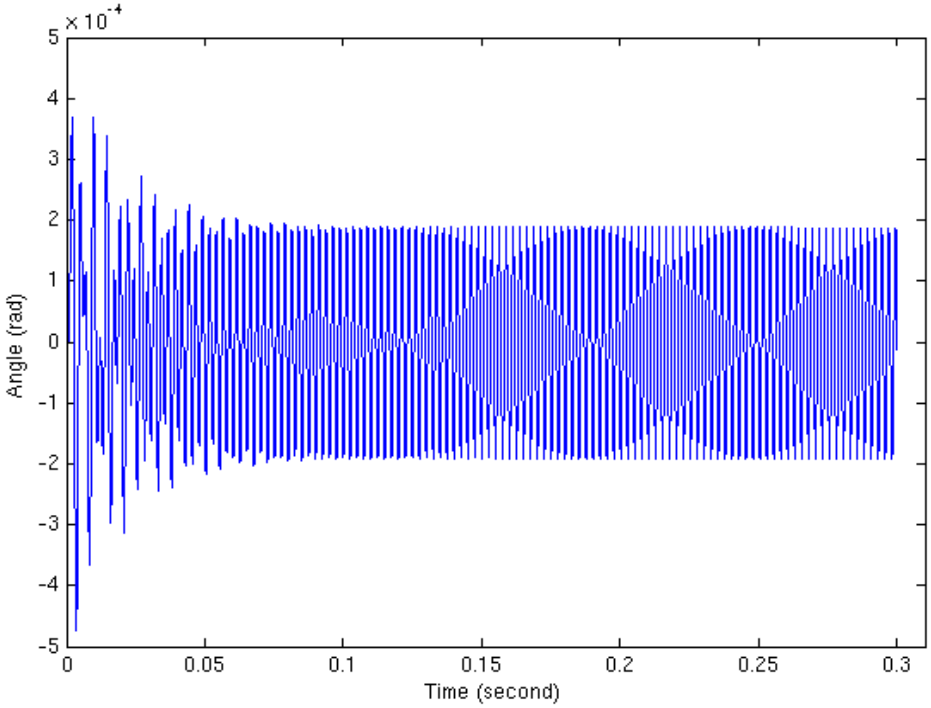

Figure 3-8: Transient of θ

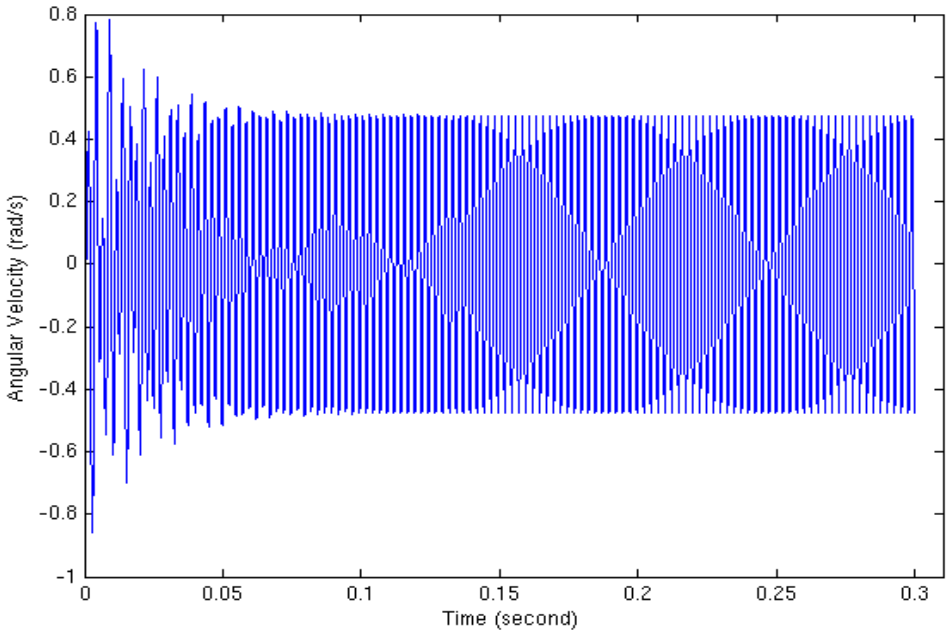

Figure 3-9: Transient of $\dot{\theta}$

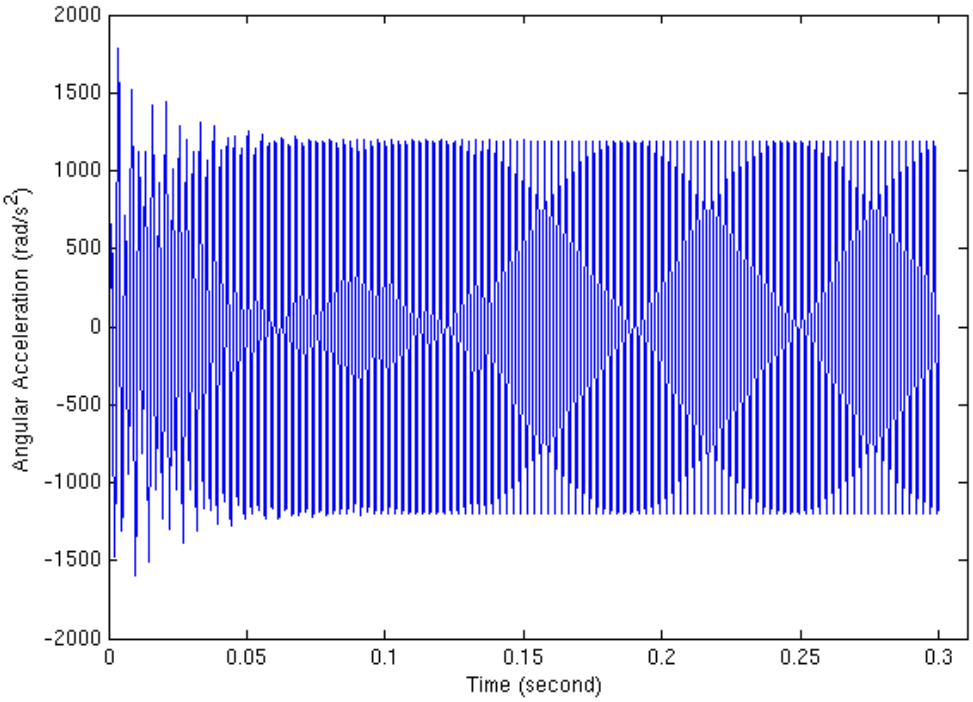

Figure 3-10: Transient of $\ddot{\theta}$

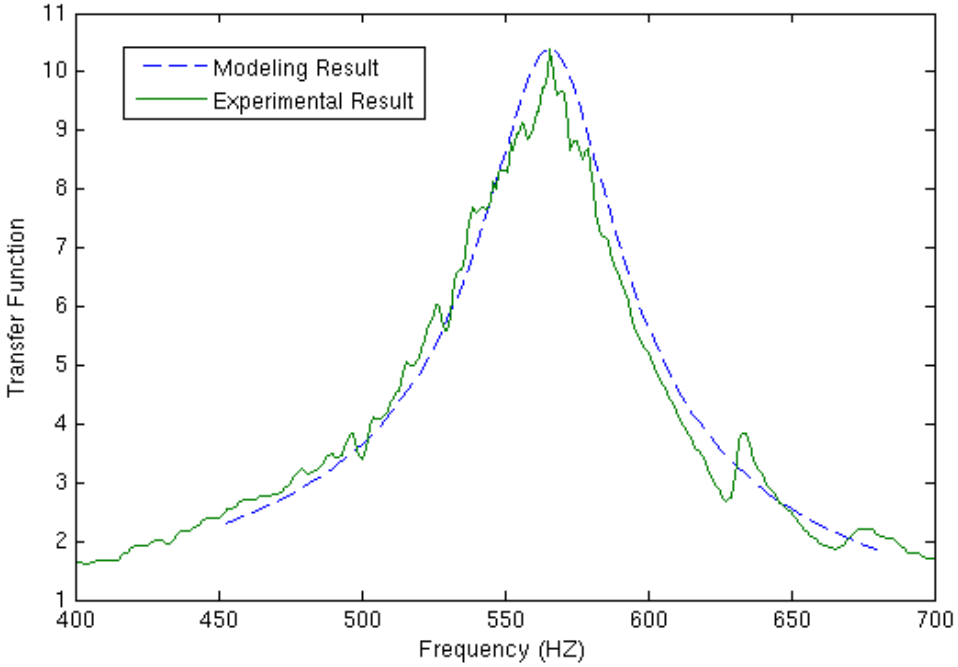

Figure 3-11: Comparison of Experimental and Modeling Transfer Functions (Wire Length = 2cm)

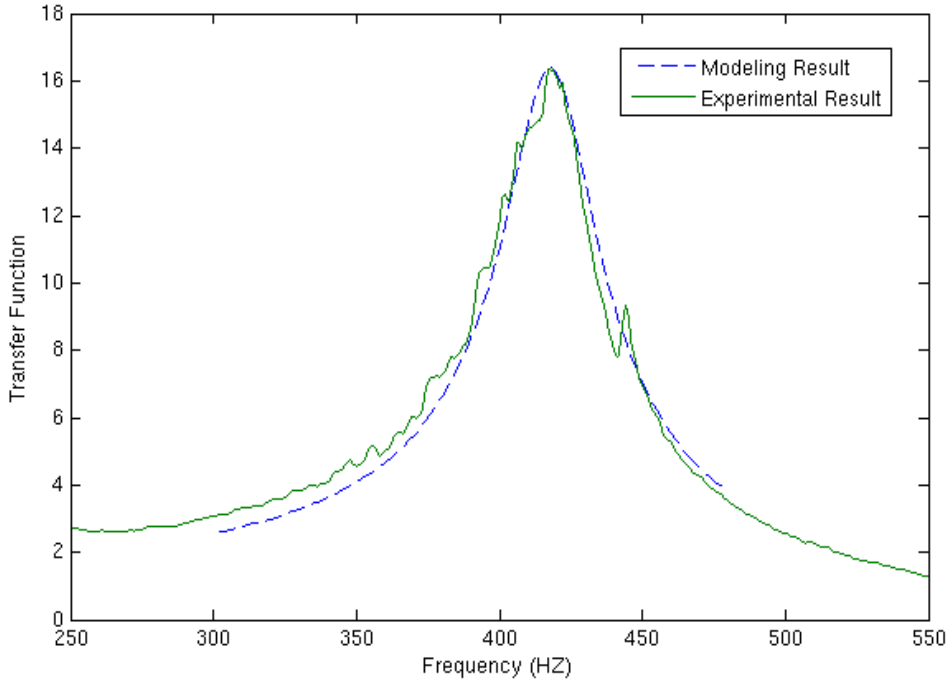

Figure 3-12: Comparison of Experimental and Modeling Transfer Functions (Wire Length = 3cm)

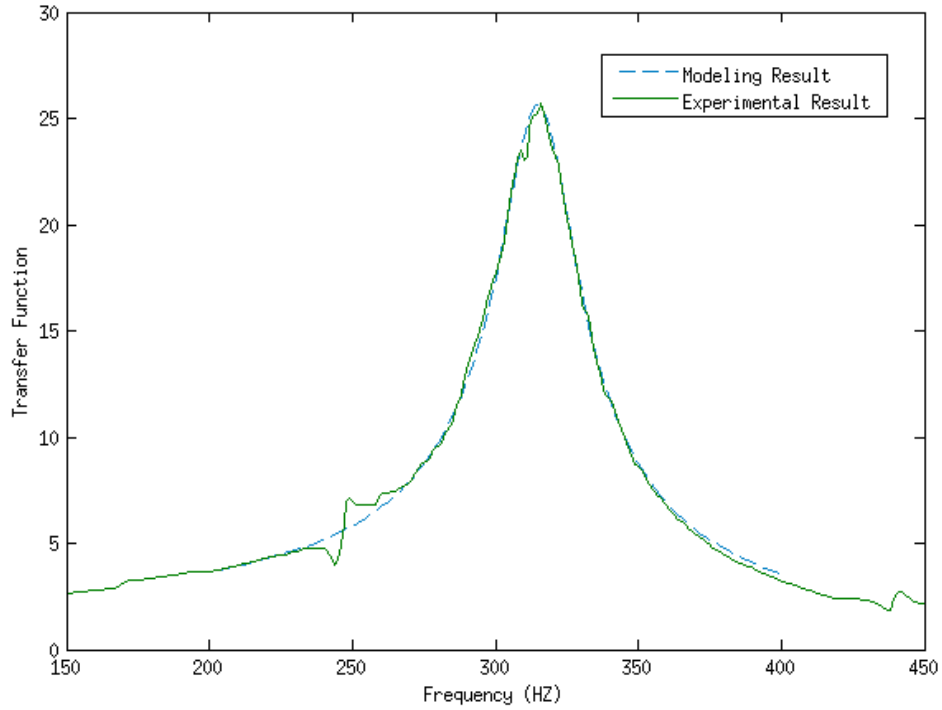

Figure 3-13: Comparison of Experimental and Modeling Transfer Functions (Wire Length = 4cm)

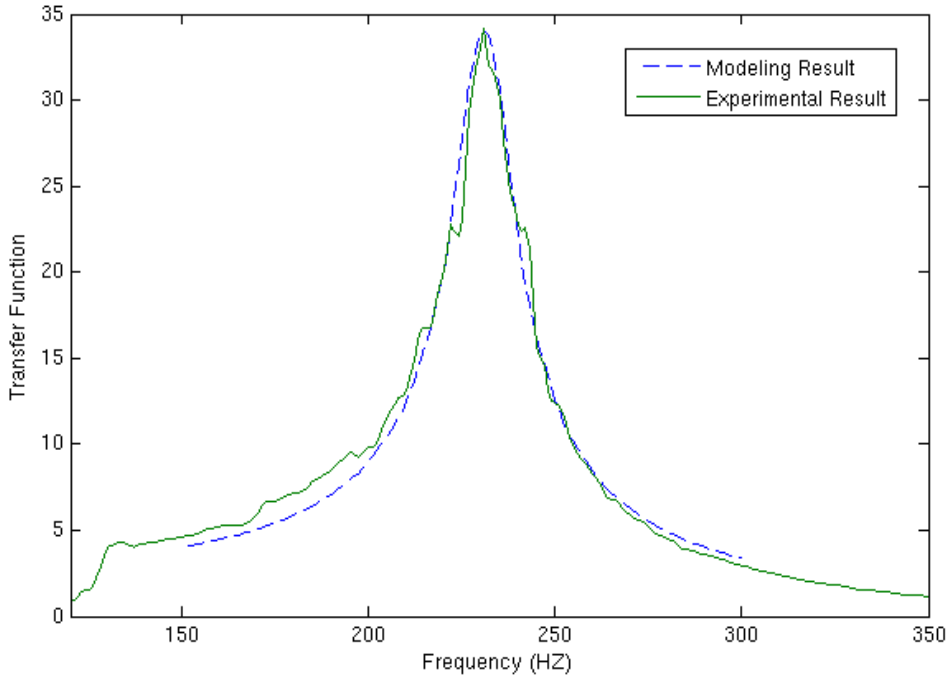

Figure 3-14: Comparison of Experimental and Modeling Transfer Functions (Wire Length = 5cm)

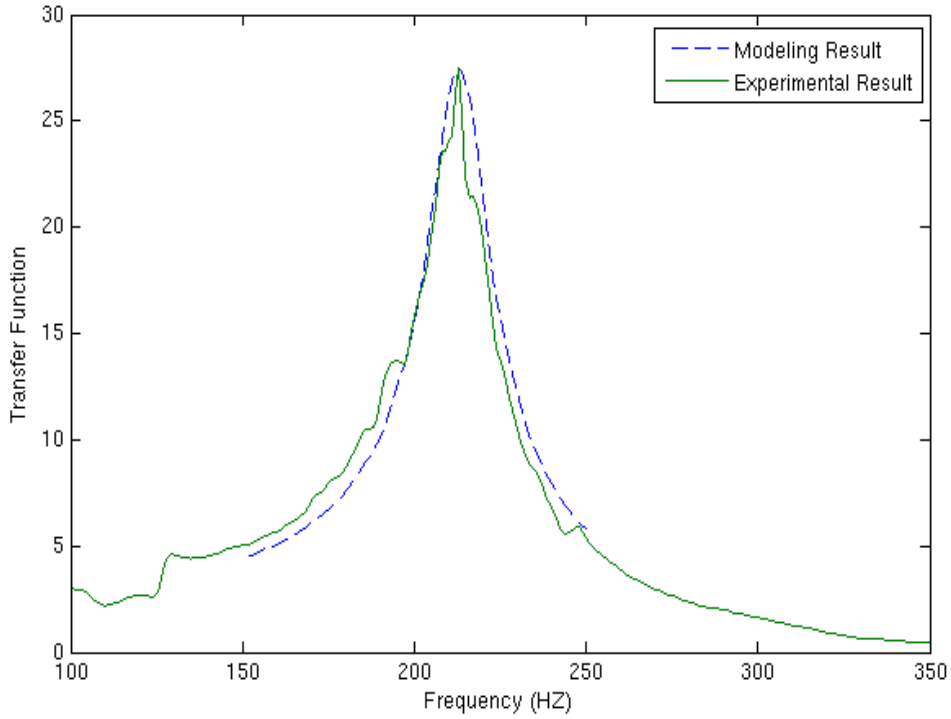

Figure 3-15: Comparison of Experimental and Modeling Transfer Functions (Wire Length = 6cm)

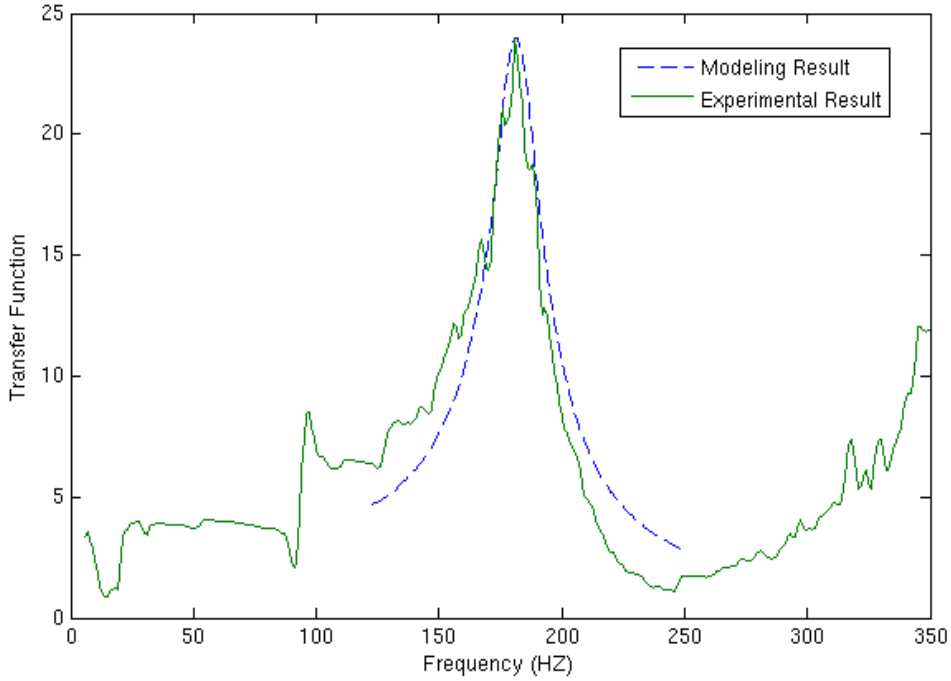

Figure 3-16: Comparison of Experimental and Modeling Transfer Functions (Wire Length = 8cm)

The output of the threshold prediction equation is the transient of friction force at the contacting interface of the connector pair. For each trial of the calculation, the output friction force is in the condition of single frequency and single amplitude vibration input. As shown in Figure 3-17, the transient of friction force with a specific amplitude and frequency input is a periodic function with a fixed magnitude. For this result, the fretting corrosion happens while the maximal absolute value of the transient friction force is over than the nominal static friction force. By the iteration of frequencies and increased input amplitudes in the range of interest, the friction force at various frequencies with the modeling threshold amplitudes are shown in figure 3-18 to figure 3-23.

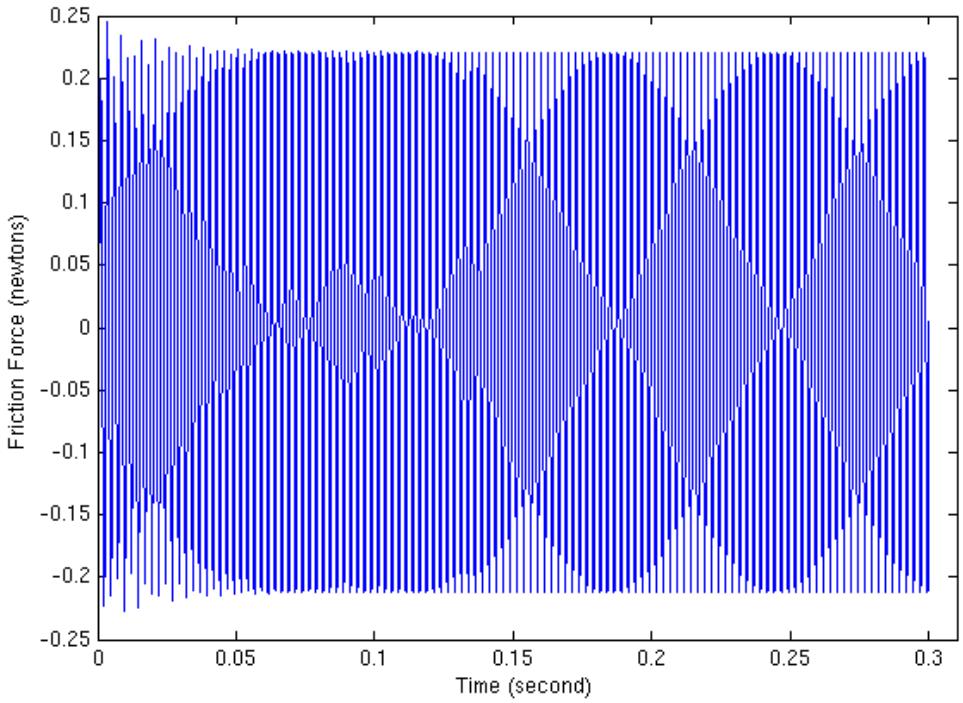

Figure 3-17: Transient of Friction Force at Contacting Interface

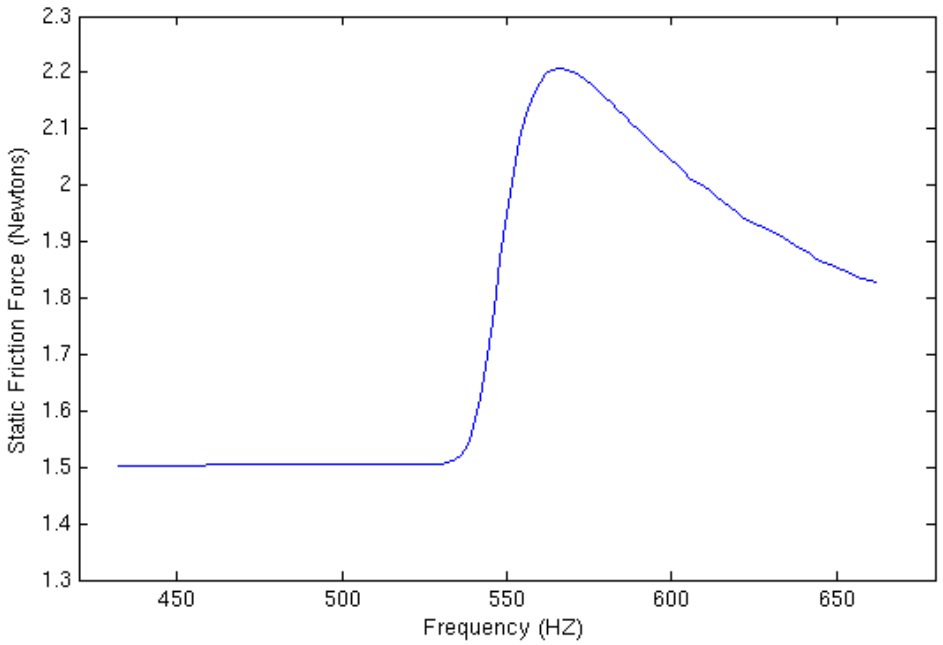

Figure 3-18: Maximal Absolute Value of Friction Force at Various Frequencies under Vibration with Threshold Amplitude (Wire Length = 2cm)

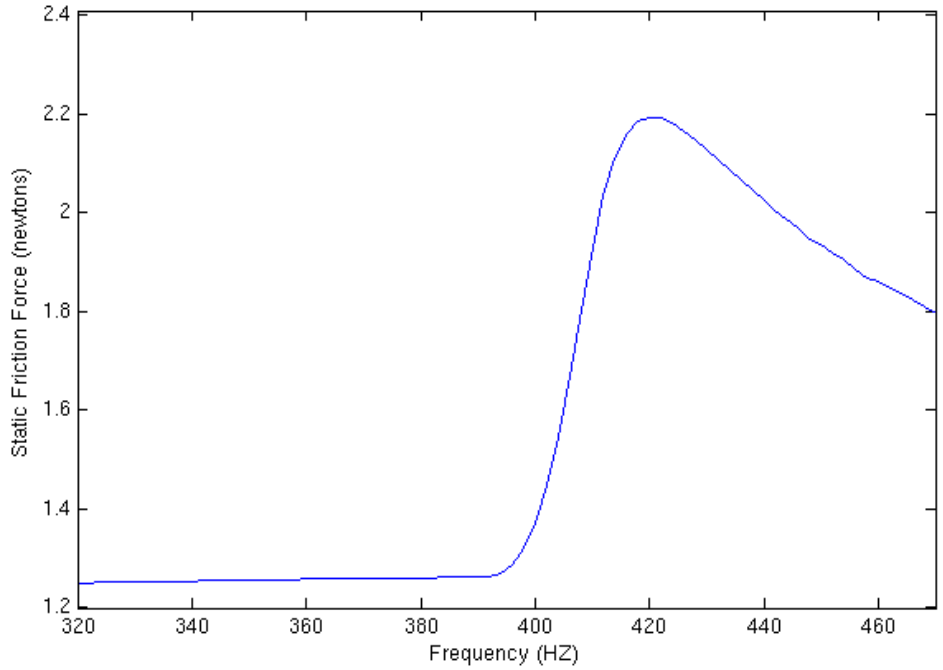

Figure 3-19: Maximal Absolute Value of Friction Force at Various Frequencies under Vibration with Threshold Amplitude (Wire Length = 3cm)

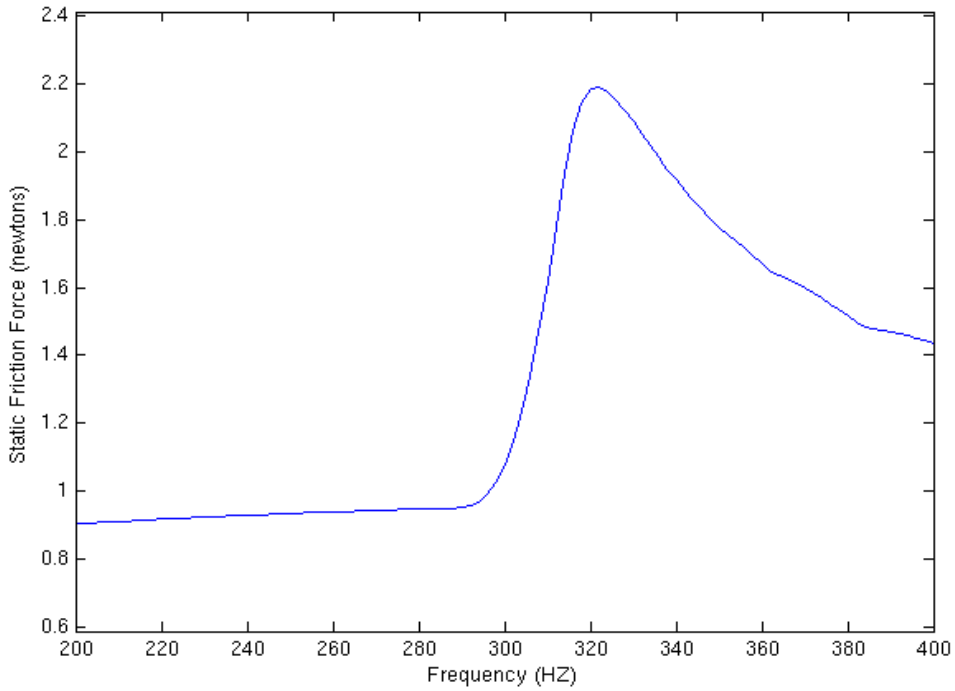

Figure 3-20: Maximal Absolute Value of Friction Force at Various Frequencies under Vibration with Threshold Amplitude (Wire Length = 4cm)

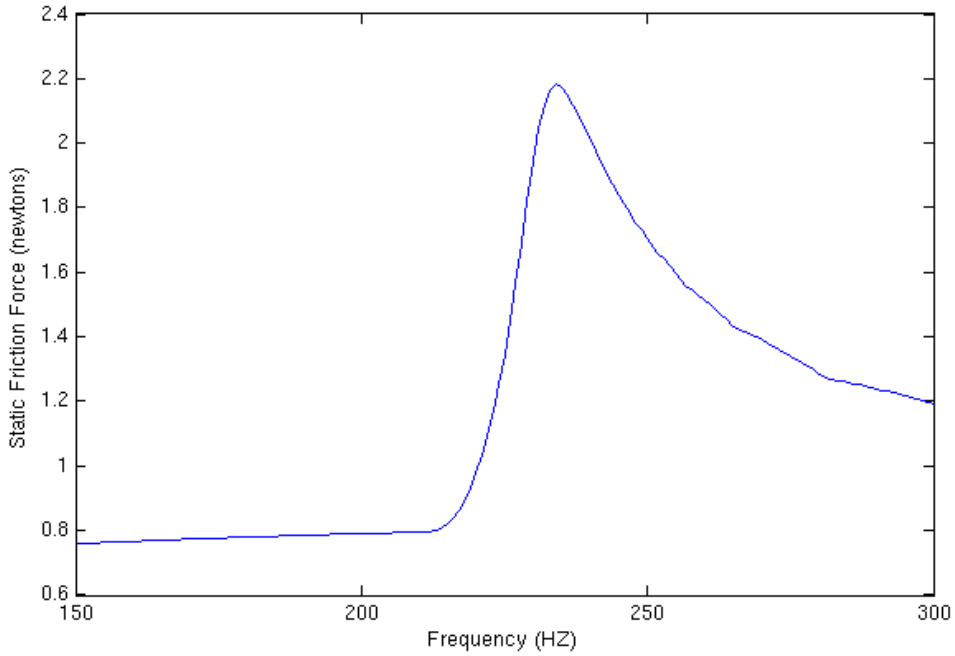

Figure 3-21: Maximal Absolute Value of Friction Force at Various Frequencies under Vibration with Threshold Amplitude (Wire Length = 5cm)

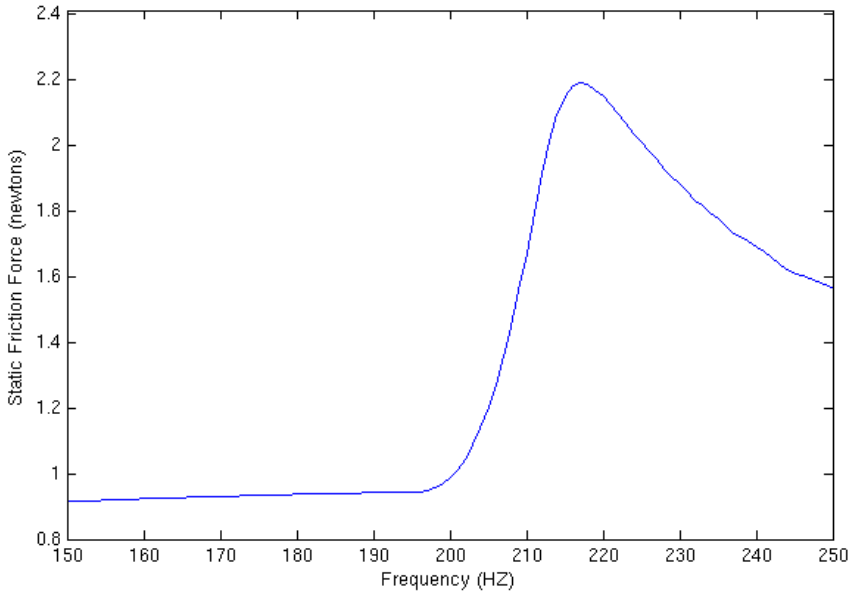

Figure 3-22: Maximal Absolute Value of Friction Force at Various Frequencies under Vibration with Threshold Amplitude (Wire Length = 6cm)

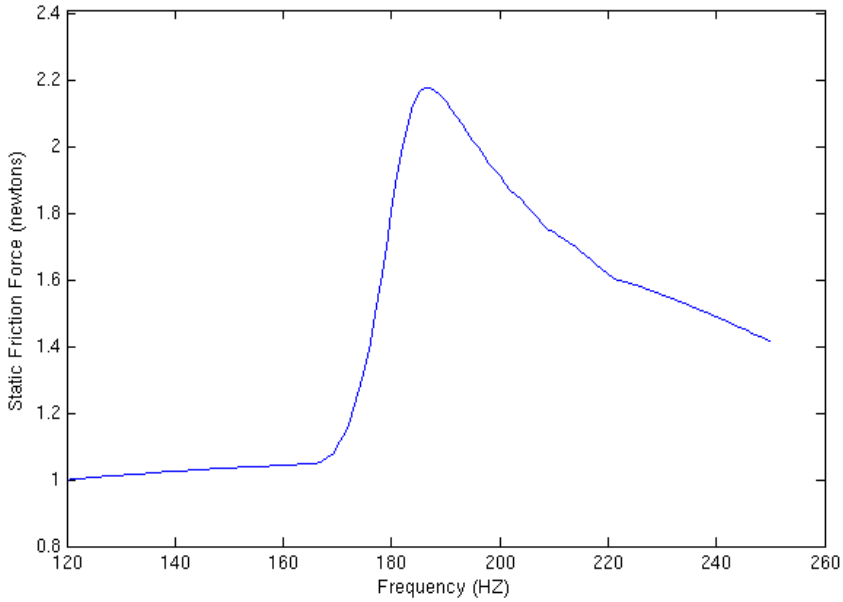

Figure 3-23: Maximal Absolute Value of Friction Force at Various Frequencies under Vibration with Threshold Amplitude (Wire Length = 8cm)

Based on the results as shown in figures above, the peaks of modeling friction forces are located at the natural frequencies of Mode A- A, which obeys the

threshold behavior measured experimentally, as shown in Figure 2-20. The comparison of experimental and modeling threshold amplitudes at Mode A-A for connectors with various wire lengths. A high correlation of the experimental and modeling results are shown. However this well correlation only exists for the connectors with short wires, and as the wire length is increased, the modeling threshold is larger and larger than the experimental thresholds. This phenomenon is in accord with the estimation of the styles of relative motions that induce fretting corrosion for connector with different wire lengths. Under the single frequency vibration at the frequency of Mode A- A, relative rocking motion happens in the connectors with long wires.

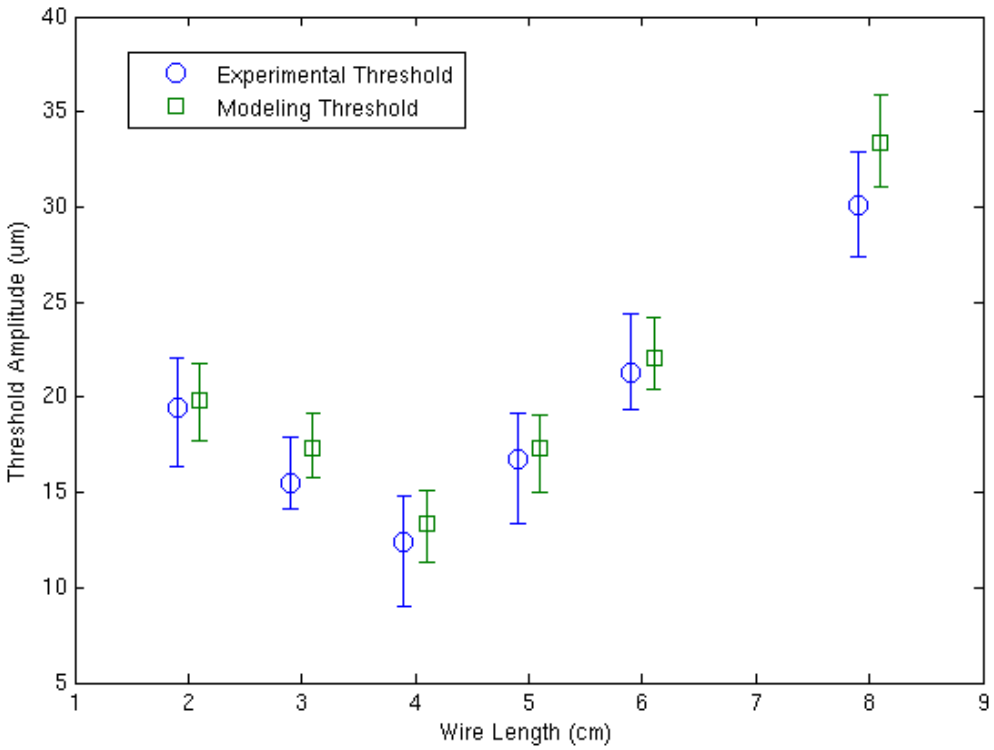

Figure 3-24: Comparison of Experimental and Modeling Thresholds at Mode A- A for Connectors with Various Wire Lengths

For the models of connectors with various wire lengths, the stiffness and damping parameters are different due to the variance of wires. The total stiffness and damping data for connector with various wire lengths are shown in figures 3-25 and 3-26. For a vibration model, higher stiffness and lower damping tend the system to vibrate more strongly under a given input amplitude and frequency. In the case of the mechanical system of electrical connectors, a smaller input amplitude can cause the relative motion between blade and receptacle with the higher stiffness and lower damping. As shown in these figures, with the increase of wire lengths, stiffness and damping both decrease. The combination of the two factors can be an explanation of the non-monotonic trend of threshold amplitudes, as shown in Figure 2-33.

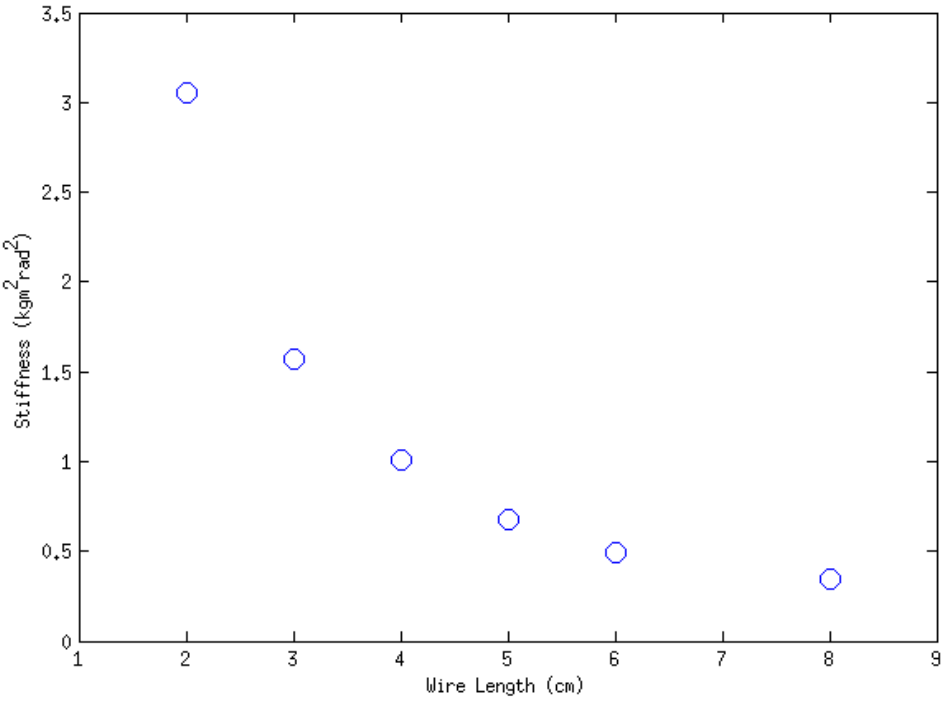

Figure 3-25: Total Stiffness of Connectors with Various Wire Lengths

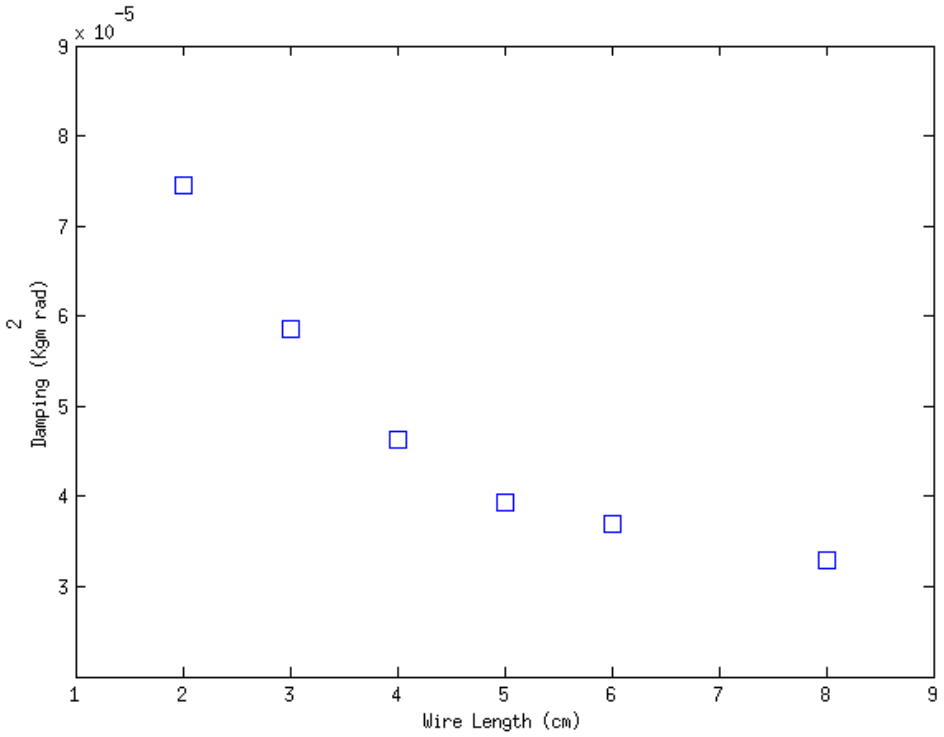

Figure 3-26: Total Stiffness of Connectors with Various Wire Lengths

CHAPTER 4 CONCLUSION AND FUTURE WORK

Two experiments and one mathematical model have been presented in this thesis to research the single frequency vibration threshold amplitudes that can trigger the fretting corrosion in electrical connector systems. In the experimental parts, frequency response and threshold behavior of the connector system was studied. Some processes are operated on connector samples for convenience of tests. The first experiment was aimed to find the frequency where threshold is lowest, and the second experiment was focused on the lowest thresholds for connector systems with various wire lengths. A spring-mass-damper discrete vibration model was applied to estimate the threshold behavior of fretting corrosion of the sample connectors. After synthesizing the experimental and modeling results, the following conclusions can be obtained for the present research:

- The electrical connectors with various wire lengths vibrate transversely under the axial vibration excitation.
- The electrical connector systems vibrate at multiple modes.
- Micro-meter scale amplitudes of the axial vibration trigger the fretting corrosion of this type of electrical connectors.
- At natural frequencies, threshold amplitudes are relatively low. And the lowest threshold appears at Mode A-A of this type of connector samples.
- With the increase of the wire length, the natural frequency of Mode A- A of

connector system decreases.

- With the increase of the wire length, the threshold amplitudes vary as a function with a non- monotonic trend. This phenomenon can be explained by the change of vibration modes based on experimental results, and decreased stiffness and damping according to the modeling results.
- The results of the mathematical model are well correlated with the experimental results.

Progress has been made in the area of fretting corrosion, but more can be done. The following are some suggestions for future research in this field:

- Research on threshold behavior of modes, other than Mode A-A.
- Create 2-D and 3-D FEA models to validate the vibration and threshold behaviors of connector systems with various wire lengths
- Design an experiment combining the axial and transverse excitation, and FEA models to validate the experimental results.

REFERENCES

[1] R. B. Waterhouse, “Fretting Corrosion”, Oxford Pergamon Press, USA.1972

[2] M. G. Fontana, Corrosion Engineering, McGraw-Hill Book, New. York, 1986

[3] J. Williams, Engineering Tribologhy, New York: Cambridge University Press, 2005

[4] I-Ming Feng and H. Uhlig, Journal of Applied Mechanics, 21, 395 (1954)

[5] M. D. Bryant, “Resistance Buildup in Electrical Connectors Due to Fretting Corrosion of Rough Surfaces”, IEEE Transactions on Components, Packaging And Manufacturing Technology, Part A, vol. 17, 1994, pp. 86-95

[6] E.M. Bock and J.H. Whitley, “Fretting Corrosion in Electric Contacts”, Proceedings of Holm Conference on Electrical Contacts, 1974, pp. 128-138.

[7] S. V. Angadi, W. E. Wilson, R. L. Jackson, G. T. Flowers, B.I. Rickett “A Multi-physics Finite Element Model of an Electrical Connector Considering Rough Surface Contact”, Proceedings of Holm Conference on Electrical Contacts ,vol. 54 ,2008, pp. 168-177.

[8] S. Wada, K. Sawa, “Degradation Phenomena of Electrical Contacts Using Hammering Oscillating Mechanism and Micro-sliding Mechanism- Contact Resistance and Its Model”, Proceedings of Holm Conference on Electrical Contacts, vol. 57 ,2011, pp. 11-14.

[9] P. Jedrzejczyk, S. Fouvry, P. Chalandon, "A Fast Methodology to Quantify Electrical-contact Behaviour under Fretting Loading Conditions", Wear, vol. 267, 2009, pp. 1731-1740

[10] L. Tristani, E.M. Zindine, L. Boyer, G. Klimek, "Mechanical Modeling of Fretting Cycles in Electrical Contacts", Wear, vol. 249, 2001, pp. 12–19

[11] R. D. Ibrahim, C. Chen, and G. T. Flowers, "Modeling and Analysis of a Blade/Receptacle Pair for the Prediction of Thermal Cycling and Temperature Dependent Vibration Driven Fretting Corrosion", Proceedings of Holm Conference on Electrical Contacts, vol.56, 2010, pp. 4-7

[12] K. Lee, D. Jeong, J. Kim, "Simulational Study of Electrical Contact Degradation under Fretting Corrosion", Tribology International, vol. 44, 2011, pp. 1651–1658

[13] S. Hsu, K. Liao "Wear Analysis and Verification of Metallic Terminals for Electronic Connectors", Engineering Failure Analysis, vol. 25, 2012, pp. 71–80

[14] K. Mashimo, Y. Ishimaru, "Computational Modeling and Analysis of a Contact Pair for the Prediction of Fretting Dependent Electrical Contact Resistance", Proceedings of Holm Conference on Electrical Contacts, vol. 57, 2011, pp. 11-14

[15] M. Antler, "Survey of Contact Fretting in Electrical Contacts", Proceedings of the Twenty Ninth IEEE Holm Conference on Electrical Contacts, 1984, pp 3-22.

[16] Ed P. Slade, "Electrical Contacts: Principles and Applications", Chapter 6,

1990

[17] S. Hannel S. Fouvry. Ph. Kaaspa, L. Vincent 'The Fretting Sliding Transition as a Criterion for Electrical Contact Performance', Wear, vol. 249, 2001, 761-770

[18] A. Lee and M.S. Mamrick "Fretting Corrosion of Tin-Plated Copper Alloy", IEEE Trans. CHMT- 10, 1987, p63

[19] J. Swingler, J.W. Bride, and C. Maul, "The Degradation of Road Tested Automotive Connectors", IEEE Transactions on Components and Packaging Technology (CPMT), 2000, 23(1), p. 157- 164

[20] J. Song, C. Koch, and L. Wang, "Correlation betweenWear Resistance and Lifetime of Electrical Contacts", Hindawi Publishing Corporation Advances in Tribology, vol. 2012, pp. 9.

[21] A. Bouzera, E. Carvou, L. Tristani, E.M. Zindine, N. Ben Jemaa and R. Elabdi "Minimum Fretting Amplitude in Medium Force for Connector Coated Material and Pure Metals", Proceedings of Holm Conference on Electrical Contacts, VOL. 56 ,2010, pp. 4-7

[22] S. Fouvry, P. Jedrzejczyk, P. Chalandon, "Introduction of an Exponential Formulation to Quantify the Electrical Endurance of Micro-contacts Enduring Fretting Wear: Application to Sn, Ag and Au Coatings", Wear, vol. 271, 2011, pp. 1524– 1534

[23] X. Lin, L. Xu, Y. Shao, G. Luo, H. Zhang "Research on Fretting Resistance and Fretting Wear Property of Ni-Au Contact Pair", Proceedings of Holm

Conference on Electrical Contacts, vol. 57, 2011, pp. 11-14

[24] T.S.N. S. Narayanan, Y. Park, K. Lee, "Fretting Corrosion of Lubricated Tin Plated Copper Alloy Contacts: Effect of Temperature", Tribology International, vol. 41, 2008, pp. 87–102

[25] Y. Park, T.S.N. S. Narayanan, K. Lee, "Fretting Corrosion of Tin-plated Contacts", Tribology International, vol. 41, 2008, pp. 616–628

[26] Y. Park, T.S.N. S. Narayanan, K. Lee, "Effect of Temperature on the Fretting Corrosion of Tin Plated Copper Alloy Contacts", Wear, vol. 262, 2007, pp. 320–330

[27] K. Y. Lee, D. K. Jeong, H. G. Joo and Y. W. Park, "Simulation for Fretting Corrosion of Tin-coated Copper Contacts", Materials and Corrosion, vol. 62 2011, pp. 352-356

[28] S. Noël, D. Alamarguy, S. Correia, P. Laurat, "Fretting Behavior of Nickel Coatings for Electrical Contact Applications", Proceedings of Holm Conference on Electrical Contacts, vol. 57, 2011, pp. 11-14

[29] R. D. Malucci, "Multispot Model of Contacts Based on Surface Features", Electric Contacts- 1990, IEEE- HOLM, Montreal, 1990, p.625

[30] R.D. Malucci, "Impact of Fretting Parameters on Contact Degradation", Proceedings of the 42nd IEEE Holm Conference on Electrical Contacts, 1996, pp. 395- 403

[31] F. Xie, Thesis "A Study of Electrical Connector Performance in Fretting", Auburn University, 2003

[32] G Villeneuve, D. Kulkami, P. Batnagel and D. Berry, "Dynamic Finite Element

Analysis Simulation of the Terminal Crimping Process", Electrical Contacts, 1996, Proceedings of the Forty- Second IEEE Holm Conference Joint with the 18th International Conference on Electrical Contacts, Sept. 1996, pp. 156-172

[33] A. Monnier, B. Froidurot, C. Jarrige, R. Meyer and P. Teste, "A Mechanical Electrical, Thermal Coupled- field Simulation of a Sphere- plane Electrical Contact", Electrical Contacts, 2005. Proceedings of the Fifthy- First IEEE Holm Conference on Sept. 26- 28, 2005, pp: 224-231

[34] G. T. Flowers, F. Xie, and M. J. Bozack, Robert D. Malucci "Vibration Thresholds for Fretting Corrosion in Electrical Connectors" IEEE Transactions on Components and Packaging Technologies, vol.27, 2004, pp.65-71.

[35] G. T. Flowers, F. Xie, M. J. Bozack, R. Horvath, R. D. Malucci, B. I. Rickett "Modeling Early Stage Fretting of Electrical Connectors Subjected to Random Vibration", Proceedings of Holm Conference on Electrical Contacts, vol. 49, 2003, pp. 45-50.

[36] G. T. Flowers, F. Xie, M. J. Bozack, X. Hai, B. I. Rickett, and R. D. Malucci," A Study of the Physical Characteristics of Vibration-Induced Fretting Corrosion" . Proceedings of Holm Conference on Electrical Contacts, vol. 50, 2004, pp 31-319.

[37] F. Xie, G. T. Flowers, C. Chen, M. Bozack, J. Suhling, B. I. Rickett, R. D. Malucci, and C. Manlapaz, "Analysis and Prediction of Vibration-Induced Fretting Motion in a Blade/Receptacle Connector Pair", Proceedings of Holm

Conference on Electrical Contacts, vol. 53, 2007, pp. 222-228

[38] C. Chen, G. T. Flowers, M, J. Bozack, J. Suhling, B.I. Rickett; B.J. Malucci, C. Manlapaz, "Modeling and Analysis of a Blade/Receptacle Pair for the Prediction of Vibration-Induced Fretting Degradation" Proceedings of Holm Conference on Electrical Contacts, vol. 54, 2008, pp: 276-283

[39] C. Chen, G. T. Flowers, M. J. Bozack; J. Suhling, "Modeling and Analysis of a Connector System for the Prediction of Vibration-induced Fretting Degradation", Proceedings of Holm Conference on Electrical Contacts, vol. 55, 2009, pp. 131-137

[40] J. Gao, C. Chen, G.T. Flowers, R.L. Jackson and M.J. Bozack "The Influence of Particulate Contaminants on Vibration- Induced Fretting Degradation in Electrical Connectors", Proceedings of Holm Conference on Electrical Contacts, vol. 56, 2010, pp. 1-5

[41] L. Lam, J. W. McBride, C. Maul and J. K. Atkinson, "Displacement Measurement at the Connector Contact Interface Employing a Novel Thick Film Sensor", Electrical Contacts, 2005. Proceedings of the Fifty- First IEEE Holm Conference on 26-28, 2005 pp: 89-96

[42] R. Fu, S. Choe, R. L. Jackson, G. T. Flowers. "Experimental Study of the Vibration-induced Fretting of Silver-plated High Power Automotive Connectors", Proceedings of Holm Conference on Electrical Contacts, vol. 56, 2010, pp. 4-7

[43] Model 2010 Multimeter User's Manual, Keithley Instruments, Inc., USA, 1999

[44] Laser Vibrometer User Manual, Controller OFV-2610/2620, Sensor Head OFV-353, POLYTEC Co., Germany

[45] HP 35665A Dynamic Signal Analyzer Installation and Verification Guide, Hewlett-Packard Company, USA, 1991

[46] S. N. Patek (2001). "Spiny lobsters stick and slip to make sound". *Nature* **411** (6834): 153–154

APPENDIX A MATLAB CODE OF EXAMPLE OF MATHEMATICAL MODEL

```
%%%% Main File

global g I m1 m2 L Lg Lgg beta gama delta k0 w a k1 k2 c1 c2

g= 9.81; % gravity 9.81 m/s^2

I=264e-9; % moment of inertia is 246e-9 m^2*kg

m1=1.1e-3; % total mass is 1.1e-3 kg

m2=0.45e-3; % receptacle mass is 0.45e-3 kg

L=36.84e-3; % length of connector is 36.84e-3 m

Lg= 15.77e-3; % length of (G) mass center of connector is 15.77e-3 m

Lgg= 24.11e-3; % length of (G') mass center of receptacle is 24.11e-3 m

beta=0.0283; % initial angle of bar is 0.0283 rad

gama= 0.0205; % initial angle of OG to Y axis is 0.0205 rad

delta= 0.0208; % initial angle of OG' to Y axis is 0.0208 rad

k1=-1403; % stiffness 1

c1=0.019; % damping 1

k2=0.083e6; % stiffness  2

c2=0.0014; % damping 2

I0= 36.9229e-9; % moment of inertia of blade

f0=1275;
```

```
w0=f0*2*pi; % connector beam natural frequeny

k0=I0*w0^2; % stiffness of connector root

a=5e-6; % threshold amplitude e-6m=um.

n=0; % number of magnitude

spm= [390:5:400]; % frequency spectrum

for f=spm

    n=n+1; % number of magnitude
    f

    w=f*2*pi;


    options = odeset('RelTol',1e-6,'AbsTol',[1e-6 1e-6 1e-6 1e-6 1e-6 1e-6]);
    [S,Y] = ode45(@sub,[0 0.3],[0 0 0 0 a/2*w 0],options);

    ly=length(Y(:,1)); % length of numerical result

    for i=1:1:ly
        input(n,i)=Y(i,4)+cos(Y(i,1))*10.54e-3-10.54e-3;

    end



magnitude(n)=range(sin(Y(ly-500:ly,1)+beta))*15e-3/range(input(n,ly-1e3:ly));

    i=0; % number of friction force

    for i=1:1:length(Y(:,1))


        forc(n,i)= (-(-L*sin(beta + Y(i,1))-(-L* sin(beta)))*k1 - (-L*cos(beta +
                Y(i,1))*Y(i,2))*c1)*sin(Y(i,1)) - (-m2*g - (Y(i,4)+ L*cos(beta
                + Y(i,1)) - L*cos(beta))*k2- (Y(i,5)- L*sin(beta +
                Y(i,1))*Y(i,2))*c2)*cos(Y(i,1))+ m2*( ( Y(i,6) -
                Y(i,2)^2*(Lgg*cos(Y(i,1) + delta)) + Y(i,3)*(-Lgg*sin(Y(i,1)
                + delta)) )*cos(Y(i,1)) - ( -Y(i,2)^2*(-Lgg*sin(Y(i,1) + delta))
                - Y(i,3)*(Lgg*cos(Y(i,1) + delta)) )*sin(Y(i,1)) );
```

```
    end

    force(n)=max(abs(forc(n,:)));

end

% experimental result comparison
load('/home/me_h3/hzy0011/Desktop/connector_testing/GOODSHAPE/goodshapeto
o/54.TXT');

for i=1:401
    mg(i)=sqrt(X54(i,2)^2+X54(i,3)^2);
end


figure(1)

subplot(2,1,1)
plot(spm,magnitude,X54(1:401,1),mg(1:401))
title('magnitude')

subplot(2,1,2)
plot(spm,force)
title('force')




%%%% Function File

function dy=sub(t,y)

dy=zeros(6,1);

global  I   m1   m2   L   Lg   Lgg   beta   gama   delta   k0   w   a   g   k1
        k2   c1   c2

%   y(1) is angle theta
dy(1)=y(2);

%   y(2) is anglular velocity theta'
dy(2)=y(3);
```

```
%    y(3) is anglular acceleration theta"

% Xg= -Lg*sin(gama + theta);
% position of G at X axis

% Xg'= -Lg*cos(gama + theta)*theta';
% velocity of G at X axis

% XA= -L*sin(beta + theta);
% position of A at X axis

% XA0= -L* sin(beta);
% intial XA

% XA'= -L*cos(beta + theta)*theta';
% velocity of XA

% XA"= L*theta'*theta'*sin(beta + theta) - L*theta"*cos(beta + theta);
% acceleration of XA

% YA= s0+ L*cos(beta + theta);
% position of A at Y axis

% YA0= L*cos(beta);
% initial position of YA

% YA'= v0- L*sin(beta + theta)*theta'
% velocity of YA

% YA"= a0 - L*theta'*theta'*cos(beta + theta) - L*theta"*sin(beta + theta)
% acceleration of YA

% Y0= s0;
% position of shaker head at Y axis


% dy(3)= ( -m1*Xg'*a0 - m1*Xg*v0 - k0*theta' + XA'*(YA-Y0)*k1 +
            (XA-XA0)*(YA'-Y0')*k1 + XA"*(YA-Y0)*c1 + XA'*(YA'-Y0')*c1 -
            YA'*XA*k2- (YA-YA0)*XA'*k2 - YA"*XA*c2 - YA'*XA'*c2 -
            m1*g*Xg' )/I

% dy(3)=( -m1*(-Lg*cos(gama + theta)*theta')*a0 - m1*(-Lg*sin(gama + theta))*v0
          - k0*theta' + (-L*cos(beta + theta)*theta')*(L*cos(beta + theta))*k1 +
```

```
(-L*sin(beta + theta)+L* sin(beta))*(- L*sin(beta + theta)*theta')*k1 +
(L*theta'*theta'*sin(beta + theta) - L*theta''*cos(beta + theta))*(L*cos(beta
+ theta))*c1 + (-L*cos(beta + theta)*theta')*(-L*sin(beta +
theta)*theta')*c1 - (v0- L*sin(beta +theta)*theta')*(-L*sin(beta + theta))*k2
- (s0+ L*cos(beta + theta) - L*cos(beta))*(-L*cos(beta + theta)*theta')*k2 -
(a0 -% L*theta'*theta'*cos(beta + theta) - L*theta''*sin(beta +
theta))*(-L*sin(beta + theta))*c2 - (v0- L*sin(beta +
theta)*theta')*(-L*cos(beta + theta)*theta')*c2 - m1*g*(-Lg*cos(gama +
theta)*theta') )/I;


% dy(3)= ( -m1*(-Lg*cos(gama + y(1))*y(2))*y(6) - m1*(-Lg*sin(gama +
          y(1)))*y(7) - k0*y(2) + (-L*cos(beta + y(1))*y(2))*(L*cos(beta +
          y(1)))*k1 + (-L*sin(beta + y(1))+L* sin(beta))*(- L*sin(beta +
          y(1))*y(2))*k1 + (L*y(2)*y(2)*sin(beta + y(1)) - L*y(3)*cos(beta +
          y(1)))*(L*cos(beta + y(1)))*c1+ (-L*cos(beta + y(1))*y(2))*(-L*sin(beta
          + y(1))*y(2))*c1 - (y(5)- L*sin(beta + y(1))*y(2))*(-L*sin(beta +
          y(1)))*k2 - (y(4)+ L*cos(beta + y(1)) - L*cos(beta))*(-L*cos(beta +
          y(1))*y(2))*k2- (y(6) - L*y(2)*y(2)*cos(beta + y(1)) - L*y(3)*sin(beta +
          y(1)))*(-L*sin(beta + y(1)))*c2 - (y(5)- L*sin(beta +
          y(1))*y(2))*(-L*cos(beta + y(1))*y(2))*c2 - m1*g*(-Lg*cos(gama +
          y(1))*y(2)) )/I;

dy(3)= ( -m1*(-Lg*cos(gama + y(1))*y(2))*(-a/2*w*w*sin(w*t)) -
        m1*(-Lg*sin(gama + y(1)))*(-a/2*w*w*w*cos(w*t)) - k0*y(2) +
        (-L*cos(beta + y(1))*y(2))*(L*cos(beta + y(1)))*k1 + (-L*sin(beta +
        y(1))+L* sin(beta))*(- L*sin(beta + y(1))*y(2))*k1 + (L*y(2)*y(2)*sin(beta
        + y(1)) - L*y(3)*cos(beta + y(1)))*(L*cos(beta + y(1)))*c1 + (-L*cos(beta +
        y(1))*y(2))*(-L*sin(beta + y(1))*y(2))*c1 - (y(5)- L*sin(beta +
        y(1))*y(2))*(-L*sin(beta + y(1)))*k2 - (y(4)+ L*cos(beta + y(1)) -
        L*cos(beta))*(-L*cos(beta + y(1))*y(2))*k2 - (y(6) - L*y(2)*y(2)*cos(beta +
        y(1)) - L*y(3)*sin(beta + y(1)))*(-L*sin(beta + y(1)))*c2 - (y(5)- L*sin(beta
        + y(1))*y(2))*(-L*cos(beta + y(1))*y(2))*c2 - m1*g*(-Lg*cos(gama +
        y(1))*y(2)) )/I;


dy(4)=y(5);       %   s0                y(4) = a/2*sin(w*t)
% y(4) is displacement of shaker head

dy(5)=y(6);   %   v0    y(5) = a/2*w*cos(w*t)
% y(5) is velocity of shaker head

dy(6)=-a/2*w*w*w*cos(w*t);   % a0      y(6) = -a/2*w*w*sin(w*t)
% y(6) is acceleration of shaker head
```

```
% dy(7)=a/2*w*w*w*w*sin(w*t); % a0' y(7)= -a/2*w*w*w*cos(w*t)
```

APPENDIX B TESTING FIXTURE DIMENSIONS

The following pages include the dimensions of fixture used for vibration and threshold experiments. They are intended for use in machining a fixture which allows axial vibration of electrical connectors with different lengths of cables. The unit of the dimensions is millimeter. All of the materials used in this fixture are aluminum. The assembly and operation is described in Chapter 2.

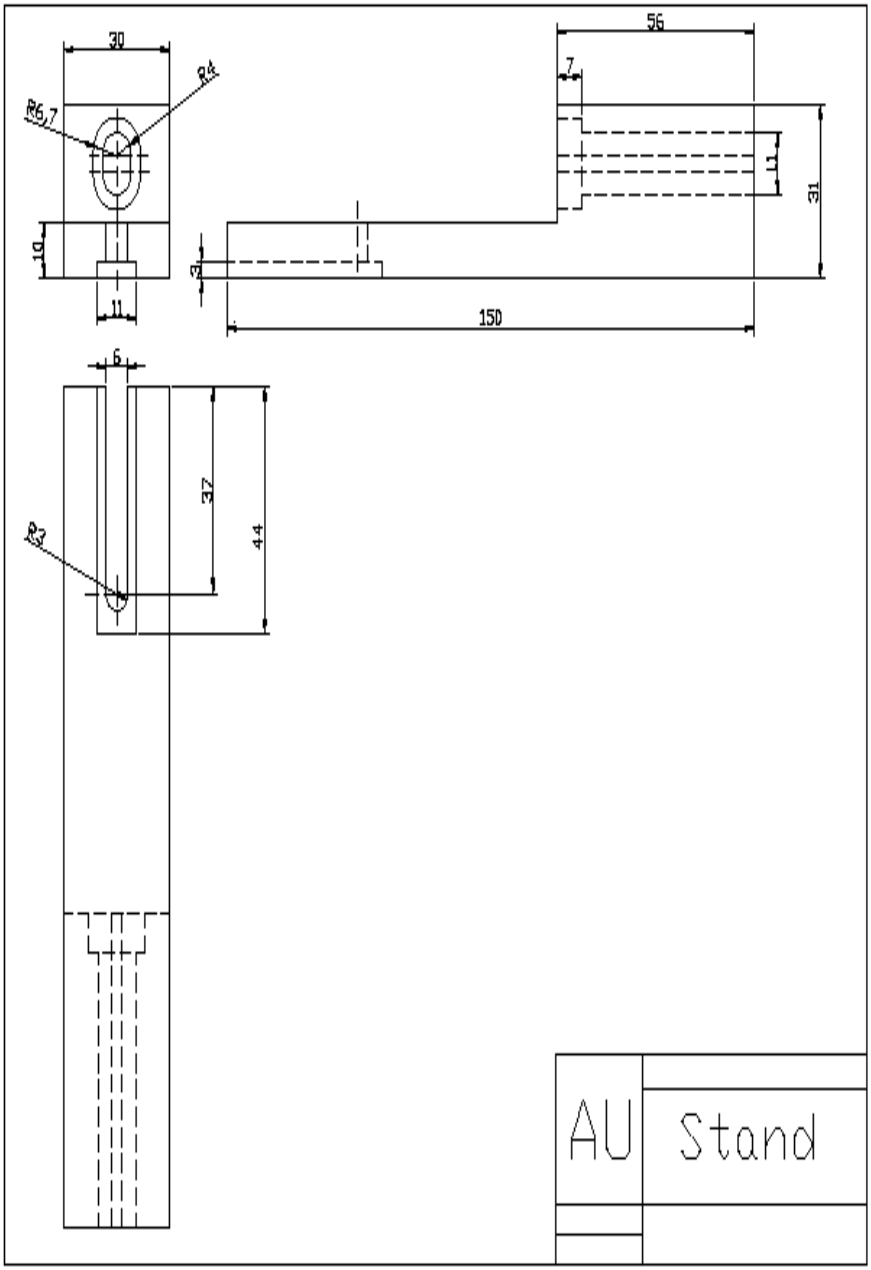
30
R6,7
10
1
56
7
11
31
3
150
6
37
44
R3
AU
Stand

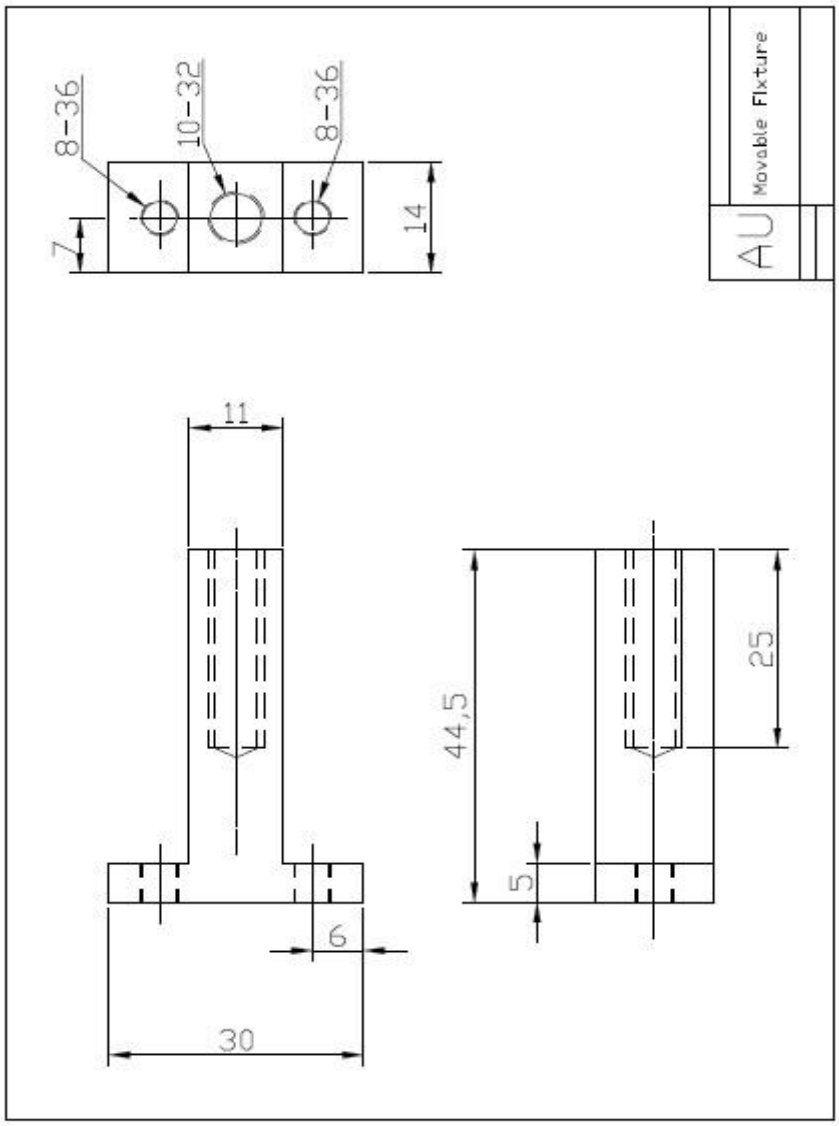
8-36
10-32
8-36
14
7
Movable Fixture
AU
11
44,5
25
5
6
30

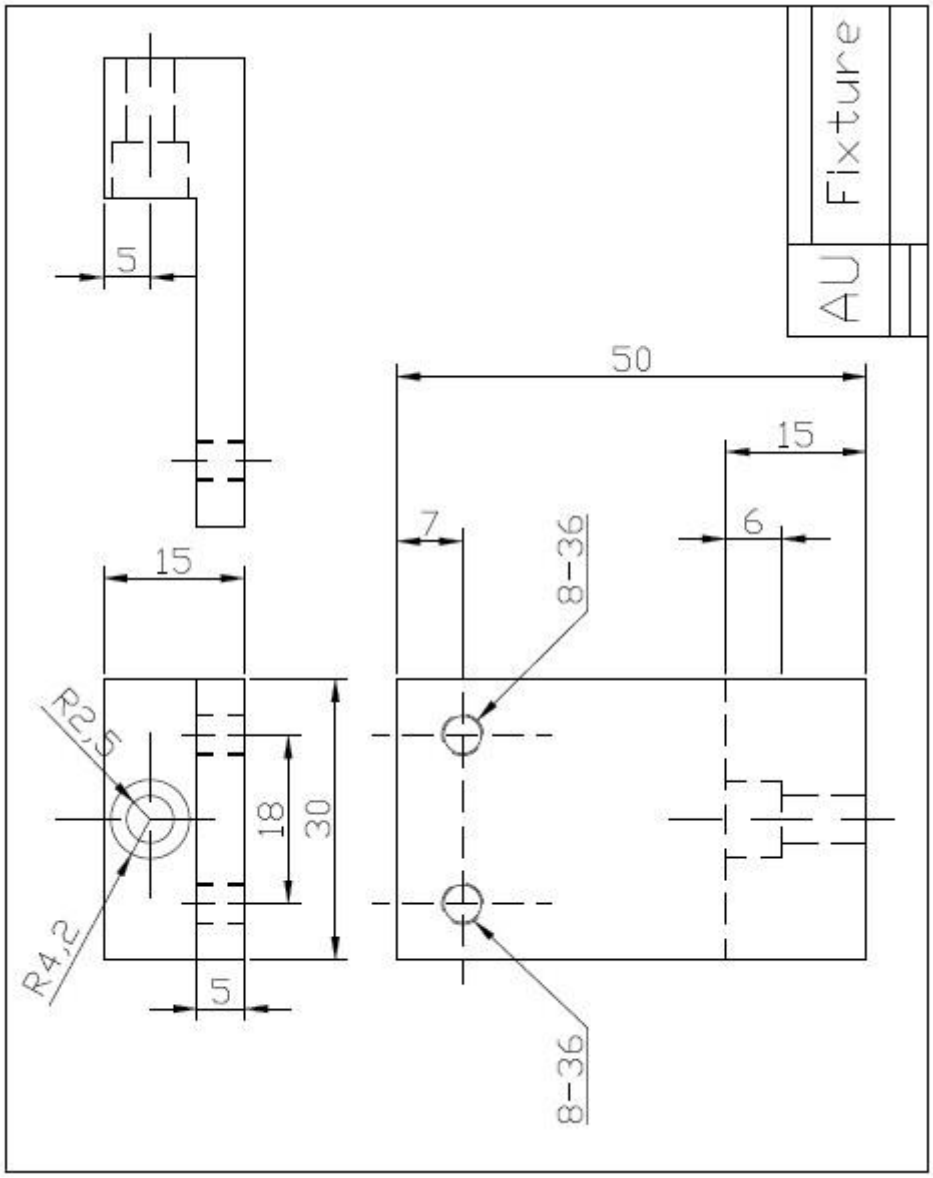
AU Fixture
5
50
15
7
8-36
6
15
R2,5
18
30
R4,2
5
8-36

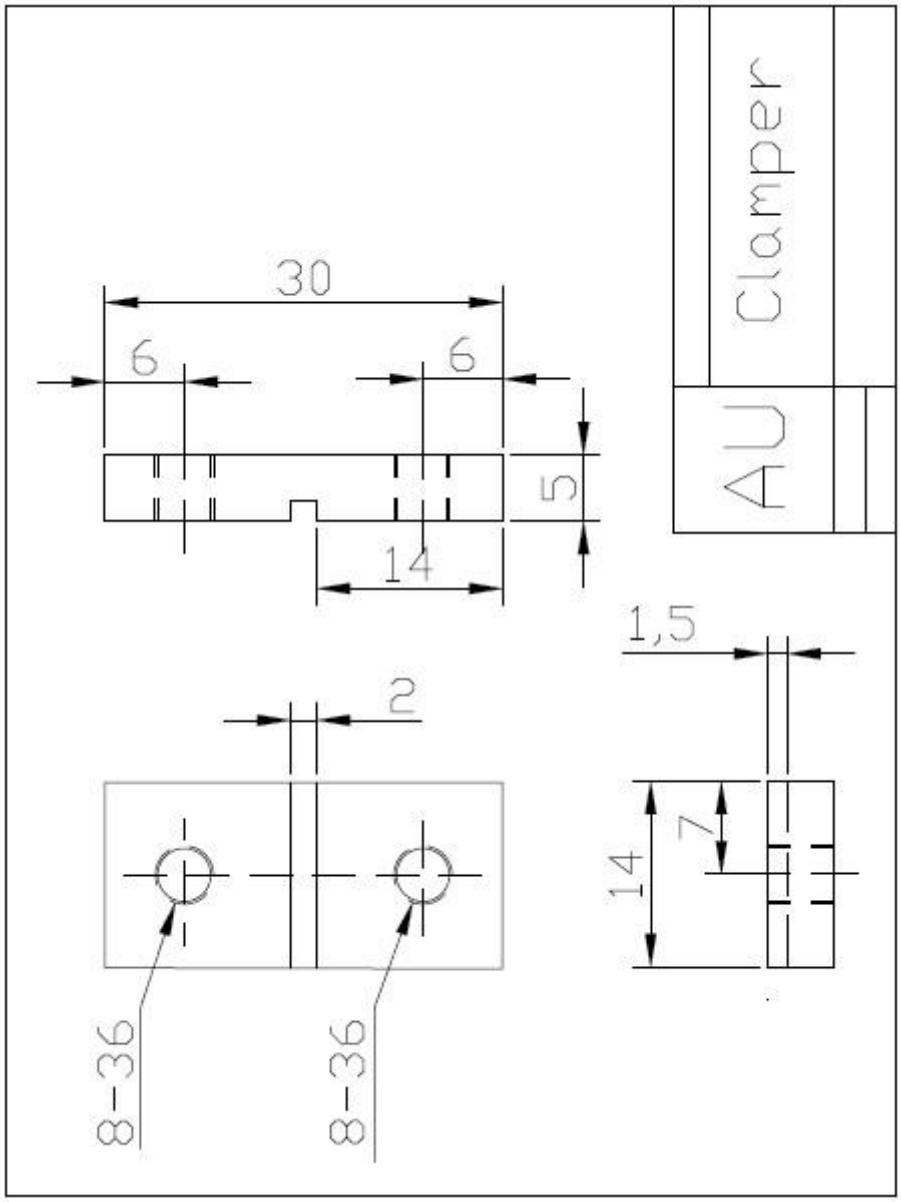
Clamper
AU
30
6
6
5
14
1,5
2
7
14
8-36
8-36